Advanced Applications of Periodic Fibre Structures in Chemical Sensing

Tan Xiao, Rex

School of Electrical & Electronics Engineering

Nanyang Technological University

Optoelectronics Research Centre

University of Southampton

A thesis submitted to the Nanyang Technological University and University of Southampton in partial fulfilment of the requirement for the joint degree of

Doctor of Philosophy

2019

Statement of Originality

I hereby certify that the work embodied in this thesis is the result of original research, is free of plagiarised materials, and has not been submitted for a higher degree to any other University or Institution.

10th Apr 2019

……. …….

Date Tan Xiao, Rex

Authorship Attribution Statement

This thesis contains material from 4 papers published in the following peer-reviewed journals and papers accepted at conferences in which I am listed as an author.

Part of Chapter 4 is published as:

Rex Xiao Tan, Stephanie Hui Kit Yap, Swee Chuan Tjin. "Fiber gratings enabled interrogation of Mach-Zehnder interferometer tapered fiber sensor.," Lasers and Electro-Optics Pacific Rim (CLEO-PR), 2017 Conference on. IEEE, 2017. DOI: 10.1109/CLEOPR.2017.8119019.

The contributions of the co-authors are as follows:

- Prof. Swee Chuan Tjin provided an initial project direction.
- I designed the study and prepared the manuscript.
- Stephanie Hui Kit Yap and I conducted the experiments, analysed experimental data and optimised proposed designs at the Centre for Optical Fibre Technology.

Part of Chapter 4 is also published as:

Stephanie Hui Kit Yap, Yi-Hsin Chien, **Rex Xiao Tan**, Abdul Rahman Ahiak Alauddin, Wen Bin Ji, Swee Chuan Tjin, Ken-Tye Yong, "An advanced handheld microfiber-based sensor for ultra-sensitive lead ion detection," ACS Sensors, Nov. 2018. DOI: 10.1021/acssensors.8b01031.

The contributions of the co-authors are as follows:

- Prof. Swee Chuan Tjin and A/Prof. Ken-Tye Yong and Dr. Wen Bing Ji provided an initial project direction and edited the manuscript drafts.
- Stephanie Hui Kit Yap and I designed part of the study.
- Stephanie Hui Kit Yap, Yi-Hsin Chien, Abdul Rahman Ahiak Alauddin, and I conducted the experiments at the Centre for OptoElectronics and Biophotonics.
- Stephanie Hui Kit Yap prepared the manuscript.

Chapter 5 is published as part of:

Rex Xiao Tan, Stephanie Hui Kit Yap, Yung Chuen Tan, Swee Chuan Tjin, Morten Ibsen, Ken-Tye Yong, and Wenn Jing Lai, "Functionalized Fiber End Superstructure Fiber Bragg Grating Refractive Index Sensor for Heavy Metal Ion Detection," MDPI Sensors, vol. 18, no. 6, p. 1821, Jun. 2018. DOI: 10.3390/s18061821

The contributions of the co-authors are as follows:

- I proposed the initial project direction and designed the study in consultation with Prof. Swee Chuan Tjin and A/Prof. Morten Ibsen.
- The experiments were conducted by Dr Yung Chuen Tan and I at the Centre for Optical Fibre Technology.
- The manuscript was drafted by me and revised by Dr. Yung Chuen Tan and Dr. Wenn Jing Lai.
- A/Prof. Ken-Tye Yong and Stephanie Hui Kit Yap shared expertise on metal ion chelation properties of Ethylenediaminetetraacetic acid.
- Prof. Swee Chuan Tjin and A/Prof. Morten Ibsen further edited the revised manuscript.

Chapter 6 is published as:

Rex Xiao Tan, Yung Chuen Tan, Daryl Ho, Chun Ho Tse, Seong Woo Yoo, Swee Chuan. Tjin and Morten Ibsen, "Birefringent Bragg Grating in C-Shaped Optical Fiber as a Temperature-Insensitive Refractometer," MDPI Sensors, vol. 18, no. 10, p. 3285, Sept. 2018. DOI: 10.3390/s18103285

The contributions of the co-authors are as follows:

- I proposed the initial project direction and designed the study in consultation with Prof. Swee Chuan Tjin and A/Prof. Morten Ibsen.
- Experiments were conducted by Dr Yung Chuen Tan and I at the Centre for Optical Fibre Technology.

- Experimental data were analysed by me with the advice of Dr Yung Chuen Tan.
- Special fibre was fabricated by Daryl Ho, Dr. Chun Ho Tse and A/Prof Seong Woo Yoo
- The manuscript was drafted by me and revised by Dr. Yung Chuen Tan.
- Prof. Swee Chuan Tjin and A/Prof. Morten Ibsen conducted final edits of the manuscript.

Part of Chapter 7 is published as:

Rex Xiao Tan, Stephanie Hui Kit Yap, Yung Chuen Tan, Swee Chuan Tjin, Morten Ibsen, Ken-Tye Yong, and Wenn Jing Lai, "Functionalized Fiber End Superstructure Fiber Bragg Grating Refractive Index Sensor for Heavy Metal Ion Detection," MDPI Sensors, vol. 18, no. 6, p. 1821, Jun. 2018. DOI: 10.3390/s18061821

The contributions of the co-authors are as follows:

- I proposed the initial project direction and designed the study in consultation with Prof. Swee Chuan Tjin and A/Prof. Morten Ibsen.
- The experiments were conducted by Dr Yung Chuen Tan and I at the Centre for Optical Fibre Technology.
- The manuscript was drafted by me and revised by Dr. Yung Chuen Tan and Dr. Wenn Jing Lai.
- A/Prof. Ken-Tye Yong and Stephanie Hui Kit Yap shared expertise on metal ion chelation properties of Ethylenediaminetetraacetic acid.
- Prof. Swee Chuan Tjin and A/Prof. Morten Ibsen further edited the revised manuscript.

10th Apr 2019
……. …….

Date Tan Xiao, Rex

ACKNOWLEDGEMENT

I am grateful to my supervisors. To Prof. Tjin Swee Chuan whom from the start of my PhD studies have allowed me the freedom to widely explore the field of photonics in search of my interest. No matter what I proposed to explore, your positive support and encouragement is vital to pushing me through the challenges that I have encountered in the course my research. To A/Prof Morten Ibsen, for rescuing me on my first night in a foreign land stranded with an unliveable nightmare house I so unwisely rented on the internet. You have taught me precious skills, and so generously shared your knowledge. Not to mention that you have one of the coolest cars I have sat in.

My eternal gratitude to my parents. I have almost never done you proud academically for the first 20 years of my life, but you have not given up on me. We did not live a life of abundance but both of you have always made sure that I have everything I need to succeed. I was too young and foolish to appreciate your sacrifices. It is only with your support that I am who I am today. I am eternally grateful.

To my fiancée, my wife to be a month from now. Thank you for standing behind my decision to pursue a career in science. Despite my frequent absence during these years for long periods, you have remained an encouraging partner. As I near the end of my PhD studies, I look forward to my next chapter in life together with you.

Finally, a big thank you to my "EEE PhD band of brothers", awesome friends and colleagues. Live long and prosper everyone!

ABSTRACT

Optical fibres had found applications in a wide range of engineering fields including but not limited to manufacturing, medical technology and structural monitoring since its discovery. With the maturity of optical fibre technology and demand to monitor the environment, optical fibre environmental sensors received increased attention.

Optical fibres can detect changes in its environment in the form of refractive index (RI), temperature, strain and other perturbances. Changes in environmental RI is particularly of interest to this thesis as it can be indicative of pollution amongst other issues. Furthermore, optical fibre sensitivity of RI can be exploited for sensing selected chemicals with simple surface coatings, enabling targeted chemical sensing in the environment.

This thesis presents two new fibre Bragg grating (FBG) based RI sensing schemes designed to address the issues of temperature and strain cross-sensitivity that are plaguing most state-of-the-art fibre RI sensors. Both proposed schemes can measure RI and temperature simultaneous with no cross-sensitivity effect. The first of the sensing scheme adopts a low finesse Fabry-Perot (FP) cavity formed between an FBG and the cleaved end of the optical fibre, with the cleaved fibre end as the sensing interface. This sensor measures the RI through the modulation of the resulting FP interference while measuring temperature change from spectral shifts. A maximum RI sensitivity of 230dB/RIU in the RI range of 1.333 to 1.471 and temperature sensitivity of 8.43pm/^{o}C were achieved.

The second scheme makes use of a birefringent FBG inscribed into a special C-shaped birefringent optical fibre where one polarisation mode is purposefully exposed to the environment. The birefringence of this special fibre is affected by changes in environmental RI and causes spectral response to the birefringent FBG in the form of polarisation mode separation, while temperature change induces a common spectral shift regardless of polarisation. A maximum RI sensitivity of 1300pm/RIU in the RI range of 1.333 to 1.410 was achieved.

Work on the first RI sensing scheme was further explored by coating the sensing fibre end with Ethylenediaminetetraacetic acid (EDTA) and Molybdenum disulphide (MoS_2) for heavy metal ion in water and ethylene gas sensing respectively. Both the sensors achieved high sensitivity, being able to detect traces of heavy metal ion in water from 10ppm and ethylene gas from 500ppb.

TABLE OF CONTENTS

Acknowledgement vi

Abstract vii

List of Tables xv

List of Figures xv

1 Introduction 1

1.1 Optical Fibre Chemical sensor 1

1.2 Motivation 2

1.3 Objectives 4

1.4 Major Contributions of Thesis 4

1.5 Organization of Thesis 5

1.6 Concluding Remarks 7

2 An Overview of Optical Fibre Technology and Grating-Based Optical Fibre Chemical Sensors 8

2.1 Optical Fibre 8

2.1.1 Geometrical Structure of Optical Fibres 8

2.1.2 Waveguiding Principles 9

2.1.3 Other Important Parameters 10

2.2 Optical Fibre Gratings 12

2.2.1 Photosensitivity of Optical Fibres 12

2.2.2 Fibre Bragg Grating 17

2.2.3 Long Period Fibre Grating 28
2.3 Optical Fibre Grating Refractometers 30
2.3.1 Cladding Thinned Fibre Bragg Grating Refractometer 31
2.3.2 Polarization Assisted fibre Bragg Grating Refractometer 32
2.3.3 Fibre Bragg Grating Fibre End Ratio-meter 34
2.3.4 Long Period Grating Refractometer 36
2.4 Surface Functionalized Optical Fibre Refractometers for Chemical Sensing Applications 36
2.4.1 Examples of Surface Functionalised Optical Fibre Chemical Sensors 36
2.4.2 Surface Functionalisation Techniques 37
3 High Germanium Core Content Optical Fibres for Grating Applications 40
3.1 Introduction 40
3.2 Photosensitivity Characterisation 41
3.2.1 Photosensitivity Characterisation Through Fibre Bragg Grating Inscription 41
3.2.2 Photosensitivity Characterisation Experiment of High Germanium-Doped Optical Fibre with 266nm Ultra-Violet Irradiation 42
3.3 Results and Discussions 44
3.4 Discussion and Conclusion 45
4 Grating Interrogation of Mach-Zehnder Interferometric Optical Fibre Chemical-sensors 46
4.1 Fibre Bragg Grating's Role in Chemical-Sensing as Interrogators 46

4.2 Mach-Zehnder Interferometry Based Tapered Fibre Refractometer.....47
4.2.1 Theory.....47
4.2.2 Sensor Fabrication and Characterisation.....48
4.3 Grating Enabled Interrogation Circuit Design for Mach Zehnder Interferometric Refractometers.....49
4.3.1 Duo Fibre Bragg Grating Interrogation Circuit Design.....49
4.3.2 Fibre Bragg Grating Fabrication.....50
4.4 Experiment.....51
4.5 Results and Discussions.....52
4.6 Concluding Remarks.....54
5 Bragg Grating to Fibre End Fabry-Perot interferometric Refractometers.....55
5.1 Introduction.....55
5.2 Theory.....55
5.2.1 Fibre-End Fresnel Reflection.....55
5.2.2 Fibre Bragg Grating to Fibre End Fabry–Perot Cavity.....57
5.2.3 Sensing Scheme.....60
5.2.4 Temperature Sensitivity of Fibre Bragg Gratings.....61
5.3 Sensor Fabrication.....62
5.3.1 Fabrication of Chirped Fibre Bragg Grating Sensor.....62
5.3.2 Fabrication of Superstructure Fibre Bragg Grating Sensor.....63
5.4 Experiment and Results.....64
5.4.1 Experimental Set-Up.....64

5.4.2 Refractive Index Response Characterisation 66
5.4.3 Temperature Response Characterisation 70
5.4.4 Further Discussions on Results 71
5.5 Fibre Host Comparative Studies for Superstructure Fibre Bragg Grating Sensors 72
5.5.1 Sensor Fabrication 72
5.5.2 Refractive Index Response 74
5.5.3 Temperature Response Characterisation 76
5.5.4 Further Discussions 77
5.6 Concluding Remarks 77
6 Birefringent Fibre Bragg Grating Refractometers 79
6.1 Introduction 79
6.2 Theory 80
6.2.1 Fibre Bragg Grating Inscribed Birefringent Waveguides 80
6.2.2 Side Exposed Single Mode Fibre 81
6.2.3 Fibre Bragg Grating In C-Shape Optical Fibre 82
6.2.4 Temperature-Refractive Index Decoupling of C-Fibre Bragg Grating Refractometer 83
6.3 Sensor Fabrication 83
6.3.1 Fabrication of C-Shape Optical Fibre 83
6.3.2 Fibre Bragg Grating Inscription 86
6.4 Experiment 87

6.5 Results and Discussions 89
6.5.1 Sensor Response to Refractive Index Change 89
6.5.2 Sensor Response to Temperature Change.....91
6.6 Concluding Remarks 92
7 Surface Functionalized Grating Based Refractometers for Chemical Sensing Applications 93
7.1 Introduction 93
7.2 Heavy Metal Detection.....94
7.2.1 Ethylenediaminetetraacetic Acid as Chelating Agent for Metal Chelates 94
7.2.2 Ethylenediaminetetraacetic Acid Coating Process on Fibre End for Heavy Metal Sensitivity 95
7.2.3 Experiment and Results 96
7.3 Ethylene Gas Sensing.....98
7.3.1 Molybdenum Disulphide for Ethylene Gas Sensing.....98
7.3.2 Molybdenum Disulphide Coating Process on Fibre End for Ethylene Gas Sensitivity 99
7.3.3 Experiment and Results 100
7.4 Concluding Remarks 102
8 Final Discussions, Conclusion and Recommendations For Future Work 104
8.1 Final Discussions.....104
8.1.1 Advantages and Limitation of Fibre Bragg Grating Refractometers....104

8.1.2 Advantages and Limitation of Surface Functionalisation of Fibre Refractometers 105

8.2 Conclusion 106

8.3 Recommendations for Future Work 108

8.3.1 Detail Study of High Germanium Doped Fibres 108

8.3.2 On Tower Inscription of C-Fibre Bragg Gratings 108

8.3.3 Further Investigation of Molybdenum Disulphide Interaction with Ethylene Gas Molecules 109

References 110

List of Publications 119

LIST OF TABLES

Table 1: List of high Germanium-doped optical fibres. 42

Table 2: Refractive index response comparison table for superstructure fibre Bragg grating sensors hosted in PS1250 and UHNA 4 optical fibres. 75

LIST OF FIGURES

Figure 1: (a)Cross section of a standard optical fibre with core of radius a and cladding of radius b. (b)Schematic of a standard optical fibre's structural profile with polymer coating. 9

Figure 2: Ray representation of total internal reflection of light as mechanism of light guiding in a length of optical fibre. 9

Figure 3: Schematic depiction of acceptance cone of an optical fibre. 11

Figure 4: Possible GODC candidates - Ge-E' centre and Ge(1) and Ge(2) electron trap centres. 14

Figure 5: Schematic diagram of a uniform fibre Bragg grating. 18

Figure 6: Distributed Fresnel reflection at index fringe boundaries along a length of fibre Bragg grating. 18

Figure 7: Schematic diagram of tilted fibre Bragg grating. 19

Figure 8: Typical transmission spectrum of a tilted fibre Bragg grating. 20

Figure 9: Schematic diagram of a chirped fibre Bragg grating 21

Figure 10: Reflection spectrum of chirped fibre Bragg grating. 21

Figure 11: Schematic diagram of a superstructure fibre Bragg grating. 22

Figure 12: Reflection spectrum of a superstructure fibre Bragg grating. 22

Figure 13: Holographic fibre Bragg grating method. 24

Figure 14: Schematic diagram of a phase-mask 25

Figure 15: Typical scanning phase mask set up.....26

Figure 16: Point by point fibre Bragg grating system.....27

Figure 17: Draw tower grating technique 28

Figure 18: Schematic diagram of a long period fibre grating. 28

Figure 19: Typical spectral response of a long period fibre grating. 29

Figure 20: Schematics of (a.) a silica plate phase mask and (b.) a metal plate amplitude mask. 30

Figure 21: Schematic diagrams of (a.) unmodified fibre Bragg grating, (b.) etched fibre Bragg grating and (b.) tapered fibre Bragg grating.....31

Figure 22: Typical spectral response of etched/tapered fibre Bragg grating refractometers 32

Figure 23: Schematic diagram of (a.) etched D-shape, (b.) etched panda H-shaped and (c.) etched side hole H-shape fibres refractometers.....33

Figure 24: Typical spectral response of birefringent fibre Bragg grating refractometers. 33

Figure 25:Schematics of a fibre Bragg grating-Fibre end Fresnel reflection ratiometer. 34

Figure 26: Typical spectral response of a fibre Bragg grating fibre end ratiometer for RI measurement. 35

Figure 27: Procedure of dip coating.....37

Figure 28: Optical deposition set up. 39

Figure 29: RI profiles of UHNA4 from Nufern and A0641 from Optoelectronics Research Centre (University of Southampton).....43

Figure 30: Experiment setup. 44
Figure 31: Refractive index modulation and effective index evolution of a.) UHNA4 and b.) A0641 45
Figure 32: Schematic diagram of a typical single mode fibre taper. 47
Figure 33: Transmission spectrum of tapered fibre refractometer 48
Figure 34: Schematic of two fibre Bragg grating interrogator design. 49
Figure 35: Transmission spectrum of interrogation fibre Bragg grating pair. 50
Figure 36: Experimental setup. 51
Figure 37:Transmission spectrum of tapered fibre sensor in three different refractive index environments. 52
Figure 38: (a) Reflected optical power by fibre Bragg grating 1 and fibre Bragg grating 2. (b) Ratio of reflected power by FBG1 and FBG2. 53
Figure 39: (a.) Superstructure fibre Bragg grating to fibre cleaved end Fabry–Perot cavity. (b.) Chirped fibre Bragg grating to fibre cleaved end Fabry–Perot cavity. 58
Figure 40: Bragg grating - fibre cleaved end Fabry–Perot interference pattern of (a.) chirped fibre Bragg grating sensor (b.) superstructure fibre Bragg grating sensor. 58
Figure 41: chirped fibre Bragg grating fabrication method. 62
Figure 42: Sensor schematics diagram of sensor configuration and refractive index modulation resulting in chirped fibre Bragg grating sensor. 63
Figure 43: superstructure fibre Bragg grating fabrication method. 63
Figure 44: Sensor schematics diagram of sensor configuration and refractive index modulation resulting in superstructure fibre Bragg grating sensor. 64
Figure 45: Experimental set up for refractive index measurement. 65
Figure 46: Experimental setup for temperature characterisation of fibre sensors 66

Figure 47: Reflection spectrum when interfaced with DI water (refractive index:1.333) and Glycerine solution(refractive index: 1.410 for chirped fibre Bragg grating and 1.433 for superstructure fibre Bragg grating) for (a.) Chirped fibre Bragg grating fibre end sensor, (b.) Chirped fibre Bragg grating fibre end sensor zoomed to 1 nm spectral width and (c.) Superstructure fibre Bragg grating fibre end sensor. 66

Figure 48: Spectral response of chirped fibre Bragg grating sensor interfaced with de-ionised water, with top and bottom envolop functions. 67

Figure 49: Refractive index response for chirped fibre Bragg grating sensor. 68

Figure 50: (a.) Spectral response of superstructure fibre Bragg grating sensor interfaced with de-ionised water, (b.) expended view of peak 0 of the spectrum. 69

Figure 51: Refractive index response for superstructure fibre Bragg grating sensor ...69

Figure 52: Reflection spectrum when submerged in 20°C and 60°C DI water for (a.) Chirped fibre Bragg grating fibre end sensor, (b.) Superstructure Bragg grating fibre end sensor measured at lower resolution to remove interference fringes. 70

Figure 53: Temperature response for chirped fibre Bragg grating and superstructure fibre Bragg grating sensor. 71

Figure 54:Schematics diagram of sensor configuration and refractive index modulation resulting in superstructure fibre Bragg grating sensor hosted in UHNA 7 high Ge-doped Optical fibre. 73

Figure 55:Spectral response of superstructure fibre Bragg grating sensor interfaced with deionised water of (a.) Sensor A and (b.) Sensor B. (c.) expended view of peak -2 of the spectrum for Sensor B. 74

Figure 56: (a.) Reflection spectrum of Sensor B when interfaced with DI water (refractive index:1.333) and Glycerine solution (refractive index: 1.4710) and (b.) expanded view of peak -2. 74

Figure 57: Refractive index response for superstructure fibre Bragg grating sensor B 75

Figure 58:Reflection spectrum when submerged in 20°C and 60°C DI water for Sensor B. 76

Figure 59: Temperature response for superstructure fibre Bragg grating Sensor B. 77

Figure 60: Schematic of (a.) D-shape and (b.) C-shape single mode fibres. 81

Figure 61: Schematics of C-fibre with FBG spliced to standard single mode fibres as inline refractive index sensor. 82

Figure 62: Milling of preform on customized milling stage with Standard Series 10 Rotary Knee mill from SONIC-MILL. 84

Figure 63: (a.) Preform of standard single mode fibre with quadrant cut out. (b.) fibre end image of C-shaped fibre. 85

Figure 64: Thin cladding layer formed through fibre drawing process. 85

Figure 65: Index profile of C-Shape optical fibre along x and y axes. 86

Figure 66: C-Shape optical fibre with fibre Bragg grating inscribed affixed to a nylon block with V-groove. 87

Figure 67: Experimental setup. 88

Figure 68: Spectral response in deionized water and Glycerine solution of refractive index 1.410. 89

Figure 69: Sensor response to change in ambient refractive index. 90

Figure 70: Sensor response to change in ambient temperature. 91

Figure 71: Superstructure fibre Bragg grating refractometer fibre end coated with Ethylenediaminetetraacetic acid. 96

Figure 72: Experimental set up for metal ion detection with EDTA coated sensor. 96

Figure 73: Ethylenediaminetetraacetic acid coated sensor response when exposed to air and in deionized water 97

Figure 74: Ethylenediaminetetraacetic acid coated Sensor response when exposed to deionized water and in 100 ppm and 200 ppm solution of Cd2+ 97
Figure 75: Superstructure fibre Bragg grating refractometer fibre end coated with Molybdenum Disulphide 100
Figure 76:Experimental set up for metal ion detection with MoS^2 coated sensor.....100
Figure 77: Molybdenum Disulphide coated Sensor response when exposed to air and ethylene gas of 0.5ppm and 1ppm of ethylene gas. 101
Figure 78: Central peak of Molybdenum Disulphide coated Sensor response when exposed to air and ethylene gas of 0.5ppm and 1ppm of ethylene gas. 102

1 INTRODUCTION

This chapter provides the pretext to the search of a perfect solution in optical fibre chemical sensing. It does so by first outlining some of the major progresses over the past five decades of optical fibre sensor research and development. It then goes on to highlight the motivation behind this fervent pursuit of a more elegant sensor designs, lay out the objectives of this thesis and summarizes its major contributions. Lastly, an outline of the thesis was included for reader's reference.

1.1 Optical Fibre Chemical sensor

Mechanism of light guiding in fibre light structures was discovered in the 1850s as light was observed to be directed in a bent path in streams of water. This discovery eventually lead to the first published paper on low refractive index (RI) material clad glass fibre imaging bundle [1] in the 1950s. The genesis of optical fibre sensors arguably began when the first low loss optical fibre [2] was made in the late 1960s to early 1970s. Hence this is the point in history, five decades ago, that this thesis recognizes as the beginning of modern optical fibre sensors as we know today.

Optical fibre sensors had received a huge amount of attention from the sensor community for its superiority in many areas when compared to its electronics counterparts. Researchers around the world had first glimpsed the impact of optical fibre sensors [3] in the early 1980s. Members of the optics and sensors community began work in vast areas of applications for optical fibre sensors in acoustic, magnetic, force, temperature and chemical sensing just to name a few.

Optical fibre chemical sensors are of huge research interest due to optical fibre's various inherent advantages such as robustness, electromagnetic immunity and short time to results using real time interrogation as compared to many existing solutions such as bulk spectrometers. These properties of the optical fibre gave rise the immense potential of optical fibre chemical

sensors to be applied in environmental sensing. The base of environmental sensing for optical sensors are commonly refractometers which has a wide range of applications including water quality [4], humidity [5] and temperature [6] measurements and monitoring. The need to constantly monitor our environment, both water and air is ever increasing in this age. Water source purity and air quality are of national security concern for many countries like Singapore [7] where the author of this thesis is based. Robust fibre sensors can be designed and deployed in large bodies of water such as reservoirs and ground water sources, as permanent monitors or simple portable probes. Works in this area had been actively researched and published for three decades [8, 9].

Another part of our environment which is of interest other than water, is of air. Air can be rich in both polluting and non-polluting chemicals and particulate matters. These particles in air can result in environmental and health hazard but often goes undetected. A failure in monitoring air quality resulting in lack or delay in rectification actions can lead to problems such as asthma prevalence [10] or even high premature mortality [11]. Air, or more specific gas monitors can also benefit the society in other ways such as in agriculture and occupational health. Fruit farming can benefit from sensors deployable in the field that monitors ethylene levels for better management of produce [12]. On the other hand, in indoor environments [13], a range of gases, air particulates and other pollutants can cause adverse impacts to inhabitants in homes and offices.

This thesis contributes in this effort of advancing optical fibre sensors by focusing on the development of novel optical fibre chemical sensors for water and air environment monitoring based on fibre Bragg grating (FBG) technology. The motivation and objectives are more adequately spelled out in the following sections.

1.2 Motivation

The ability to monitoring our environment in real time continuously, had long been desired. As the science and technology community continue pushing boundaries towards

solutions of all-round real time online environmental monitoring, optical fibre sensors emerged as a branch of technology with high suitability for the potential fulfilment of the market's pursuit of high performance and low-cost.

The performance of a sensor is commonly judged by its sensitivity, resolution, operating range and robustness while low cost arises from simplicity of design, easy integration with existing infrastructures and cost-effective manufacturing. Being photonic devices, optical fibre sensors are inherently capable of relatively high performance as compared to electronic sensors. Coupled with the advancement of optical fibre technology and the ever-expanding adoption of fibre optics devices in a wide range of applications, optical fibre is seemingly the right solution to work towards.

However, optical fibre sensors might not yet be ready for rapid adoption as many sensing schemes are plagued with some unique problems which prevented such sensors from achieving the desirable characteristics discussed here. Three of these problems are:

1. Highly cross sensitive to other attributes of the test samples such as temperature changes and induced strain.
2. Complicated optical design requiring complex fabrication processes and designs involving more than one strand of optical fibre for temperature and strain compensation.
3. Highly complex equipment and optical circuitries needed for interrogation which also result in high cost.

Therefore, more research is needed to be taken on by the optical fibre sensor community to address these problems for optical fibre sensors to become the undisputed standards in chemical sensing.

1.3 Objectives

The objectives of this thesis are to demonstrate new optical fibre chemical sensing schemes that fulfils the above discussed characteristics, placing emphasis on simplicity of design and low cost in implementation. The sensing schemes should be free from cross sensitivity issues, easy to fabricate and do not require expensive and complex interrogation equipment and circuits.

An emerging type of optical fibre with extremely high Germanium dopant was studied for both their photosensitivity, RI modulation characteristics and suitability as host fibre for chemical sensors. A design of all fibre interrogation circuit using cascading FBGs was proposed and implemented for MZI based chemical fibre sensor, eliminating the reliance of these sensors on lab based bulk interrogation systems. Two types of sensing scheme based on FBGs were designed and fabricated to study their performance as refractometers. Based on these refractometers, two chemical sensing applications were demonstrated by applying special chemical coatings on the refractometers' sensing surfaces.

This forms a complete study of novel FBG chemical sensors based on surface functionalized FBG RI sensing schemes. It begins from fundamental study of grating inscription in new optical fibre types, adaptation of FBGs in fibre chemical sensors as interrogators, design and implementation of new FBG based RI sensing schemes, and lastly on chemical surface functionalization of these fibre refractometers for a couple of chemical sensing applications.

1.4 Major Contributions of Thesis

This thesis revisited grating inscription fundamentals with a new class of photosensitive optical fibres with extremely high doping concentration of germanium in their fibre cores. The claimed capability of such fibres being highly UV photosensitive host for grating based applications and suitability and superiority as compared to standard fibres as host of fibre sensors was evaluated. The high germanium content fibres used in this study came from three sources, including research centres and commercial manufacturers.

It also proposed and showed that FBGs can contribute to existing fibre chemical sensors by providing a sensor interrogation scheme that is not reliant on lab-based equipment. This was demonstrated in the form of duo FBG interrogation circuit for a type of well-studied tapered fibre Mach-Zehnder Interferometric refractometer.

The thesis then proposed two types of FBG based refractometers that are free from issues of cross sensitivity to fluctuating environmental attributes that plague many reported fibre sensors. The two sensor types adopt FBG technologies in radically different manners, presenting different advantages.

Lastly, chemical sensing on top of RI sensing was studied by the means of chemical functionalization of light-environment interaction surface of the demonstrated refractometers. Two of such applications, one each in liquid (heavy metal ion in water) and air (ethylene gas) were demonstrated using specific chemicals chosen for their interaction and chelating properties with target chemicals.

1.5 Organization of Thesis

This thesis is organized as such where chapter one introduces the history, development, demand and common principles of optical fibre chemical sensors. The motivation behind the works reported in this thesis were discussed, objectives laid out and major contributions summarized. The chapter concludes with an outline of this thesis.

Chapter 2 provides an overview of the various sciences and technologies involved in the study of optical fibre chemical sensors. It first reviews the fundamental wave-guiding principles of optical fibres, fibre gratings and variation of such gratings fabricated through periodic modulation of optical fibre's core refractive index with controlled UV irradiation. It then reviews grating based refractometers that laid the ground works for the studies in this thesis and lastly discussed surface functionalization techniques for the transformation of optical fibre refractometers into chemical targeted sensors.

In chapter 3, high germanium doped fibres were studied for their photosensitivity and it discusses a unique characteristic for RI modulation common to all sample fibres with small doses of UV irradiation. Grating inscription characteristics were investigated. The chapter concludes with an evaluation of the suitability of this class of fibres as host fibre for grating based chemical sensors.

Chapter 4 takes a retrospective look at some reported fibre chemical sensors and proposes additional role of FBGs in chemical sensor designs. This proposal is in a form of a full fibre grating-based interrogation circuit for the replacement of lab-based interrogators. This concept was implemented on a tapered fibre Mach–Zehnder interference refractometer to demonstrate its simplicity, ease of implementation, and cost effectiveness.

Chapter 5 begins by introducing a new concept of FBG to Fibre-end Fabry–Perot interferometric refractometer. The study designed and implemented two of such sensors using two different special grating types. The chapter discusses the theory, fabrication and experiment for both sensor schemes in detail and concludes with analysis of the performance of these sensors, comparing the advantages and limitations of each design.

In chapter 6, a new design of a side exposed FBG refractometer based on FBG inscription in a point exposed C-shape special fibre was demonstrated. The special fibre was fabricated in house and it’s waveguiding characteristics at the FBG site leading to its sensing properties was discussed. Fabrication of the sensor and experimental procedure to characterize the sensor was elaborated in detail. The chapter concludes with an analysis of the sensor performance and potential “off-the-tower” one step fabrication of such sensors.

The penultimate chapter 7 of this thesis first discusses the surface functionalization of optical fibre refractometer as refractometer sensitization technique for targeted chemical sensing. It then introduces two chemicals used to functionalized fibre refractometers discussed in chapter 5 for chemical sensing applications in specific liquid and gas, i.e. heavy metal ion in water and ethylene gas in air respectively. Surface functionalization methods and experimental procedures

were described in detail and performance of each sensor discussed. The chapter concludes with remarks on the flexibility, ease of fabrication and robustness of such chemical sensors.

The final chapter provides the last remarks of the author, providing a conclusion to this thesis, and proposes directions for future work.

1.6 Concluding Remarks

The maturity of optical fibre technologies has led to the diversification of applications for optical fibres. These advancements have placed optical fibre sensors as a feasible optoelectronic replacement for a wide range of traditional electronic sensors as they are of superior performance and can be more cost effective. Several issues in such sensors remain to be addressed with further research by the community, to enable wider optical fibre sensor adoption.

2 An Overview of Optical Fibre Technology and Grating-Based Optical Fibre Chemical Sensors

The glass optical fibre operates on simple law of physics, guiding light wave from one point to another by confining the radiation within the fibre structure based on the principle of total internal reflection. Besides its obvious application in long distance, high speed transmission of data through the modulation of guided light, the optical fibre is also a good host and platform for photonic sensors of both physical and chemical sensing applications.

This chapter lays out the fundamentals of the science and technology behind silica based optical fibres, optical fibre photosensitivity and optical fibre grating devices. It then goes on to provide a brief survey of optical fibre sensors for refractive index (RI) sensing with a focus on grating-based refractometers, discussing the working principles of the sensors and their merits and limitations. Lastly, the chapter concludes with an introduction of the concept of targeted chemical sensing through surface functionalization of optical fibre refractometers.

2.1 Optical Fibre

An optical fibre is a long, thin and traditionally cylindrical waveguide made of dielectric materials with a few exceptions [14, 15] for special applications. It is able to capture light at one end, traps and guide the radiation along its length to the other end [16]. The light guiding principles of the optical fibre is simple. However, the light-fibre interactions do present many interesting nonlinear phenomena such and Raman scattering and light dispersion that had been discussed in very great details in many literatures [17].

2.1.1 Geometrical Structure of Optical Fibres

The standard optical fibre today generally refers to the telecommunication optical fibre optimized for guiding light of wavelengths around 1550nm over long distances. These optical fibres are silica glass based with cross sectional diameter of around 125μm. The structure of a

standard optical fibre (Figure 1) consists of a relatively thick pure silica cladding surrounding a thinner germanium-doped silica core of few micrometres in diameter. Optical fibres are also usually coated with a thin layer of polymer for protection against breakages.

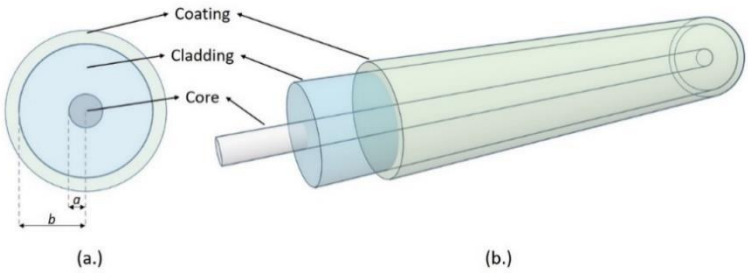

Figure 1: (a)Cross section of a standard optical fibre with core of radius a and cladding of radius b. (b)Schematic of a standard optical fibre's structural profile with polymer coating.

The optical fibre can be characterized by its core and cladding radius, a and b, and their respective RIs. The RI of the fibre core and cladding are commonly denoted as n_{core} and n_{clad} respectively. Effective RI of an optical fibre is radiation mode dependant, varying for light of different wavelength.

2.1.2 Waveguiding Principles

Light is guided within and along the optical fibre core by confining them in the optical fibre core. This is achieved by selecting appropriate n_{core} and n_{clad} to meet the condition for total internal reflection of the light within the wavelength range, at the core-cladding boundary.

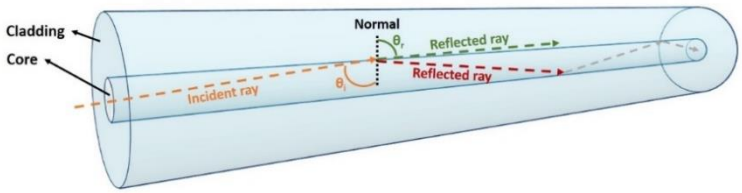

Figure 2: Ray representation of total internal reflection of light as mechanism of light guiding in a length of optical fibre.

With RI of the fibre core higher than that of the cladding (i.e. $n_{core} > n_{clad}$), the following condition for total internal reflection, angle of incident to be higher than that of critical angle (θ_C), can be satisfied.

$$n_{core} \sin \theta_C = n_{clad} \sin 90 \quad (1)$$

$$\theta_C = \sin^{-1} \frac{n_{core}}{n_{cladd}} \quad (2)$$

A silica optical fibre's core is also predominantly silica. To raise the RI of the core to be higher than the cladding, Germanium is commonly used as a dopant. This could be done by the means of gradual doping from the fibre cladding to the centre of the fibre core, resulting in a graded index increase, or as an abrupt step increase of index at the core-cladding interface.

The standard telecommunication optical fibre is doped in the core with germanium [18] in the range of few molecular percentage, which actual doping concentration differs slightly with manufacturers. The RI of the doped core can be derived through the linear relationship between mole percentage of doped material and permittivity as follows:

$$n_{core}^2 = n_{SiO_2}^2 + \frac{m}{m_{dopant}} (n_{dopant}^2 - n_{SiO_2}^2) \quad (3)$$

where n_{SiO_2} is the RI of fibre host material silica, m is the mole-percentage of doping in the fibre core fabricated and n_{dopant} and m_{dopant} are the RI of doping material and mole-percentage of dopant in the doping material used. An interesting direction of advancement in optical fibre technology is in the research in core dopant materials that gives the fibres special characteristics such as light amplification [19-21], better waveguiding with low loss at higher wavelengths [22] and photosensitivity [23, 24].

2.1.3 Other Important Parameters

2.1.3.1 Numerical Aperture

Due to the dependence of optical fibre waveguiding characteristics on the angle of incidents of light at fibre end, an optical fibre can also be characterized by an acceptance angle θ_A. The acceptance angle denotes an acceptance cone (Figure 3) within which incidental light will be efficiently confined in and guided by the optical fibre.

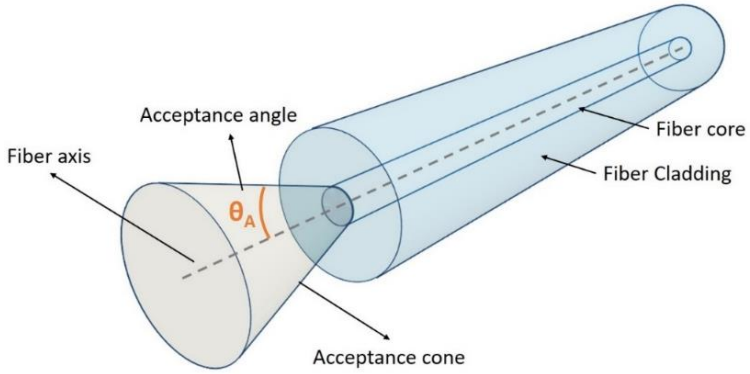

Figure 3: Schematic depiction of acceptance cone of an optical fibre.

The acceptance cone therefore determines how light couples from an external light source into the fibre. From the acceptance angle, one can also represent this ability to accept light as the numerical aperture (NA) of the optical fibre.

$$NA = \sin \theta_A \tag{4}$$

$$NA = \frac{1}{n_0}\sqrt{n_{core}^2 - n_{clad}^2} \tag{5}$$

where n_0 is the RI of the medium surrounding the optical fibre in which light source propagates in before its incidences with the optical fibre end.

The NA is always smaller than 1 as it is a function of the optical fibre's RIs. A large NA optical fibre though will able to collect light from a wider angle, improves waveguiding ability and lowers bending losses, but also results in large beam divergence for the fundamental guided mode thus increasing nonlinearity in the fibre.

2.1.3.2 Transmission Loss

Unavoidable loss of power for light guided through a length of optical fibre can be due to various reasons. Common causes of power attenuation are bending [25-27] including micro-bending where light that are incident at the core-cladding boundary no longer satisfy conditions of total internal reflection, impurities in optical fibre materials or the occurrence of different types of scattering mechanisms [28].

Transmission loss of the fibre can be represented by an attenuation constant (α) and hence the optical power transmitted (P_0) over a length of optical fibre (L) is given by:

$$P_T = P_0 e^{-\alpha L} \tag{6}$$

From equation (6), one can then derive an empirical mathematical representation of total fibre loss contributed by all loss mechanisms regardless of types with the following relation:

$$\alpha_{dB} = -\frac{10}{L}\log\frac{P_T}{P_0} \tag{7}$$

here α_{dB} is the actual power loss of the fibre per unit length quantified in decibels. It is also interesting to note that light of different frequencies interacts with optical materials differently, resulting in frequency dependent losses. Therefore, optical fibres are usually characterized at specific operating wavelengths of interest.

2.2 Optical Fibre Gratings

Optical gratings are periodic structures inscribed into optical materials or waveguides that diffracts light incident onto it. In optical fibre waveguides, grating structures can be inscribed using a couple of methods to change its waveguiding properties in a desired manner. The most common and efficient method to create these structures is to irradiate a length of optical fibre periodically with ultra-violet (UV) light, modulating the RI of the UV photosensitive germanium doped core.

Two main types of fibre gratings exist, long period gratings, which couples guided modes of an optical fibre into forward propagating cladding modes, and Bragg gratings, that reflects a specific wavelength of light and is transparent to all others. These structures have found a wide range of applications in fibre lasers, filters and sensors.

2.2.1 Photosensitivity of Optical Fibres

The photosensitivity of optical fibres is the basis for grating inscription since its discovery [29] in 1978. Despite the recent research into grating inscription using femtosecond

lasers which do not depend on fibre photosensitivity, photoinduced RI modulation remains the most popular method for its many advantages.

2.2.1.1 Mechanism of Optical Fibre Photosensitivity

Germanium is commonly used as dopant for optical fibre core, raising the RI of the core to satisfy light confinement and guiding conditions. At a concentration of 3-5 mole-percent for typical standard single mode optical fibres, this addition of germanium atoms introduces defects into the silica glass matrix by forming oxygen deficient bonds [30]. Evidence suggest that these defects that occurs in germanosilicate fibres are the reason for such optical fibres to exhibit photosensitivity [31-35], especially in the UV region.

The most prevailing defect in germanosilicate glass structure is the Ge-O defect, forming an energy gap of 5eV. This energy gap happens to coincide the energy of one photon from a UV laser such as an excimer laser or frequency doubled argon ion laser. Absorption of photonic energy equivalent to that of the energy gap of the Ge-O defects, breaks the bond resulting in Ge-E′ centre, introducing free electrons to the germanosilicate glass matrix. These free electrons, when trapped at hole-defect sites, forms Ge(1) and Ge(2) colour centres, causing the light absorption characteristics of the glass to change, thus affecting its RI according to the Kramers-Kronig relation:

$$\Delta n(\omega') = \frac{c}{\pi}\int_0^{\infty} \frac{\Delta\alpha(\omega)d\omega}{\omega^2\omega'^2} \tag{8}$$

where $\alpha(\omega)$ is the original absorption spectrum and $\Delta n(\omega')$ is the spectrum dependent RI change after formation of Ge(1) and Ge(2) colour centres with light absorption.

As the photosensitivity is directly related to the number of Ge-O defects in the glass, photosensitivity of standard telecommunication optical fibres is limited due to the low dopant concentration in its core. Pristine standard telecommunication optical fibres exhibit a saturated RI change through UV irradiation in the order of 10^{-4}. There are several methods of enhancing the photosensitivity of optical fibres including increasing germanium doping concentration, co-

doping of fibre cores with other materials and hydrogenation. These photosensitization methods are discussed in the immediately following sections.

2.2.1.2 Enhancing Optical Fibre Photosensitivity

Since the discovery of optical fibre photosensitivity in Ge-doped optical fibres, multiple techniques to enhance this nonlinear effect have been reported, mainly by works on fibre grating inscription. A couple of main methods have been studied in great details by the research community and each result in different advantages and limitations. These methods are increasing optical fibre core Ge dopant concentration and hydrogenation of the optical fibres.

Highly Germanium-Doped Germanosilicate Optical Fibres

As established, the photosensitivity of germanosilicate fibres depends on the number of defect sites, specifically Ge-O defects in the fibre core [35]. Naturally, optical fibre fabricators have increased the concentration of Ge dopant in fibre core to raise photosensitive of the fibre. The increase in Ge in the optical fibre core increases occurrence of Ge-O defect sites which translate to a higher fibre photosensitivity [36].

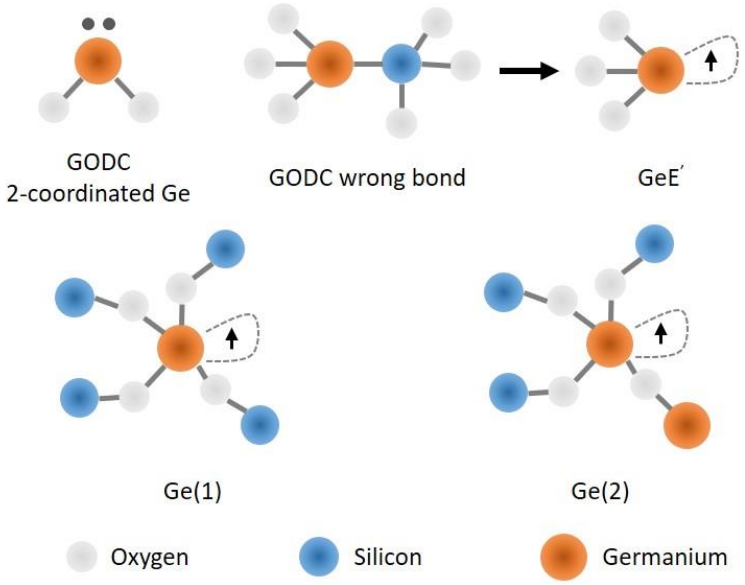

Figure 4: Possible GODC candidates - Ge-E' centre and Ge(1) and Ge(2) electron trap centres.

High Ge-doped fibres of up to 30% have since been commercially available as high NA and bend insensitive photosensitive fibres. These fibres' RI can be modulated with UV

irradiation up the order of 10^{-2}. This degree of photosensitivity is an order of 2 in improvement as compared to standard telecommunication optical fibres.

Due to the high Ge-dopant level, NA of these step index optical fibres are also high, resulting in high *V* number. The *V* number is a dimensionless parameter, value of which should be kept below approximately 2.4 for a step index optical fibre to be single mode at the operating wavelength of interest.

$$V = \frac{2\pi}{\lambda} a \cdot NA \tag{9}$$

where λ is the operating wavelength of guided modes and *a* is the radius of the optical fibre core. The *V* number also indicates the ratio of optical power of a guided mode confined in the fibre core as compared to the cladding. To keep high Ge-doped optical fibres single mode at telecommunication wavelength of around 1550nm, boron is sometimes added to the fibre core to lower the RI of the core.

The same can also be achieved by reducing the core diameter *a*, but results in reduced mode field diameter (MFD) of the fundamental mode in the optical fibre. The MFD of a guided mode in a length of optical fibre is a measure of the transverse extend of that mode in the fibre and can determined by approximating [37] the mode radius (*w*) using the Marcus Formula.

$$\frac{w}{a} \approx 0.65 + \frac{1.619}{V^{\frac{3}{2}}} + \frac{2.879}{V^6} \tag{10}$$

$$MFD = 2w \tag{11}$$

When a segment of optical fibre with MFD mismatched with the rest of the optical fibre system, usually using standard telecommunication fibres, significant coupling loss can be resulted. Hence, Ge/B co-doped photosensitivity enhanced fibre capable of achieving MFD matching with standard telecommunication fibres are sometimes referred to as MFD matching photosensitive fibres.

More recently, work have been reported on photosensitivity studies of extremely high Ge-doped germanosilicate fibres in the range of 70-90% mole percent [23, 38]. These fibres

have good waveguiding characteristics beyond the operating wavelength of standard optical fibres due to lower attenuation at higher wavelengths. However, the photosensitivity mechanism appears to be highly complex and will be discussed in more detail in Chapter 3 of this thesis.

Hydrogenation of Optical Fibres

The most effective way to increase photosensitivity of an optical fibre is through hydrogenation, also known as hydrogen loading [39]. This process involves soaking the optical fibres in a chamber filled with pressurized hydrogen gas at high temperature. Depending on conditions and time allowed for the process, the chamber pressure can be up to 600-800 bar and temperature of up to 150ºC. However, given enough time, soaking the optical fibre in hydrogen gas of 200 bar at room temperature for 2 weeks is sufficient for diffusion of hydrogen into the optical fibre core glass matrix [39]. With hydrogenation, RI modulation in the order of 10^{-2} is possible [40, 41] for a standard telecommunication optical fibre. An index modulation of this magnitude is as high as the core-cladding index step.

The mechanism of photosensitization [42] using hydrogen loading techniques depends on promoting the population of germanium oxygen deficiency centres (GODCs) within the fibre core glass matrix. After hydrogen loading, the optical fibres show increased attenuation in the water absorption bands, indicating the formation of OH absorption species. It was suggested [43, 44] that the GODC and OH species are formed from thermal reaction between hydrogen and the germanosilicate fibre core. These GODCs bleached by UV irradiation results in a change of RI at the point of irradiation [40].

One important parameter for photosensitization of optical fibres through hydrogenation is the concentration of hydrogen in the optical fibre core, which is dependent on pressure, temperature and duration of the process. The concentration of hydrogen (C) in the optical fibre [30] can be calculated from the diffusion equation with diffusion coefficient of hydrogen (D) as follows:

$$C(\rho,t) = 2C_0 \sum_{n=1}^{n=\infty} \frac{J_0(\mu_n \rho)}{J_1^2(\mu_n)} e^{(D(\frac{\mu_n}{b})^2 t) \int_0^1 \varphi(\rho)\rho J_0(\mu_n \rho) d\rho} \quad (12)$$

$$D = 2.83 \times 10^{-4} e^{\frac{-40.19kJ/mol}{RT}} \quad (13)$$

where $C(\rho,t)$ is the normalized radial position (ρ) and time (t) dependent concentration of hydrogen, C_0 is the initial concentration of hydrogen, b is the fibre radius, $\varphi(\rho) = 1$ for hydrogen diffusion into the fibre, μ_n are the nth zeroes of the Bessel function J_0 , D is the diffusion coefficient of hydrogen, R =8.311J/(K-mol) and T is temperature in Kelvin.

Despite the premise of a simple photosensitization technique for optical fibres, hydrogenation do bring about limitations such as the occurrence of water (-OH) absorption in hydrogenated optical fibres at 1320nm and increased attenuation of the fibre. However, for most applications of photosensitive optical fibres, only a small segment of such fibres will be required in the optical system. Hence, the increase in attenuation will usually not warrant significant concern.

2.2.2 Fibre Bragg Grating

Fibre Bragg gratings (FBG) are optical fibre devices fabricated by periodically modulating the RI of an optical fibre core, usually in sub micrometre pitch [45]. The RI perturbance results in reflection of light within a narrow wavelength band of light called the Bragg wavelength.

2.2.2.1 Fundamentals of Fibre Bragg Grating

Reflection of a FBG is a band of light (λ_{Bragg}) which satisfies the Bragg condition.

$$\lambda_{Bragg} = 2n_{eff}\Lambda \quad (14)$$

where n_{eff} is the effective RI of host fibre and Λ is the pitch of RI modulation or grating fringes.

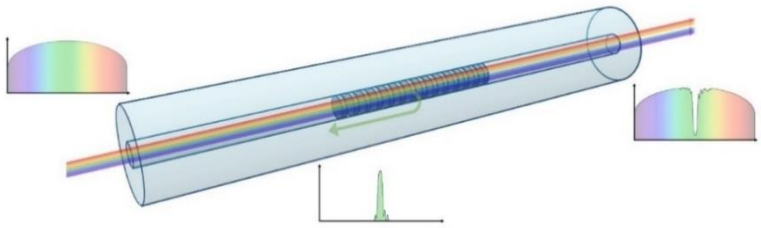

Figure 5: Schematic diagram of a uniform fibre Bragg grating

One of the design parameters as presented in equation (14), is the grating pitch in a specific host fibre. Light of matching phase as the grating pitch reflects at each fringe through Fresnel reflection (r) due to the RI difference at the fringe boundaries.

$$\mathrm{r} = \left(\frac{n - (n + \delta n)}{n + (n + \delta n)}\right)^2 \tag{15}$$

All the Fresnel reflected light throughout the length of the FBG are in phase due to the specific grating pitch and therefore constructively contributing to the overall reflection as in Figure 6.

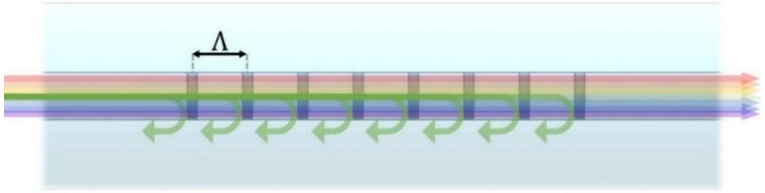

Figure 6: Distributed Fresnel reflection at index fringe boundaries along a length of fibre Bragg grating.

The peak reflectivity (R_{peak}) of an FBG as derived from coupled-mode theory [30] is as follows,

$$\mathrm{R} = \tanh^2(\kappa L_{gr}) \tag{16}$$

$$\kappa(z) = \frac{\pi \cdot (\eta \cdot \delta n(z))}{\lambda_{Bragg}} = \frac{\pi \cdot \delta n_{eff}(z)}{\lambda_{Bragg}} \tag{17}$$

$$\delta = 2\pi \cdot n_{eff} \cdot \left(\frac{1}{\lambda} - \frac{1}{\lambda_{Bragg}}\right) = \beta - \frac{\pi}{\Lambda} \tag{18}$$

where κ is coupling coefficient of the grating, δ is detuning and L_{gr} is the effective length of the grating.

Other parameters of interest for a FBG is the bandwidth of the reflected light. Bandwidth of the FBG reflection of a specific wavelength is a function of the grating length (L_{gr}), effective RI (n_{eff}) of the optical fibre and coupling coefficient (κ).

$$\Delta\lambda = \frac{{\lambda_{Bragg}}^2}{\pi \cdot n_{eff}} \cdot \sqrt{\kappa^2 + \left(\frac{\pi}{L_{gr}}\right)^2} \tag{19}$$

From (19), it is obvious that a longer grating length can result in narrower spectral response of a Bragg grating. An FBG design can thus be generally defined by its Bragg wavelength (λ_{Bragg}), reflectivity (R) and bandwidth ($\Delta\lambda$).

2.2.2.2 Fibre Bragg Grating Types

On top of the usual uniform Bragg grating structure, there exist a range of special Bragg gratings designed for different applications. The common grating types, apart from a uniform Bragg grating, includes tilted, chirped and superstructure Bragg gratings.

Tilted Fibre Bragg Grating

Often used in sensing applications, the tilted FBG (TFBG) encourages mode coupling between core and cladding modes, including radiation modes of an optical fibre.

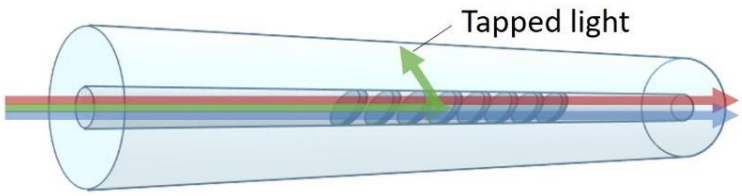

Figure 7: Schematic diagram of tilted fibre Bragg grating.

The RI modulation planes of a TFBG is at an angle to the light guiding axis of the optical fibre as shown in Figure 7. This angle results in coupling of core guided light into the cladding as loosely guided modes propagating in the optical fibre cladding.

As the cladding propagating modes can interface with the optical fibre's immediate environment, the TFBG's transmission spectrum is altered by the optical fibre's ambient environment RI. Hence, a TFBG is by itself, with sufficient tilt angle, an evanescent-field RI sensor [46].

The TFBG transmission spectrum is characterised by its core, ghost and cladding modes. Core mode of the TFBG is the longest wavelength reflected, which is also the fundamental mode of light propagating along and tightly confined in the fibre core with no interaction with the environment. Ghost modes are strongly guided near the core-cladding interface with little interaction with the environment, and the resonances of these ghost modes occur spectrally near the core mode. Cladding modes are guided by the environment-cladding boundary and hence, is inherently sensitive to the RI of the ambient environment [47].

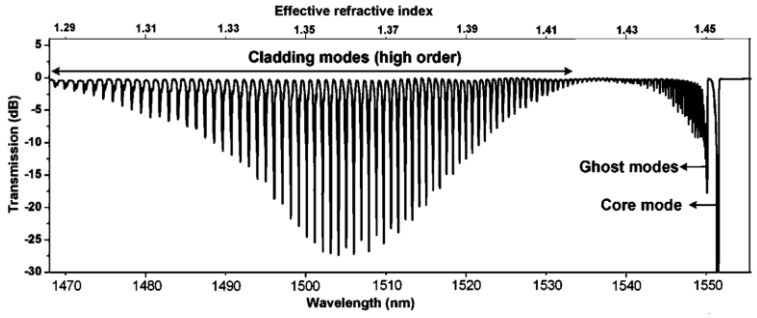

Figure 8: Typical transmission spectrum of a tilted fibre Bragg grating. Figure adapted from Optics & Laser Tecnology, Vol. 78, T. Guo et al., Tilted fiber grating mechanical and biochemical sensors, Pages 19-33., under Creative Commons Attribution-NonCommercial-No Derivatives License (CC BY NC ND).

Environmental RI can be inferred from a few spectral evolutions of the TFBG transmission spectrum. Two main methods are, measurement from cladding mode resonance envelope [48], and observation of individual cladding mode [49].

The first method takes into consideration the lossy nature of cladding modes. As the ambient RI increases, the difference between the ambient RI and cladding RI decreases. Hence, critical angle for total internal reflection become smaller and more cladding mode leaks into the ambient environment. Therefore, the cladding modes becomes more lossy. By measuring the area of the cladding mode spectrum envelope, the ambient environmental RI can be inferred.

Individual cladding mode response can also be monitored for RI measurement. As the ambient RI increases, each cladding mode approaches their cut-off condition at different levels of ambient RI. As each mode nears its cut-off condition, the mode extends further into the ambient environment and the wavelength of their resonance shifts increasingly with further

increase in ambient RI. As each cladding mode has different cut-off condition, the range of RI measurement from this method is extended.

Chirped Fibre Bragg Grating

Chirped fibre Bragg gratings (CFBG) are fibre gratings that reflect a board wavelength band of light with a non-uniform index modulation along the grating length. The distribution of grating pitch can be linearly increasing[50], discretely incremented, quadratic [51], or even random.

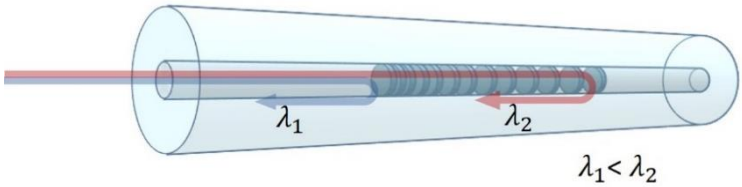

Figure 9: Schematic diagram of a chirped fibre Bragg grating

Figure 9 shows the schematics of a common CFBG with continuous linearly increasing grating pitch. Light of different wavelength satisfies the Bragg equation (Equation (14)) at different physical points of the CFBG. Light of short and long wavelength reflects at regions of the grating where the grating pitch is shorter and longer respectively according to the following relationship:

$$\lambda_{Bragg}(z) = 2n_{eff}(z)[\Lambda_0 + \Lambda_1 z] \quad (20)$$

where Λ_0 is the shortest period and $\Lambda_1$is the positive rate of change of pitch with position z.

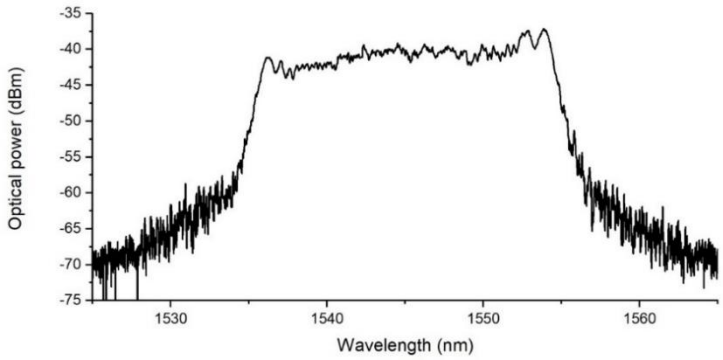

Figure 10: Reflection spectrum of chirped fibre Bragg grating.

Due to the band reflection characteristics of the CFBG where different wavelength of light reflects at different physical point of the grating, light of different wavelength propagates

varying distance before being back coupled. This property of the CFBG enables itself to be designed to either disperse of compress wavelength band of light [52] with important application in telecommunications. Over the years, CFBGs has found many other applications including optical fibre sensing as demonstrated in chapter 5.

Superstructure Fibre Bragg Grating

The superstructure fibre Bragg grating (SSFBG) is a complex grating structure with both long and short period index modulations [53]. It can be approximated with multiple short FBG segments places closed to each other, with gaps usually in the length of ~10^2 micrometres. The close interaction of each short FBG segment within the super structure results in the SSFBG's reflection characteristics.

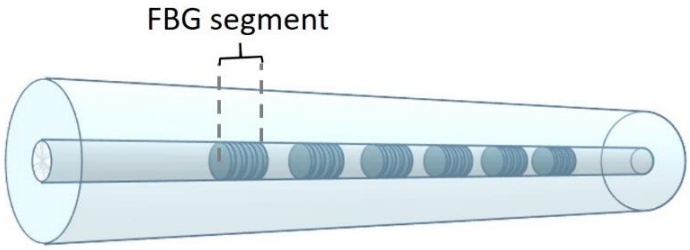

Figure 11: Schematic diagram of a superstructure fibre Bragg grating.

The reflection spectrum of the SSFBG is of infinite reflection peaks centred around the main Bragg wavelength of the FBG segments. Spectral distribution of reflected light is according to individual spatial Fourier component of the RI perturbation.

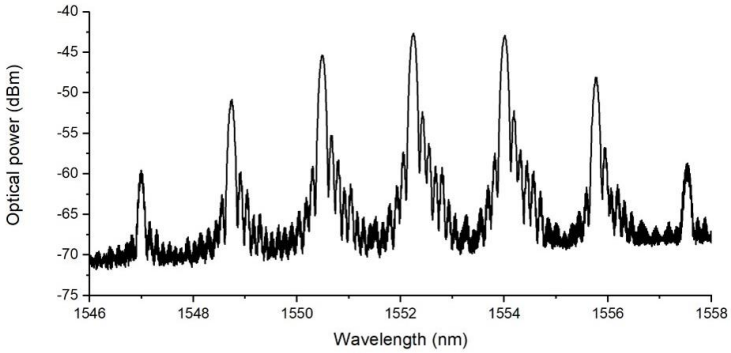

Figure 12: Reflection spectrum of a superstructure fibre Bragg grating.

This unique reflection characterises had found applications such as an inline optical fibre filter in telecommunication and multiwavelength fibre lasers. In this thesis, we discuss an application of this type of FBG in RI sensing.

2.2.2.3 Fabrication of Fibre Bragg Grating

The fabrication of FBGs involves techniques that periodically modifies the RI of the fibre core. The period of the modified RI is in the sub micrometre range and hence requires highly precise procedures. Modulation of RI is traditionally through UV irradiation of photosensitive optical fibres, although there had been significant developments in femtosecond laser inscription techniques [54]. With tightly focused ultra-short pulse lasers of high intensity, glass absorption can be achieved at the point of exposure even in non-photosensitive glass fibre cores [55].

Four techniques of grating inscription suitable for both UV laser and femtosecond laser techniques are described in the following sections. Each method presents its unique advantages and limitations.

Interferometer Technique

Interferometric or the holographic technique is the earliest developed method for grating inscription [45]. It involves splitting a UV laser beam into two paths and interfering the beams at an angle to form an interference pattern with a standard holographic set up. As a photosensitive fibre is exposed within the UV interference region, the core RI of the optical fibre is modulated with the characteristics of the interference pattern.

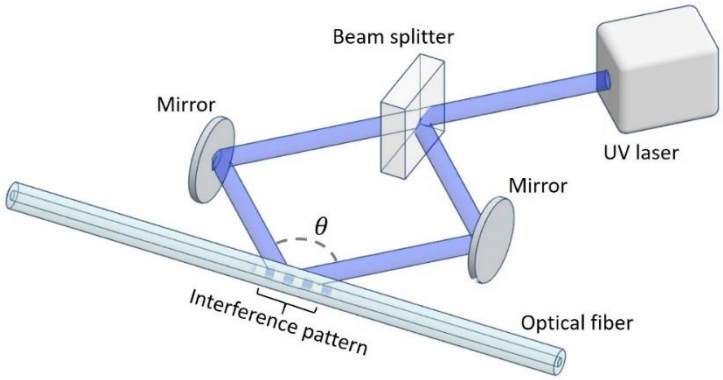

Figure 13: Holographic fibre Bragg grating method.

This method of inscription can be adjusted within physical constrains of the interferometer setup to achieve Bragg wavelength (λ_{Bragg}) design by the means of varying the two-beam path interfering angle, θ.

$$\lambda_{Bragg} = \frac{n_{eff}\lambda_{UV}}{n_{uv}\sin\left(\frac{\theta}{2}\right)} \tag{21}$$

where n_{eff} is the fundamental mode effective index of the optical fibre, λ_{UV} is the wavelength of UV irradiation used in the inscription system and n_{UV} is the RI of silica for the UV light. As θ can, in theory, be varied from 0° to 180° by adjusting the beam paths using the UV mirrors, as in Figure 13, λ_{Bragg} can be theoretically adjusted to be close to the wavelength of UV irradiation source at 180°, and upwards to infinity at 0°.

Despite the freedom to design Bragg wavelength of a wide practical range, this method for grating inscription is not widely used today for issues mainly due to the difficulty of maintaining a stable interference pattern throughout the time required for grating formation. The set up's performance is susceptible to minor disturbances arising from vibration, temperature drift of optical components, and even air turbulences affecting the beam paths.

Phase-mask Technique

The phase-mask inscription technique is arguably the most popular method for FBG inscription. This method is robust and can achieve good repeatability. The phase mask is essentially a silica plate with a relief grating etched on one side. UV beam that is incident

squarely onto the silica plate perpendicular to the grating plane is diffracted into many orders (m= 0, ±1 ….). The relief grating is designed to diffract majority of the optical power of incident light beam equally into the two first order diffraction beams (m=±1). The two first order diffraction beams then interferes forming an interference pattern which determines the pitch of a grating formed when a length of optical fibre is exposed within the interference region. Unlike the holographic method, Bragg wavelength of FBGs inscribed through a phase mask is predetermined by the period (Λ_{pm}) of the mask's grating with no tunability.

$$\Lambda_{pm} = \frac{m\lambda_{uv}}{\left(\sin\frac{\theta_m}{2} - \sin\theta_i\right)} \tag{22}$$

where m=1 for first order grating, λ_{UV} is the wavelength of UV irradiation used in the inscription system, $\frac{\theta_m}{2}$ is the angle of diffraction, and θ_i is angle of incident of UV light on the phase mask plane.

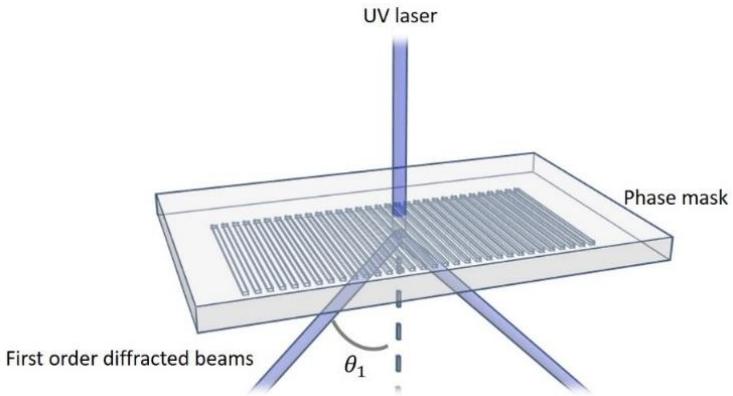

Figure 14: Schematic diagram of a phase-mask

When the UV beam is incident perpendicular to the phase mask, $\sin\theta_i = 0$, and the beam is diffracted only to the zeroth and first orders, with the first order diffraction having significantly higher power as compared to zeroth order which then, can be ignored. Equation (22) then simplifies to,

$$\Lambda_{pm} = \frac{\lambda_{uv}}{\sin\frac{\theta_1}{2}} \tag{23}$$

The ±1 order diffraction of diffraction angle of $\frac{\theta_1}{2}$ then interferes forming an interference pattern of period Λ_{FBG}.

$$\Lambda_{FBG} = \frac{\lambda_{uv}}{2\sin\left(\frac{\theta_1}{2}\right)} = \frac{1}{2}\left(\frac{\lambda_{uv}}{\sin\frac{\theta_1}{2}}\right) = \frac{1}{2}\Lambda_{pm} \quad (24)$$

Therefore, pitch of a FBG inscribed with a phase-mask can be determined as half the pitch of the phase-mask's relief grating.

The inscribing process using the phase mask method can vary slightly depending on factors such as the laser used, and length of grating being inscribed. Nevertheless, the objective is to expose the optical fibre with UV light after the phase mask. Common UV lasers such as the frequency doubled Argon ion laser, MOPA solid state lasers and excimer lasers.

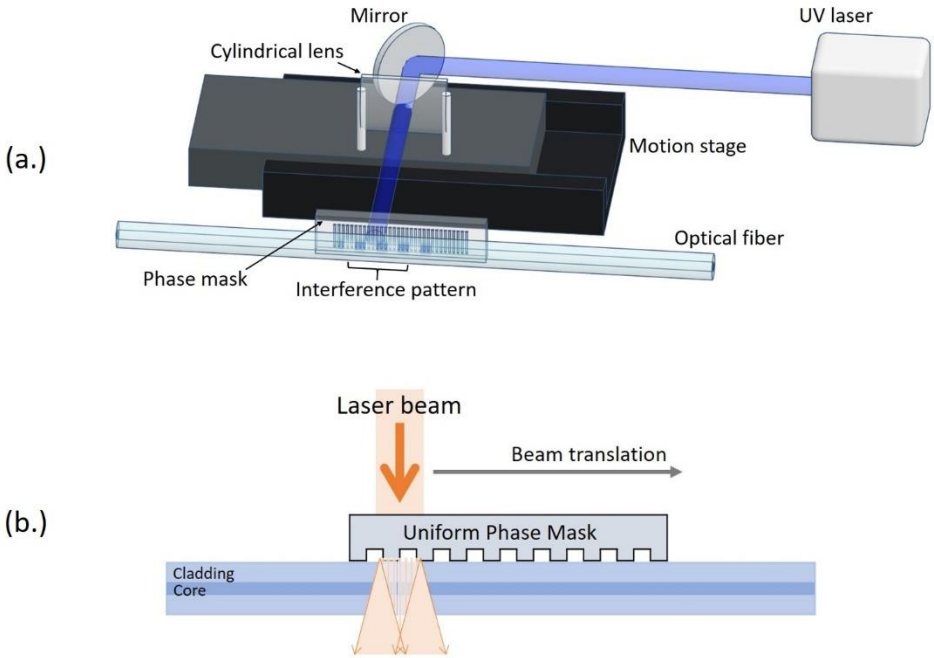

Figure 15: Typical scanning phase mask set up

In order to inscribe a longer grating that exceed the laser beam width, a motion stage is used to scan the laser beam across the desired grating length (Figure 15b). In such cases, a cylindrical lens is often used to focus the beam so that optical power from the laser can be concentrated on the fibre core for effective inscription. As the beam scans across the optical fibre though the phase mask, an FBG is being inscribed. The speed of translation of the motion stage therefore determines amount of optical power the optical fibre is exposed to at every point, affecting the strength of grating inscribed.

Point-by-point Technique

The point-by-point inscription technique for FBGs is the most direct method for grating fabrication. This method exploits the small diffraction-limited spot size of UV lasers to induced precise periodic index change along a length of the fibre, one fringe at a time, with a tightly focused UV laser beam. Although this method can, in theory, fabricate infinitely long gratings, it is limited by practical control issues. To translate either the optical fibre or the laser across a length with such high precision, elaborate control systems, including interferometric positioning lasers, must be implemented.

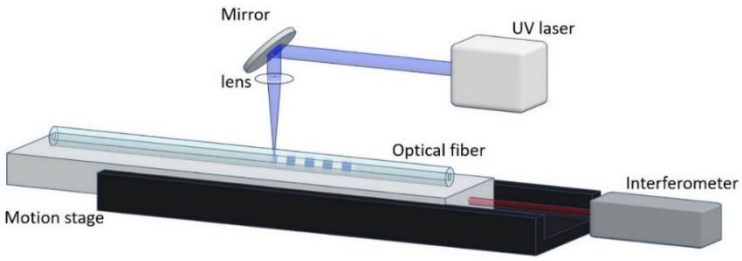

Figure 16: Point by point fibre Bragg grating system

Due to the impracticality of achieving such high precision, such a setup is better suited for inscription of long period gratings. However, some system designs have mitigated these problems by combination of phase mask method with the system, stitching multiple short gratings inscribed through the phase mask.

On Tower Inscription Technique

The fabrication of draw tower gratings received increased attention recently due to the premise of long FBG array for sensing, fabricated directly from the fibre tower [56-58]. These methods use high energy pulses either from a UV laser or a femtosecond laser in a holographic configuration as discussed earlier. The optical fibre is exposed to these pulsed interference as it is being drawn to shape on the fibre drawing tower.

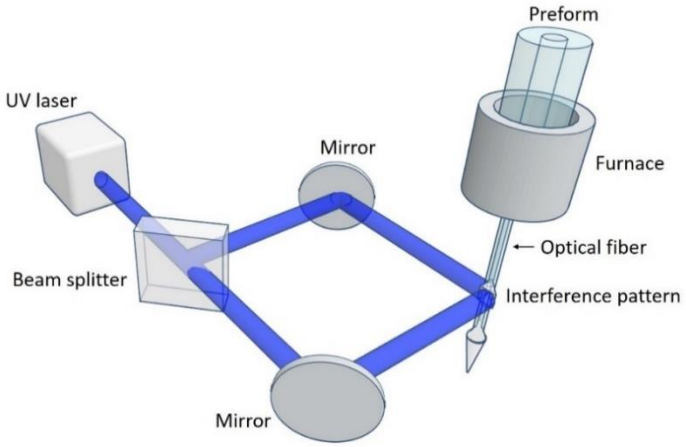

Figure 17: Draw tower grating technique

This method is essentially an adaptation of holographic technique on to a fibre drawing tower. Such systems have the potential to fabricate a continuous chain of FBGs with varying Bragg wavelengths simply by varying the angle between interfering beam paths. However, like the control system issues presented in point-by-point inscription, high quality longer length FBGs can be difficult to fabricate by this method.

2.2.3 Long Period Fibre Grating

Alike FBGs, long period fibre gratings (LPFG) are also fibre devices with periodic RI modulations in the core of an optical fibre. However, the pitch of LPFGs are much longer than that of FBGs, often in the few sub millimetres distance. First proposed as a fibre band-reject filter [59], the LPFG couples core guided modes into forward propagating cladding modes[60].

2.2.3.1 Fundamentals of Long Period Fibre Grating

As the core mode in a LPFG fibre is only coupled in the forward direction, LPFGs can only be observed in the transmission spectrum of the fibre.

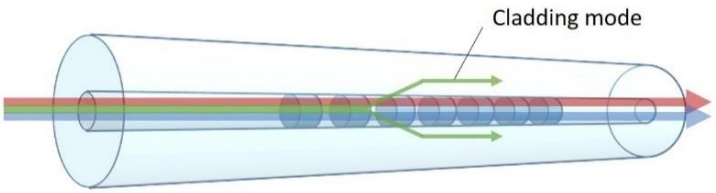

Figure 18: Schematic diagram of a long period fibre grating.

The wavelengths of the core mode which are coupled to discrete i^{th} cladding mode (resonance wavelength: λ_{LPFG}^{i}) can be determined as:

$$\lambda_{LPFG}^{i} = \Lambda_{LPFG}\left(n_{eff_{co}} - n_{eff_{cl}}^{i}\right) \quad (25)$$

where Λ_{LPFG} is the pitch of grating, $n_{eff_{co}}$ is the effective index of the core guided modes and $n_{eff_{cl}}^{i}$ is the effective index for the i[th] cladding mode. Henceforth, all wavelength of core guided modes satisfying the conditions spelt out in Equation (25) will be coupled into the cladding by the grating.

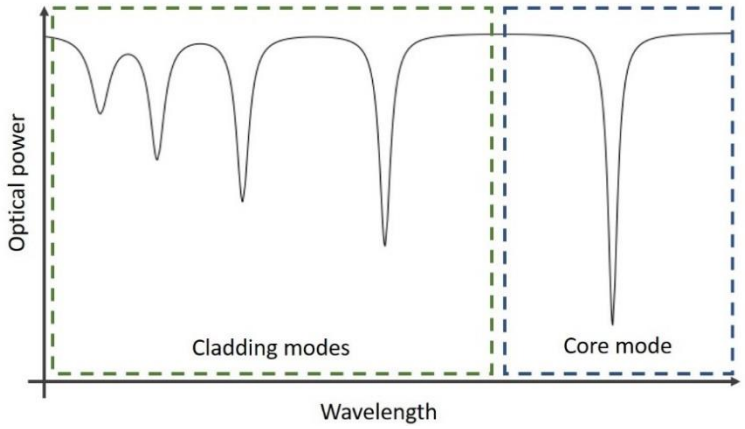

Figure 19: Typical spectral response of a long period fibre grating.

Equation (31) also shows that the LPFG response is dependent on the effective index of the core mode and all the respective cladding modes.

LPFG's spectral response is inherently sensitive to ambient RI as the loss characteristics and effective RIs of these higher order cladding modes is a strong function of ambient RI [61]. A change in ambient RI will alter $n_{eff_{cl}}^{i}$ resulting in measurable resonance wavelength (λ_{LPFG}^{i}) shifts. The sensitivity of LPFG spectral of i^{th} mode is given by:

$$\frac{d\lambda^{i}}{dn_{env}} = \left(\frac{d\lambda^{i}}{dn_{eff_{cl}}^{i}}\right)\left(\frac{dn_{eff_{cl}}^{i}}{dn_{env}}\right) \quad (26)$$

where n_{env} is the effective RI of the immediate ambient environment of the optical fibre. This characteristic of the LPFG spectral response have been widely exploited for RI sensing, to be discussed in section 2.3.4.

2.2.3.2 Fabrication of Long Period Grating

Fabrication of LPFGs is like that of FBGs but is much simpler as the grating period is large. Both the mask or point by point UV inscription methods previously described, can be adopted with small modifications. As the modulation is of sub millimetre period, precision requirement is not as stringent as that of FBG inscription. An amplitude mask instead of a phase mask is used.

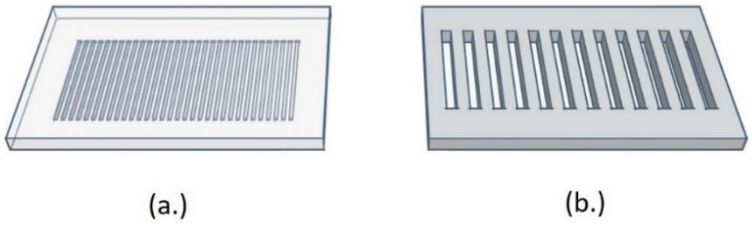

Figure 20: Schematics of (a.) a silica plate phase mask and (b.) a metal plate amplitude mask.

Essentially, the amplitude mask is an array of linearly and periodically distributed slits in an opaque plate that only allows light through the slits resulting in periodic irradiation behind the amplitude mask. Hence, RI modulation in the fibre core is localised at positions of the mask's slits.

Alternatively, the point-by-point inscription method can be used for LPFGs. With the lower requirement for precision, this method can yield longer length of LPFGs. However, in consideration of cost effectiveness and repeatability, the amplitude mask method is widely adopted.

2.3 Optical Fibre Grating Refractometers

Fibre gratings have been incorporated in optical fibre grating based refractometers in many ways. The gratings within these different systems also respond to RI changes of sample substance or the environment differently. This section reviews four different types of fibre grating based refractometer schemes.

2.3.1 Cladding Thinned Fibre Bragg Grating Refractometer

FBGs are usually written in the Ge-doped core of an optical fibre. The core guides the fundamental mode of light of which power is mostly confined within the fibre core, extending only slightly into the cladding [62, 63]. The fundamental mode does not interact with the ambient environment unlike the higher order cladding modes. Hence, the fibre Bragg grating in the core of the optical fibre is not sensitive to change in ambient RI.

To sensitise the FBG to ambient RI, etching [63-68] and tapering[69-71] of the optical fibres are methods used to extend the fundamental guided mode in an FBG into the ambient environment. Both etching and tapering are cladding reducing techniques that forces the core guided modes to be partially extended out of the fibre into the surrounding medium.

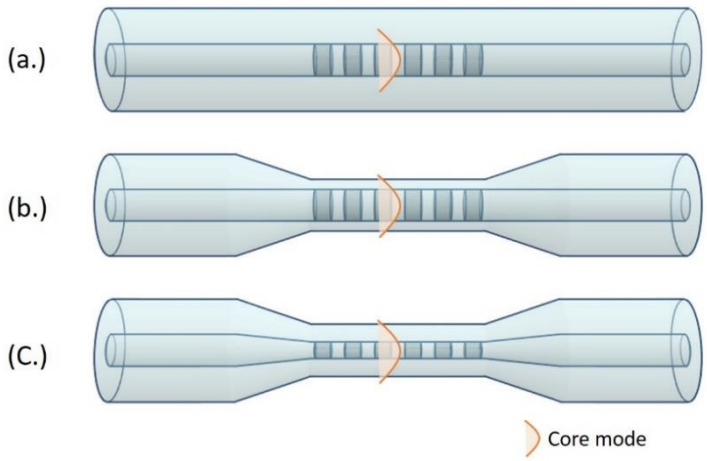

Figure 21: Schematic diagrams of (a.) unmodified fibre Bragg grating, (b.) etched fibre Bragg grating and (b.) tapered fibre Bragg grating.

By doing so, as can be seen in Figure 21, the modal effective RI of the core mode becomes a function of the ambient RI, causing a Bragg wavelength shift, along with a change in ambient RI, according to equation (14).

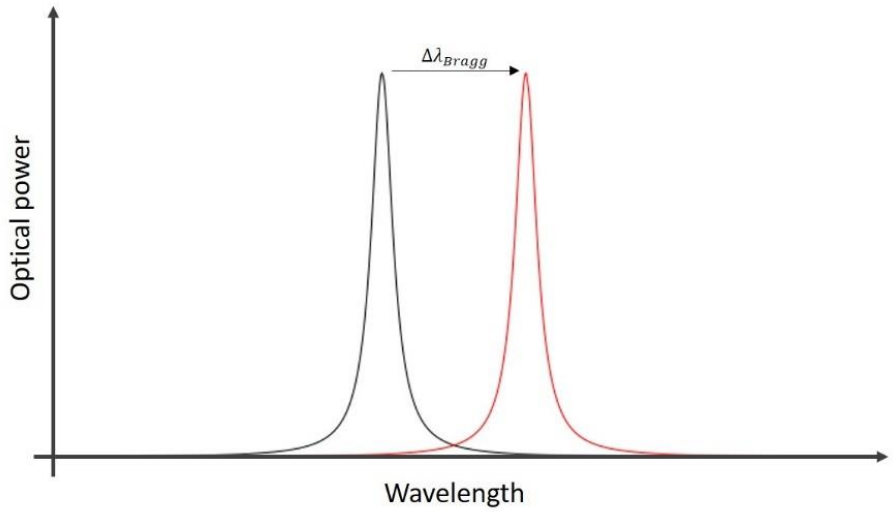

Figure 22: Typical spectral response of etched/tapered fibre Bragg grating refractometers

RI changes of the ambient environment can then be characterised by the amount and direction of shift of the Bragg wavelength in either the transmission or reflection spectrum of the FBG.

These sensor schemes are simple in principle and hence is widely explored. However, fabrication of the sensors requires complicated processing of the optical fibre. These sensors are also cross sensitive to strain and temperature fluctuation in the environment, resulting in low accuracy. Thinning of the optical fibre also decreases the structural integrity of the fibre, rendering it unfeasible in harsher environments.

2.3.2 Polarization Assisted fibre Bragg Grating Refractometer

Alike the etched or tapered FBG refractometers discussed in the earlier section, polarization assisted FBG refractometers also relies on cladding thinning as a sensitization technique. However, instead of thinning the Bragg grating fibre evenly towards the core, asymmetrically thinning of cladding biased to one polarisation axis is carried out. These modifications of the optical fibre expose the orthogonal polarisation modes propagating in the fibre to the ambient environment differently. This difference then results in ambient RI influenced birefringence in the fibre. Such a birefringence can be observed from the Bragg spectrum of an FBG inscribed at the birefringent region.

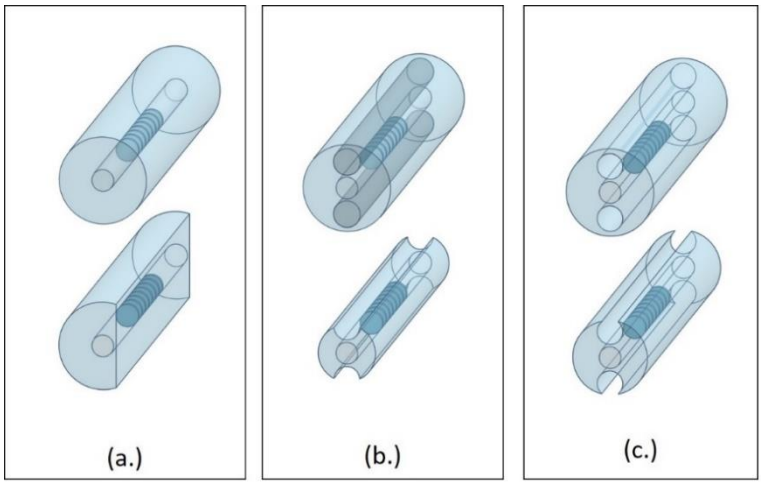

Figure 23: Schematic diagram of (a.) etched D-shape, (b.) etched panda H-shaped and (c.) etched side hole H-shape fibres refractometers

A series of designs of such sensors were reported (Figure 23) with etched fibres of different shapes to achieve birefringence. Reported schemes include the use of etched D-shape [72], panda [73], side hole [74] and rectangular fibres [75]. An unmodified side hole fibre sensor scheme [76] was also implemented by pumping test substances directly into the side holes. These side holes of the special fibre are close to the fibre core, and hence interacts with the core guided modes partially.

Each of these sensors exhibits Bragg grating polarisation split spectral response. One polarisation mode is purposefully exposed to the ambient environment. Therefore, the corresponding Bragg wavelength shifts more than the orthogonal mode when ambient environment changes.

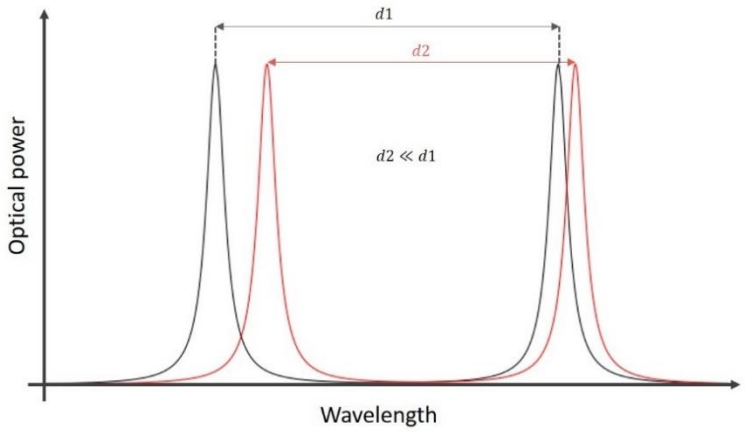

Figure 24: Typical spectral response of birefringent fibre Bragg grating refractometers.

The RI measurement from these sensors are inferred by the change of polarisation spectral differences (i.e. spectral separation between peaks of Bragg reflections). The common spectral shift of the peaks of both polarisations can be used to measure temperature change in the ambient environment.

As the cladding of the sensor fibres were partly removed, structural integrity of the sensor is affected. However, this type of FBG refractometer, effectively decoupled RI sensitivity from temperature and strain sensitivity. This not only improves accuracy, but also enables simultaneous measurement of temperature along with RI.

2.3.3 Fibre Bragg Grating Fibre End Ratio-meter

In the previous two sections, two inline FBG refractometers were discussed. While inline sensors have the advantage of easy integration into a sensor array, there are some benefits of a fibre end design as well. Fibre end optical sensors are usually implemented as a probe for rapid measurement. Having only one end of the optical fibre connected for interrogation can serve cases where there is space constraints or portability is required.

The FBG fibre end ratio-meter is one of such fibre end refractometer design [77, 78] which is an FBG enhanced version of traditional ratiometers [79]. A ratiometer makes use a reference arm interfaced with a known RI and compares with another fibre arm exposed to the substance or environment under test. This method is prone to error due to light source fluctuations and difficulty in maintaining good reference condition as the two arms are separate optical fibres. The FBG-fibre end ratiometer only consist of one single strain of optical fibre and hence is more robust.

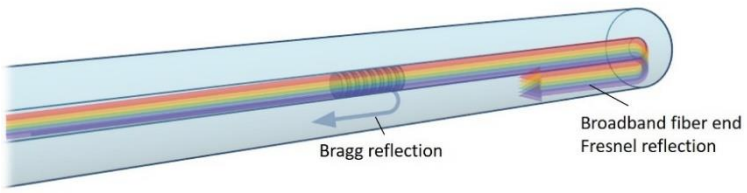

Figure 25:Schematics of a fibre Bragg grating-Fibre end Fresnel reflection ratiometer.

Bragg reflection power (R_{Bragg}) will remain a fixed ratio of total optical power delivered by the illuminating light source. Hence, the peak reflection of the Bragg grating serves as a good reference power in a ratio meter. The cleaved fibre end results in Fresnel reflection due to RI difference between the fibre and the interfacing environment.

$$R_{Fresnel} \approx \frac{\left(n_{eff} - n_{ambient}\right)^2}{\left(n_{eff} + n_{ambient}\right)^2} \tag{27}$$

where $R_{Fresnel}$ is ratio of reflection at cleaved fibre end (typically ~4% in air), n_{eff} is the effective RI of the fibre and $n_{ambient}$ is the effective RI of the interfacing ambient environment.

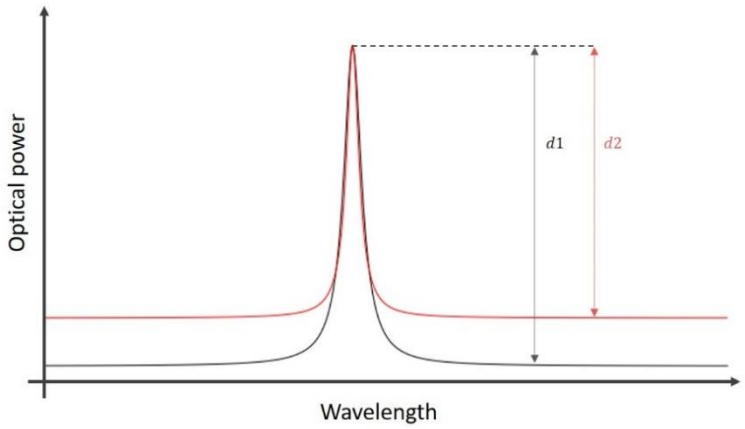

Figure 26: Typical spectral response of a fibre Bragg grating fibre end ratiometer for RI measurement.

Hence, it is obvious that as the ambient RI varies, $R_{Fresnel}$ changes accordingly while Bragg refection remain constant. The ratio between $R_{Fresnel}$ and R_{Bragg} becomes a measure of the ambient RI.

Such a ratiometer design is simple and easy to fabricate. The fibre remains unmodified and hence retains its structural strength. As the RI measurement is from power ratio between Bragg reflection and fibre end reflection, the Bragg wavelength shift can also be used to simultaneously measure temperature changes. However, the sensitivity of such design to RI is lower than the other designs discussed earlier.

2.3.4 Long Period Grating Refractometer

LPFG by itself is a sensor for RI without the need for any post processing after grating inscription. As previously discussed in section 2.2.3.1, the cladding modes of the LPFG is sensitive to ambient RI and this sensitivity is observed in the transmission spectrum of the grating. The LPFG have been widely explored [80-83] as a refractometer for decades and many sensitivity enhancing techniques [84-87] had been reported.

Such sensors are of inline configuration and array formation is possible given proper design and demodulation techniques. However, the LPFG is extremely sensitive to strain, temperature and bending, also often applied as physical sensors [88-90]. Hence the cross sensitivity of the LPFG is a major limitation on its applicability as a refractometer which many work to resolve [91], with increased complexity of design and interrogation.

2.4 Surface Functionalized Optical Fibre Refractometers for Chemical Sensing Applications

The surface functionalisation of optical fibre generally refers to the modification of the fibre surface either by modification of the surface molecules or attachment of materials to the fibre surface. The ability to functionalise the surface of a fibre expands the application of optical fibre sensing in both physical and chemical sensing applications. With this technique, a refractometer can then be transformed into targeted chemical sensors. Some common examples of the chemical sensors are discussed in the following section.

2.4.1 Examples of Surface Functionalised Optical Fibre Chemical Sensors

Chemical sensors based on functionalised fibre refractometers are of research interest for the past decade and much progress have been made collectively by the research community. These sensors can be broadly classified into gas, ion and organic sensors.

Common gas sensor applications include detection of Hydrogen with deposition of thin palladium layers [92-94], Oxygen with sol-gel coating [95, 96] and hydrocarbon gas with

refractometers coated with carbon nanotube [97] or porous silica layers[98]. Aqueous Ion detectors, such as applications in metal ions detection [99, 100] and pH measurement [101, 102] were also widely studied. Finally, organic compound sensor such as detection of nerve agents using conducting polymer polypyrrole coating[103] and Ammonia sensing with a polyaniline thin films [104] were reported.

The limitation of chemical sensing with surface functionalised fibre sensors is that it is dependent on the availability of reagent that will produce a measurable RI change or induce physical change to the host fibre, and technique of coating the fibre sensor with the chosen material.

2.4.2 Surface Functionalisation Techniques

We briefly discuss some of the most common methods used to functionalise the surface of an optical fibre. These techniques are based on different principles and hence its applications, depending on the type of fibre and the coating material.

2.4.2.1 Dip Coating

Dip coating is usually a three-step process. These steps are normally referred to as Immersion, Deposition and Curing. With precise control in each of the three steps, it is possible to deposit a mono layer of material onto the fibre surface.

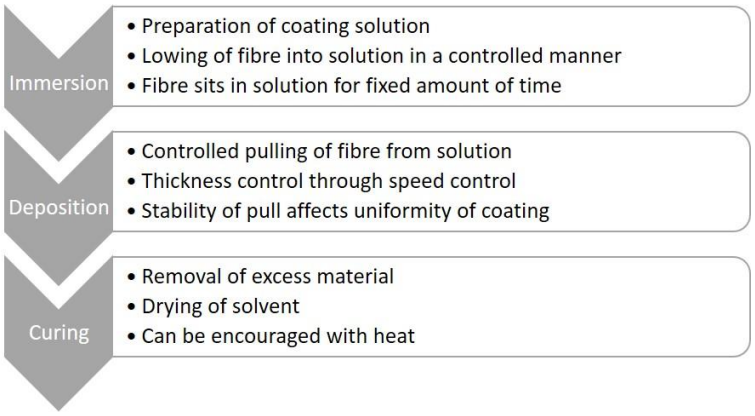

Figure 27: Procedure of dip coating

For the immersion stage, the sensor fibre is first immersed into a solution of the coating material. It is often then left in the solution for a given amount of time for the material to cling onto the fibre surface. The process is completed as the fibre is pulled out of the solution at a controlled speed. The speed of removal of the fibre from the solution is determined by the desired thickness of the material to be deposited on the surface. Precision and steadiness of the mechanical movements during the process can greatly influence the quality of the coating. Lastly, curing involves the removal of excess liquid from the fibre surface and allowing the solvent used to prepare the coating solution, to evaporate. In some cases, this part of the process can be facilitated with the introduction of heat or UV irradiation.

Some examples of materials that can be deposited onto an optical fibre surface using this method include polymers such as sol-gel [105] and hydrogel [106] and nanoparticles, including nanocrystals [107] and metal oxides.

2.4.2.2 Optical Deposition

Optical deposition can be used to deposit coating at the fibre end at the fibre core. The working mechanism of optical deposition is not clear. It was suggested that the principles of optical deposition could be either or a combination of the following two theories: (1) The heating of liquid by the optical power emitted from the fibre end, which causes a convection of the fluid, pulling coating materials toward the fibre core. (2) The material could be captured at the fibre end by the guided light through optical tweezing effect.

Optical deposition process can be controlled to deposit desired amount of material at the fibre end by in situ monitoring of reflected optical power by the fibre end during the process illustrated in Figure 28. The procedure includes connecting the fibre to a power meter and light source through a circulator. The fibre end is immersed in the coating solution and light is delivered to the fibre end while the power of the back reflected light is being monitored.

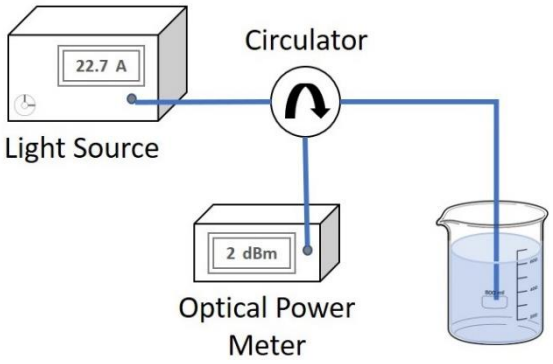

Figure 28: Optical deposition set up.

As the fibre end becomes coated with coating material, the power reflected is measured by the optical power meter. In this way, it is possible to optimise each coating process to achieve thickness of coating to a high degree of control. Optical deposition have recently become the most popular coating method for fibre ends, especially for graphene applications [108].

2.4.2.3 Drop Casting

Drop casting is a simplest method of coating. The coating material is first mixed with a suitable solvent with sonification. The optical fibre surface is then cleaned, and the solution is dropped onto the surface. The now coated optical fibre is then left to dry either naturally or with assistance of heat. This method is simple but may not be ideal for a wide range of applications due to the difficulties in control, and hence desired thickness of coating is hard to achieve.

3 High Germanium Core Content Optical Fibres for Grating Applications

3.1 Introduction

Germanosilicate optical fibres are known to be photosensitive to UV irradiation. This phenomenon is a contribution from multiple competing physical processes, dominant at different stages of irradiation. Standard germanosilicate optical fibres (i.e. SMF28) doped with low germanium concentration typically display two distinctive photosensitivity phenomena, known as Type I and Type II [109]. Type I and Type II photosensitivity result in refractive index (RI) increase and decrease of the doped fibre core respectively arising from different mechanisms. The absorption band in the UV region for such a fibre is centred at around 240nm. Hence, a 244nm Argon ion gas laser is often used for glass processing and fibre Bragg grating inscription [110]. However, it has become increasingly popular amongst the research community and commercial grating fabricators to adopt 266 nm frequency quadrupled solid-state UV laser due to its simplicity in system design and low requirement for laser peripherals such as cooling system and power delivery. The maturity of solid state 266 nm UV lasers in recent years [111, 112] has catalysed the adoption process. Despite significantly lower absorption at 266nm tail end of the absorption band for germanosilicate fibres, practical benefits of a 266nm solid state laser system often outweighs this disadvantage.

To design and fabricate fibre gratings of desired parameters, characterisation of the fibre, especially photosensitivity characterisation, is of utmost importance. The standard telecommunication fibre's photosensitivity characteristics to the common UV wavelengths (i.e. 198nm, 244nm and 266nm) are well known. Therefore, one can design and fabricate FBGs in a length of standard telecommunication optical fibre by choosing the appropriate level of fluence exposed on the fibre, grating pitch and grating lengths to a high level of confidence.

For further work into grating application in novel classes of photosensitive optical fibres such as the recent popularised extremely high Ge-doped germanosilicate fibres (HGF) [23, 38], investigations into the photosensitivity characteristic of these fibres are necessary. HGFs are of interest to fibre sensing due to their single mode waveguiding properties for higher IR wavelength above 2 micrometres, large NA for light of communication band, and high nonlinearity such as Raman scattering. This chapter studies the photosensitivity of a range of a HGFs with core Ge-doping concentration of 25% and higher. These fibres were acquired from three sources, including a commercial optical fibre fabricator and two research institutes.

3.2 Photosensitivity Characterisation

3.2.1 Photosensitivity Characterisation Through Fibre Bragg Grating Inscription

Many methods to characterise the photosensitivity of an optical fibre have been proposed [113-115]. A direct approach commonly used is to inscribe multiple uniform FBG of the same parameters but with different fluence into different lengths of optical fibre of the same type. From the FBG transmission spectral response, reflectivity and central wavelength can be measured. The resulting index modulation (Δn) can then be calculated using equation (28) with these measurements.

$$\Delta n = \frac{\kappa \lambda_{Bragg}}{\pi \eta} \tag{28}$$

$$\kappa = \frac{\operatorname{arctanh} \sqrt{R}}{L_{FBG}} \tag{29}$$

$$\eta = 1 - 2e^{-2 \log V^2} \tag{30}$$

where κ, λ_{Bragg}, R and L_{FBG} are the coupling constant, central wavelength, reflectivity and length of the grating. η and V are the mode overlap parameter and V number of the grating optical fibre host respectively. Hence, for every grating written with known length, fluence, measurable reflectivity and central wavelength, RI change due to the deposited UV fluence can be calculated.

An iteration of the method described above is to repeatably expose the same location on the same length of optical fibre with consistent dose of irradiation through a phase mask. The resulting Bragg grating can be measured and RI modulation calculated using the same method above between each additional dose of fluence [116]. Using a scanning phase mask method with controlled scanning speed, length and power, each scan of the phase mask over the optical fibre will result in the exposure of the fibre to approximately the same dose of fluence. Therefore, with each additional scan, the FBG grows with the addition of one dose of fluence. It is then possible to use measurements after each dose to calculate Δn and observe the evolution of RI from the UV irradiation.

3.2.2 Photosensitivity Characterisation Experiment of High Germanium-Doped Optical Fibre with 266nm Ultra-Violet Irradiation

3.2.2.1 Basic Optical Fibre Characterisation

Nine HGFs were gathered from three sources (commercial: Nufern, research institute: Optoelectronics Research Centre of University of Southampton and The Photonics Institute of Nanyang Technological University) and characterised for their photosensitivity with reference to a 266nm UV laser.

Table 1: List of high Germanium-doped optical fibres.

s/n	Fibre no.	%GeO_2	Core Diameter	n_{core}*	V number*	Fabricator
1	A0020	25	1.1	1.4784	1.400	University of Southampton
2	UHNA4	29	2.2	1.4852	3.152	NuFern (United States of America)
3	A0033	38	12.1	1.4984	19.618	Nanyang Technological University
4	A0641	39	3.5	1.5008	5.803	University of Southampton
5	A0032	42	13.9	1.5041	23.716	Nanyang Technological University
6	A0029	55	15.25	1.5227	29.869	Nanyang Technological University
7	A0025	62	17.24	1.5327	35.912	Nanyang Technological University
8	A0037	70	2.8	1.5442	6.209	Nanyang Technological University
9	A0803	100	3	1.5871	8.009	University of Southampton

* with respect to 1550nm light

Bragg gratings were inscribed and RI modulation due to irradiation calculated from grating parameters. All the fibres were measured using an index profiler (IFA-100). The fibres

were also inscribed with a Bragg grating with known grating pitch and measured to determine their effective index. It was found that most of the fibres are multimode at communication wavelength due to the large RI step between core and cladding and their core sizes. As only UHNA4, A0641 and A0037 are near single mode, these three fibres were selected for further investigation. However, A0037 exhibits low photosensitivity at small fluence doses of 50 J/cm^2 and so was also excluded from the study. The cause of this observation is not well known but is believed to be the lack of defect states, since the fibre core is now essentially Germanium based, with over 70% concentration of Germanium, resulting in the unlikelihood for Ge-O defects to form.

3.2.2.2 Experimental Procedure

Scanning phase mask method was employed to inscribe a 5mm gratings into two high germanium doped fibres (UHNA4 from Nufern and A0641 from ORC) under identical conditions. RI profiles of the fibres presented in Figure 29 were taken with the IFA-100 Fibre Index Profiler, giving insight on the RI distribution across the fibres and their fibre core sizes.

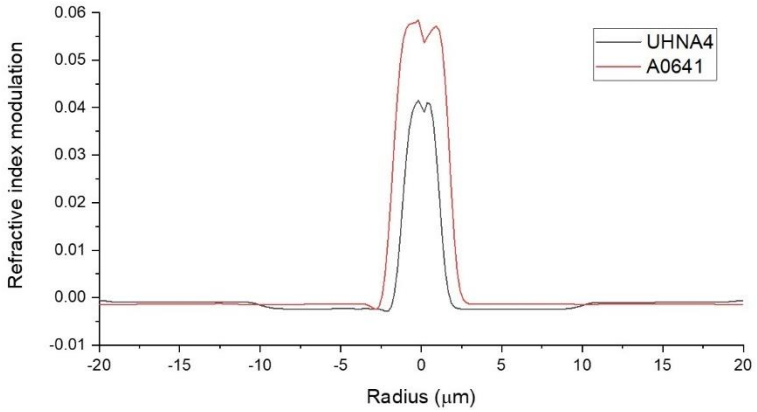

Figure 29: RI profiles of UHNA4 from Nufern and A0641 from Optoelectronics Research Centre (University of Southampton)

The UV irradiation is from a 266nm 20 Hz, 5ns pulsed laser of average power 15mW. Speed of translation and focus of beam is adjusted to expose the fibre with of 50 J/cm^2 UV optical power per scan.

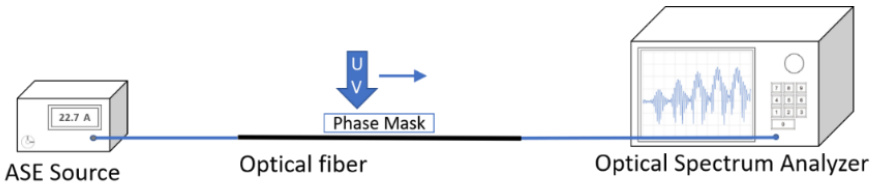

Figure 30: Experiment setup.

Both optical fibres underwent the same process with 200 UV irradiation scans amounting to a total fluence of 10 kJ/cm^2 exposed on the fibre. After each scan, the Bragg wavelength and reflectivity were immediately measured before commencing the next dose of irradiation. From the Bragg wavelength and reflectivity of the resulting FBG measured on the optical spectrum analyser, the index modulation was calculated.

3.3 Results and Discussions

Figure 31 shows the RI evolution of the fibres throughout the process. The evolution plots presented peculiar periodic features that is different from common telecommunication fibres. At small fluence, the HGFs seemingly experience competing photosensitivity mechanisms, much resembling the type I and II photosensitivities of the telecommunication fibres. However, unlike standard fibres where there is only one transition of type I to type II photosensitivity, HGFs shows multiple transition periodically with increase in fluence exposed on the fibres.

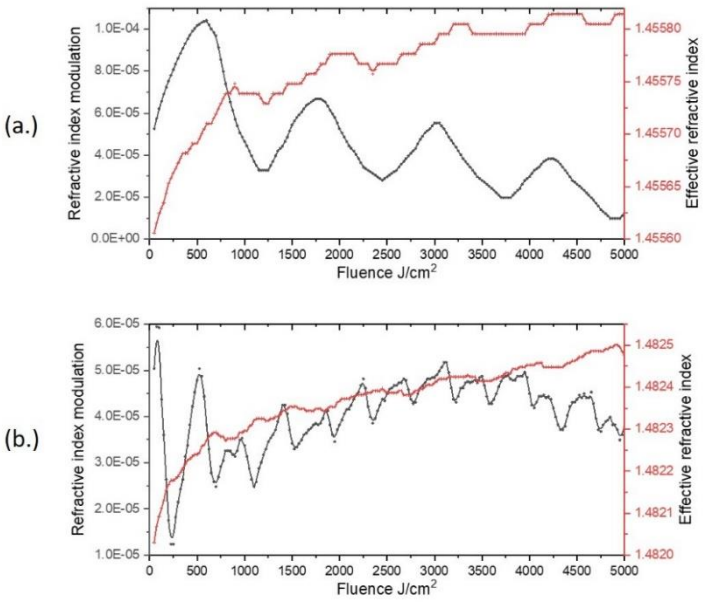

Figure 31: Refractive index modulation and effective index evolution of a.) UHNA4 and b.) A0641

There is a clear periodic positive and negative RI modulation for both fibres. When compared to the evolution of effective RI of the grating fibre, it is obvious that effective RI changes follow the periodic trend of RI modulation. This was not observed for large fluence irradiation [23] in extremely high germanium dopant level of over 90%. To eliminate the influence of any environmental factors that may cause errors in the experiment, the experiment was isolated on the optical table shielded from any potential air draft. Laser power was measured after every five scans and was found to be stable with no measurable power drift. The same experiment was repeated on different segments of the optical fibres yielding identical results.

3.4 Discussion and Conclusion

An interesting phenomenon was observed with RI evolution of silica fibres doped with a high concentration of germanium in its core. All care was taken to eliminate the possibility of external influence and measurement errors. The periodic behaviour seemingly indicates that there are competing photosensitivity mechanisms at work when the fibres were irradiated with small doses of 266nm UV irradiation. It is reasonable to postulate that this phenomenon is due to closely competing Type I (positive index change) and Type II (negative index change) photosensitivity. Type I photosensitivity is believed to be caused by optically induced densification of the glass structure, while Type II photosensitivity is believed to be due to Ge-O defects resulting in glass molecular structure dilation when irradiated with UV light. At higher concentration of GeO2 of 30-40% in core, as for the two sample fibres experimented. It is possible that type I and II photosensitivity mechanisms exhibits comparable contributions to the index change of the fibre, resulting in the observed HGF photosensitivity characteristic.

Even though the mechanisms behind this effect is not determined by this experiment. It is sufficiently conclusive that this class of fibres is not suitable for weak grating applications due to its non-linear photosensitivity from small doses of UV irradiation, until more understanding into its behaviour is gained.

4 GRATING INTERROGATION OF MACH-ZEHNDER INTERFEROMETRIC OPTICAL FIBRE CHEMICAL-SENSORS

4.1 Fibre Bragg Grating's Role in Chemical-Sensing as Interrogators

As discussed in the preceding chapters, fibre Bragg gratings (FBG) were used widely in both physical and chemical sensing applications. While serving an important purpose as the sensor itself in many reported works, FBGs have the potential to contribute in other parts of a fibre sensing system in real world applications. Optical fibre sensors in general, not limiting to grating schemes, such as fibre interferometric sensors, usually consists of two major components, namely the sensor and the interrogator. While majority of fibre grating sensor works employ the grating as the sensing element to be interrogated by bulky equipment, FBGs can also be configured to replace interrogators.

Mach-Zehnder Interferometric fibre chemical sensors have been well studied over the past decade. Many of these sensors use processed fibres such as tapered or etched fibres [117], cladding modified fibres such as D shape fibres, fibre core mismatched fibre combinations [118, 119] or special fibres and fibre structures including photonic crystal fibres [120], coreless fibres [121] and special shaped fibre structures [122] to achieve Mach–Zehnder interference (MZI) by providing two parallel light propagation paths. As each subsequent study report new applications or higher sensitivity, there is a lack of an elegant interrogation scheme applicable across the systems that do not require bulky and expensive specialized optical laboratory equipment.

In this chapter, a grating-based interrogation scheme was designed and implemented for Mach-Zehnder Interferometry based tapered fibre refractometer. This type of optical fibre sensing scheme is widely studied and reported in [123-125] and more advanced designs in [126] for gas and chemical sensing applications. By replacing the interrogating equipment with a

grating-based interrogator, cost and complexity of the overall sensing scheme can be drastically lowered through removing the reliance of expensive and bulky equipment.

4.2 Mach-Zehnder Interferometry Based Tapered Fibre Refractometer

4.2.1 Theory

A tapered fibre is a modified fibre where a part of the original fibre is thinned by a tapering process. Typically, the original fibre is pulled with a precision motion stage setup to achieve a certain reduced diameter at the tapered region as heat is applied[127]. A tapered fibre can be described by three distinct regions. In the direction of light propagation, the fibre down tapers over a down-taper length (*a*) from original diameter to designed waist diameter (*d*) with waist length of (*L*) and then gradually up tapers over an up-taper length (*b*) as depicted in Figure 32.

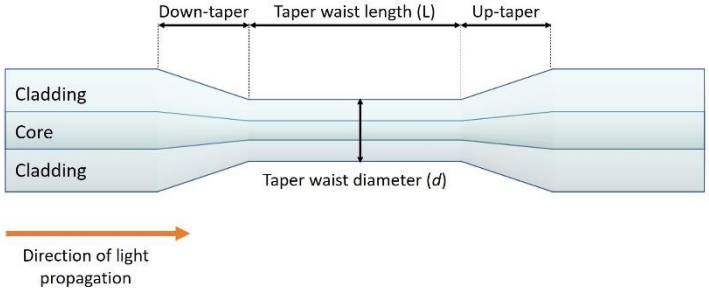

Figure 32: Schematic diagram of a typical single mode fibre taper.

As light propagates from the unmodified portion of the fibre through the down-taper region into the tapered region, higher order modes (Cladding modes) are excited and partially propagates around the surface of the fibre in the ambient environment. The number of higher order cladding modes and extend of evanescent wave is determined by wavelength of guided light, slope of taper and diameter of waist. A biconical taper profile can be designed so that mainly HE_{11} and HE_{12} modes are excited at the tapered region[125]. Design of microfiber sensors were discussed in detail elsewhere[128, 129].

Due to the differences in beam path of the cladding modes propagating through the environment, an interference pattern described by equation (31) is formed as all the modes couple back into the unmodified fibre through the up-taper region with a phase difference.

$$I = I_{core} + I_{clad}\sqrt{I_{core}I_{clad}}\cos\Delta\phi \tag{31}$$

$$\Delta\phi = \frac{2\pi}{\lambda}(\Delta n)L \tag{32}$$

where I_{core} is the intensity of core mode and I_{clad} is the intensity of cladding mode, $\Delta\phi$ is phase difference of the core and cladding modes, λ is the operating wavelength, Δn is effective refractive index (RI) difference between core and cladding modes, and L is the effective taper length. As the effective index of cladding mode is directly affected by that of ambient environmental RI, a change in ambient environmental RI will result in a shift in the MZI transmission spectrum.

4.2.2 Sensor Fabrication and Characterisation

Standard single mode fibre (sm28e) was tapered using a commercial fibre tapering machine Vytron GPX-3000. The resulted tapered fibre has an abrupt taper profile with a taper length of 10 mm and waist of 8.8 µm. As the grating enabled interrogator design requires the free spectrum range (FSR) of the resulting interference pattern to be known. The FSR was measured from the transmission spectrum and was found to be 20 nm.

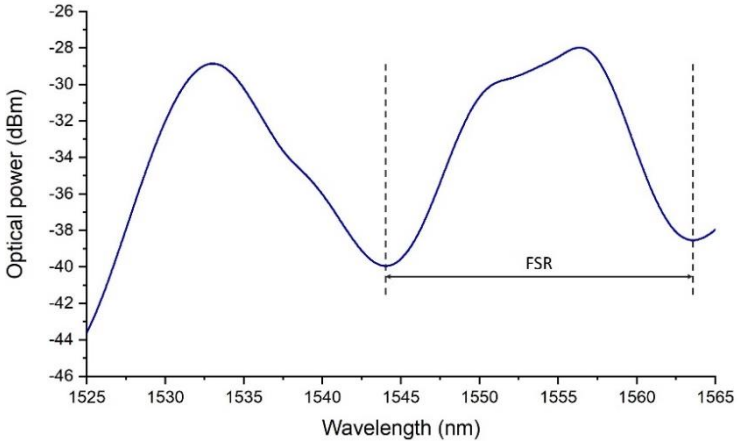

Figure 33: Transmission spectrum of tapered fibre refractometer

The tapered fibre is found to be sensitive and measurable to RI changes from 1.3398 to 1.3438, within half free spectral range wavelength shift. The same can be said of RI change of other ranges but is not the subject of this study. Hence, this work is restricted to the said range.

4.3 Grating Enabled Interrogation Circuit Design for Mach Zehnder Interferometric Refractometers

4.3.1 Duo Fibre Bragg Grating Interrogation Circuit Design

The grating enabled interrogation circuit is made up of two FBGs, two circulators, two photo detectors and a volt meter in the configuration as shown in Figure 34.

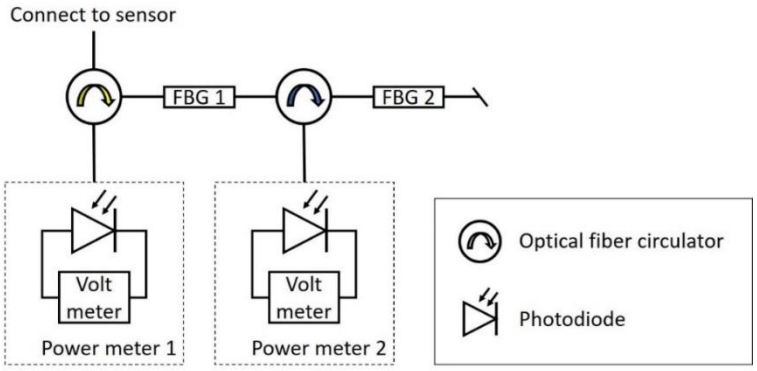

Figure 34: Schematic of two fibre Bragg grating interrogator design.

Two FBGs and two circulators were alternated and connected in series. The reflection port of each circulator is connected to a photo diode and voltmeter circuit which essentially forms the optical power meters. Each power meter will only be measuring the back reflected power from one FBG.

For example, in Figure 34, the input port of the first circulator (yellow) is connected to the sensor output and output port to FBG 1 with back reflected light of FBG 1 directed to power meter 1. Light not reflected by FBG 1 enters the input port of second circulator (blue) and output port is connected to FBG 2 with the back reflected light of FBG 2 directed to power meter 2. Operationally, the free end of FBG 2 is to be cleaved at Brewster angle or exposed to fibre effective index matching solution to remove fibre end back reflection which can interfere with results.

The FBGs were carefully designed and tuned to reflect light at two wavelengths with difference between the wavelengths being equivalent to half spectral range of the MZI. The ratio of the FBG reflected powers when connected to a MZI refractometer can then be used to resolve direction and magnitude of wavelength shifts of up to half the FSR of the MZI. This forms the basis of FBGs enabled interrogation of MZI refractometers which will be discussed in more detail in the following sections.

4.3.2 Fibre Bragg Grating Fabrication

The FBGs in this work were fabricated with a scanning phase mask technique as discussed in Section 2.2.2.3 using a 244 nm UV irradiation from a frequency doubled Argon ion laser (Coherent Fred 90C).

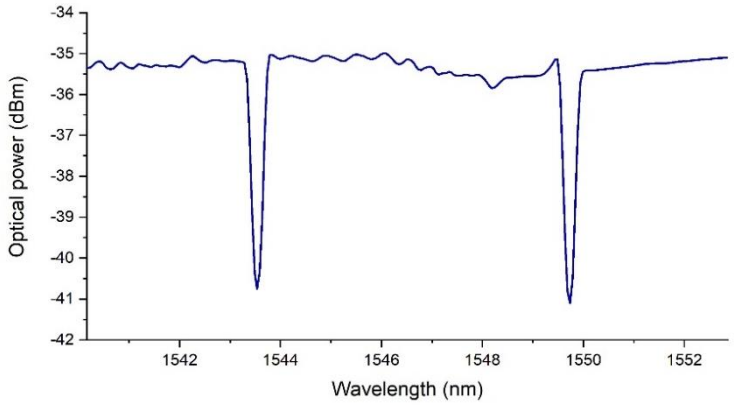

Figure 35: Transmission spectrum of interrogation fibre Bragg grating pair.

The gratings in this work are 10 mm in length with resulting FWHM linewidth of 0.15 nm and reflectivity of 90%. The two FBGs were also designed to have Bragg wavelengths difference within half of the free spectral range of the MZI of the tapered fibre sensor. The FBG pair were inscribed on a single piece of photosensitive fibre (PS1250 from Fibrecore) and was found to present Bragg wavelengths of 1543.54 nm and 1549.73 nm. The FBGs were cleaved and individually strain tuned to 1544 nm and 1550 nm resulting in a spectral distance of 6 nm between the two Bragg wavelengths.

4.4 Experiment

The tapered fibre sensor is connected to a broadband light source and transmission connected to the duo FBG interrogator circuit (Figure 36).

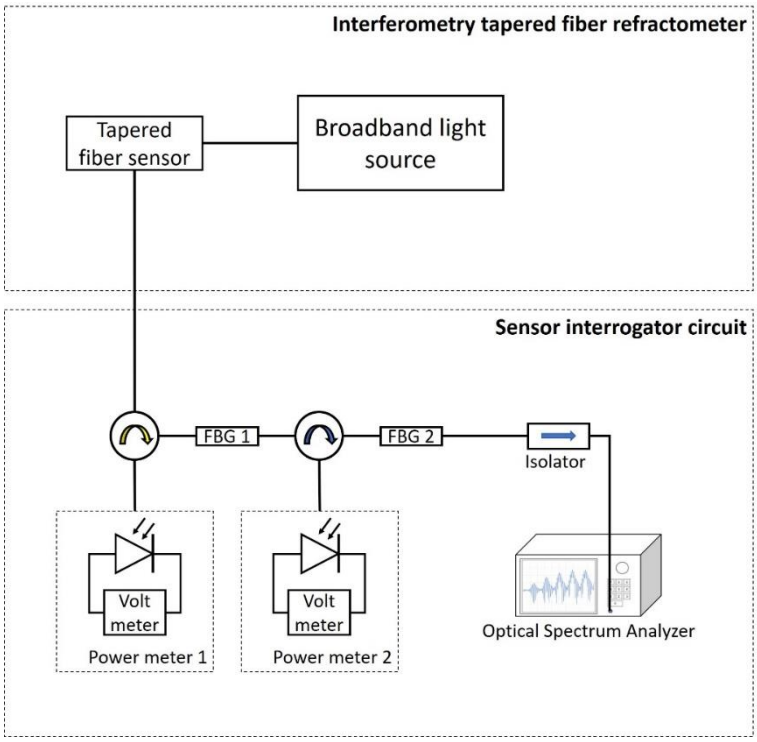

Figure 36: Experimental setup.

To obtain spectral measurements, we connected the free end of FBG 2 to an optical spectrum analyser after an isolator. The isolator acts as a one-way filter, essentially removing back reflections from the optical spectrum analyser due to the fibre connections through a mechanical connector.

The tapered fibre sensor was subjected to 7 different RI levels ranging from 1.3398 to 1.3438 by immersing the sensor into reservoirs of Glycerine solutions diluted to the appropriate RIs. Measurements were taken in random order and the tapered fibre sensor rinsed in large amount of DI water and air dried between each change of RI solution.

4.5 Results and Discussions

As we subjected the sensor to increasing RI ambient environment by changing the Glycerine solutions, the MZI spectrum of the tapered fibre sensor red shifts as showed in Figure 37.

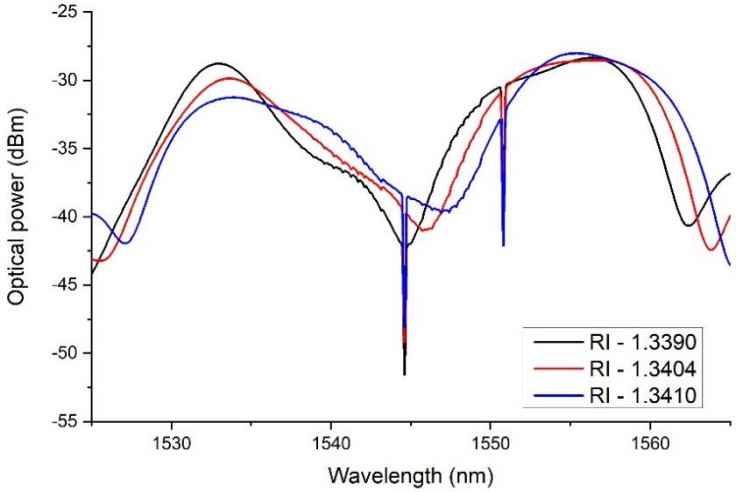

Figure 37:Transmission spectrum of tapered fibre sensor in three different refractive index environments.

Figure 37 shows clear spectral shifts of the MZI spectrum when interface with different levels of ambient RI. The two FBG Bragg wavelengths can also be observed to be fixed. From spectral measurements, the tapered fibre refractometer is found to have a sensitivity of 1200 nanometre wavelength shift per RI unit change.

The reflected optical power for the two FBGs also change as the MZI spectrum shifts. This varying optical power can then be measured by optical power meters, based on measurement of voltage resulting from irradiation of photodiodes. Two common handheld power meters were used in the experiment for measuring the two Bragg reflected optical power through respective optical circulators.

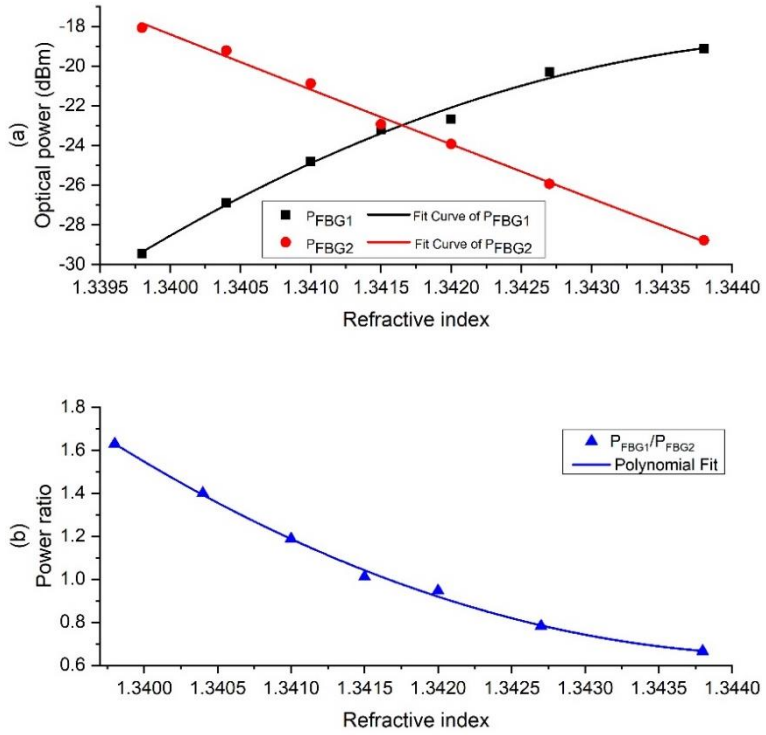

Figure 38: (a) Reflected optical power by fibre Bragg grating 1 and fibre Bragg grating 2. (b) Ratio of reflected power by FBG1 and FBG2.

Figure 38(a.) shows that Bragg reflection intensity from the two FBGs follows the spectral shape of the MZI pattern. As the MZI spectrum shifts with environmental RI changes, the optical power of the FBGs decreases and increases respectively, depending of the magnitude and direction of spectral shift. As absolute power measured from the circulators are subjected to power fluctuation of the light source and physical disturbance to the optical system, taking power ratio minimises this inaccuracy and simplifies measurement read out.

Figure 38(b.) plots the power ratio of the two FBGs and a simple polynomial relationship is observed. This observation can then be fitted to a second order polynomial relationship as follows:

$$\frac{P_{FBG1}}{P_{FBG2}} = a{n_{env}}^2 + bn_{env} + c \qquad (33)$$

where n_{env} is the ambient environmental RI. As equation (33) is a simple quadratic equation, the standard quadratic formula below can be used to solve for n_{env}. Furthermore, since n_{env} can only fall within the sensitivity range of the MZI sensor, only one acceptable solution will be obtained from the standard formula.

$$n_{env} = \frac{-b \pm \sqrt{b^2 - 4ac}}{2a} \quad (34)$$

Therefore, the tapered fiber MZI sensor with the implementation of the duo FBG interrogation circuit can be described with a simple quadratic equation. Only the two optical power measurements from the photodiodes are needed to solve for n_{env}. As power ratio is used instead of absolute power readings, the measurement is not subjected to inaccuracy due to light source power fluctuations.

4.6 Concluding Remarks

It was shown in this work that the interrogation of common MZI RI optical sensors can be done using a cost-effective optoelectronics circuit enabled by FBGs. This method also proves that FBGs can also be applied to such sensor systems as the interrogation element apart from being the sensing element.

The presented interrogation optoelectronic circuit is easily adaptable to different sensors and is relatively inexpensive when compared to traditional equipment for interrogation. The compactness of this scheme makes the design suitable for out-of-lab measurements.

5 Bragg Grating to Fibre End Fabry-Perot interferometric Refractometers

5.1 Introduction

In this thesis, we discussed two main types of grating based refractive index (RI) sensing schemes that is temperature decoupled. The first of the two schemes we investigated in depth is an indirect optical fibre Bragg grating (FBG) sensor whereby a Fabry–Perot interference (FPI) is formed between a weak reflectivity FBG and Fresnel reflection from a right-angle cleaved fibre end. This type of sensor was proposed in the late 2000s [130, 131] but remained relatively unpopular due to its limited sensing range, low sensitivity and high complexity in interrogation as compared to other demonstrated optical fibre refractometers. However, these limitations can be overcome through adaptation of special Bragg gratings. We explored different grating designs and fibre selections to optimize the sensor for specific sensitivity or range.

Two Bragg grating types were adapted to the sensing scheme, namely superstructure fibre Bragg grating (SSFBG) and chirped fibre Bragg grating (CFBG). In addition, two fibre types, Boron-Germanium co-doped photosensitive fibre (PS fibre) and ultra-high numerical aperture fibres (UHNA fibre) with high germanium dopant in core were also used in the experiments. These sensors are shown to have good RI sensing characteristics in the RI range of 1.333 to 1.471 and theoretically applicable for gas sensing for gasses of lower RIs.

5.2 Theory

5.2.1 Fibre-End Fresnel Reflection

When guided light in a length of fibre propagates towards a cleaved fibre end that is interfaced with ambient environment of mismatched RI with that of the fibre's effective RI, some light couples backwards into the fibre due to Fresnel reflection. This reflection (R_{Fr}) is commonly described by the following equation:

$$R_{Fr} = \frac{\left(n_{eff} - n_{ambient}\right)^2}{\left(n_{eff} + n_{ambient}\right)^2} \quad (35)$$

where n_{eff} is the optical fibre's effective RI as seen by the fundamental guided mode and $n_{ambient}$ is the ambient RI of the material or substance which the cleaved fibre end is directly interfaced with, at the wavelength of the optical fibre's core fundamental guided modes.

In this work, the fibres used were specialty photosensitive fibre (fibre number: PS1250) from Fibrecore (Las Vegas, NV, USA) and UHNA fibre (fibre number: UHNA 7) from Nufern (East Granby, CT, USA). The fibres were first characterized for their n_{eff} by inscribing a uniform FBG into their cores, designed to resonate in the telecommunication wavelength range. As grating pitch can be precisely controlled with the phase mask inscription method, governed by equation (36), n_{eff} can be calculated by inscribing a uniform grating in the sample fibres.

$$\lambda_{Bragg} = 2n_{eff}\Lambda_{gr} \quad (36)$$

where λ_{Bragg} is Bragg wavelength of resulting grating measurable using an optical spectrum analyser and Λ_{gr} is the pitch of grating determined by the pitch of phase mask (Λ_{PM}) used.

$$\Lambda_{gr} = 2\Lambda_{PM} \quad (37)$$

Henceforth, the n_{eff} of the sample fibres were determined to be 1.448 for PS1250 and 1.478 for UHNA7. With this information, the percentage of fibre end reflection in air for the PS1250 and the UHNA7 can be estimated using equation (35) to be approximately 3.3% and 3.7%, respectively.

It is obvious from equation (35) that a change in RI of the optical fibre's ambient environment will result in a change in the cleaved optical fibre end's Fresnel back reflection. This principle is the basis of some optical fibre refractometers [77, 79] reported, based on measuring the power change of the Fresnel back reflection. Although simple to implement as an optical fibre refractometer, these schemes are extremely susceptible to errors. The errors can arise from a range of situations such as power instability of light source and varying bending loss of the fibre in any part of the sensing system.

In the following sections of this chapter, the adaptation of this sensitivity of fibre guided light to the environment at the cleaved optical fibre ends into a noise immune grating-based design will be discussed.

5.2.2 Fibre Bragg Grating to Fibre End Fabry–Perot Cavity

A low finesse cavity adopted by some optical fibre sensing schemes[132], can also be formed between weakly reflecting FBG and its host optical fibre's cleaved fibre end. The resulting FPI pattern from such a cavity is the basis of the sensors discussed in this chapter.

Fabry-Perot interferometers (FPI) are a type of optical interference pattern usually formed by a single light source within an optical resonant cavity. This cavity can be formed by two or more mirrors manipulating beam path of light, causing interference within the cavity if the mirrors are placed at appropriate distance (cavity length) from each other. In the simplest case of an FPI, two flat mirrors reflecting at each other forming a cavity length of L, an interference pattern will be formed by incident light in the cavity if L is a multiple of the wavelength of the incident light. In this work, an FPI cavity is formed within a short length of fibber between an FBG and right-angled cleaved end of the optical fibre. An FBG is a fibre device designed to reflect light of a specific band of wavelength while a cleaved fibre end reflects a small portion of light back into the fibre that satisfy the Fresnel condition at the fibre to environment interface. The resulting FPI formed can be characterized by the intensity of it sinusoidal pattern by the following equation.

$$I = I_{R1} + I_{R2} + 2\sqrt{I_{R1} + I_{R2}} \cos\delta \tag{38}$$

where I is the interference intensity, I_{R1} is the intensity of the broadband light reflected by the fibre end and I_{R2} is the intensity of the reflected light by the FBG. δ is the phase difference between I_{R1} and I_{R2} and is given by:

$$\delta = \frac{4\pi n_{eff} L}{\lambda} \tag{39}$$

where n_{eff} is the effective index of the optical fibre at the operating wavelength, and L is the cavity. Note that I_{R1}, n_{eff} and L are usually constant in a fibre cavity not experiencing lateral

distortion. Hence, I is only dependent on I_{R2} which is a function of Fresnel reflection at the cleaved fibre end. Therefore, the FPI formed can be used to measure variation of the ambient environment RI by observing the evolution of the FPI's visibility.

Figure 39 illustrates the Fabry–Perot cavities formed by a CFBG and SSFBG with the cleaved ends of their host optical fibres.

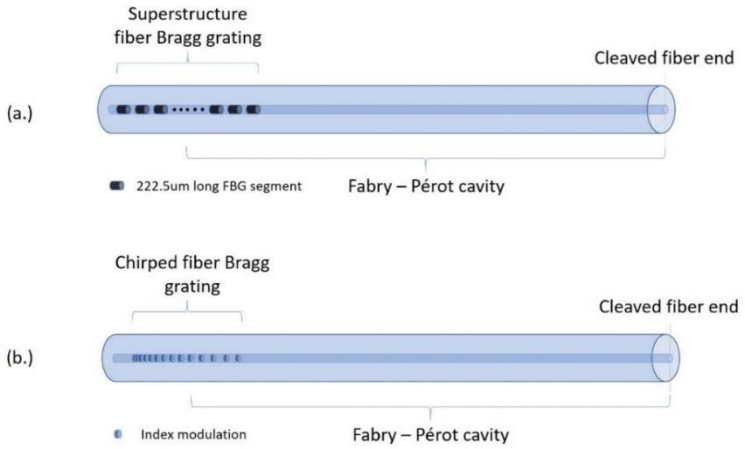

Figure 39: (a.) Superstructure fibre Bragg grating to fibre cleaved end Fabry–Perot cavity. (b.) Chirped fibre Bragg grating to fibre cleaved end Fabry–Perot cavity.

The FPI of the sensors are formed between respective characteristic reflection of the CFBG and SSFBG as discussed in section 2.2.2.2, and the broadband Fresnel reflection at cleaved fibre to environment interface end. Figure 40 shows the spectrum of two FBG-fibre end Fabry–Perot cavities with a CFBG and a SSFBG inscribed in PS1250 photosensitive optical fibre.

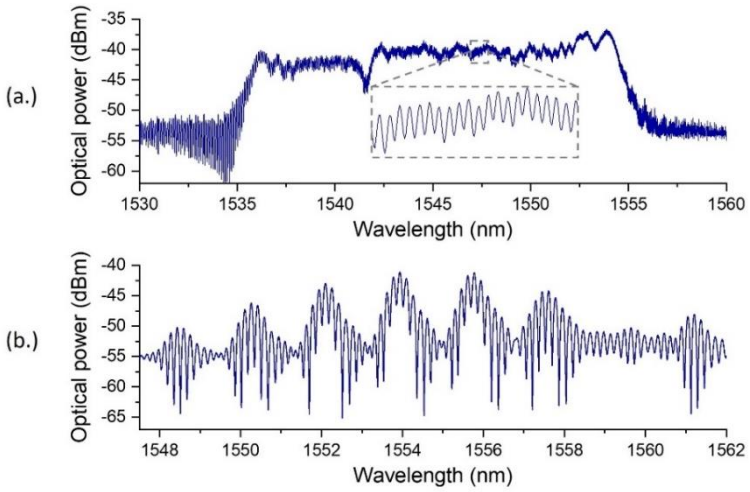

Figure 40: Bragg grating - fibre cleaved end Fabry–Perot interference pattern of (a.) chirped fibre Bragg grating sensor (b.) superstructure fibre Bragg grating sensor.

It is obvious that the sensors exhibit significantly different spectral patterns due to the characteristic Bragg reflections of the two different types of special gratings. For the SSFBG sensor, FPI can be seen to have formed on top of the multi-peak reflection spectrum of a SSFBG. For ease of explanation and referral, we label the central SSFBG peak with highest reflection as peak zero and the lower reflection peaks on the shorter wavelength side with increasingly negative labelling. In this work, we only require observation of four peaks labelled -3 to 0.

The CFBG sensor on the other hand, shows a cleaner spectrum with an almost uniform interference pattern varying slightly in amplitude due to imperfection in illuminating light source and the chirp grating structure. The imperfection in the chirped grating structure can be due to flaws in the chirped phase masks, power fluctuation in UV irradiation or slight misalignment in the grating inscription process which all can be minimised but unlikely to be eliminated. In addition, a noticeable decrease in free spectral range (FSR) was observed towards the shorter wavelength in the spectrum. This observation can be attributed to the fact that the reflection of the shorter wavelength is at a longer distance from the cleaved fibre end, resulting in a longer Fabry–Perot cavity in the optical fibre according to Equation (40).

$$FSR = \frac{{\lambda_0}^2}{2n_{eff} l \cos\theta + \lambda_0} \tag{40}$$

where FSR is the free spectral range of a FPI, defined as wavelength separation between adjacent transmission peaks, λ_0 is the central wavelength of nearest peak, n_{eff} is the effective RI of the host optical fibre at the operating wavelength, θ is the angle of incidence of light which is always 0º for optical fibre waveguides, and finally, l is the length of the Fabry-Perot cavity. It is evident from Equation (40) that FSR of interference spectrum increases with the decrease in cavity length.

The interference pattern of each sensor can further be characterized by its intensity along the spectrum. The interference at each of the reflection peaks of SSFBG sensor observed in Figure 40 can be expressed as:

$$I^m = I_{R1} + I_{R2^m} + 2\sqrt{I_{R1} + I_{R2^m}} \cos\delta \quad (41)$$

where I^m is the interference intensity at peak m, I_{R1} is the intensity of the broadband light reflected by the fibre end and I_{R2^m} is the intensity of the reflected light at each SSFBG peak. δ is the phase difference between I_{R1} and I_{R2^m} and is given by:

$$\delta = \frac{4\pi n_{eff} L}{\lambda} \quad (42)$$

where n_{eff} is the effective index of the optical fibre at the operating wavelength, L is the cavity length and λ is the operating wavelength.

On the other hand, the interference pattern formed in the CFBG sensor can be expressed as:

$$I = I_{R1} + I_{R2} + 2\sqrt{I_{R1} + I_{R2}} \cos\delta \quad (43)$$

where I is the interference intensity, I_{R1} is the intensity of the broadband light reflected by the fibre end and I_{R2} is the intensity of the reflected light by the CFBG. δ is the phase difference between I_{R1} and I_{R2} and is given by:

$$\delta = \frac{4\pi n_{eff} L_\lambda}{\lambda} \;\; ; \;\; \lambda_{blue} < \lambda < \lambda_{red} \quad (44)$$

where n_{eff} is the effective index of the optical fibre at the operating wavelength, L_λ is the cavity length at the wavelength of interest and λ is the operating wavelength of interest. λ_{blue} and λ_{red} are the longest and shortest resonance wavelength of the CFBG respectively. For the case of the CFBG, the FPI intensity (I) is a function of δ which is dependent on cavity length that varies with wavelength.

5.2.3 Sensing Scheme

As the optical fibre end comes in contact with gases or liquid of different RI, the FPI is perturbed by a change in Fresnel reflection at the cleaved optical fibre end according to Equation (45), which is a modification to Equation (35), while the Bragg reflection from the SSFBG or the CFBG remained unchanged.

$$I_{R1} = I_{ASE}\frac{\left(n_{eff} - n_{ambient}\right)^2}{\left(n_{eff} + n_{ambient}\right)^2} \quad (45)$$

where I_{ASE} is the intensity of the ASE light source, n_{eff} is the effective RI of the optical fibre at the operating wavelength, and $n_{ambient}$ is the ambient RI. The change in I_{R1} translates to a change in visibility (v) of FPI of the sensors. This interaction affects the SSFBG and CFBG sensors differently, resulting in the respective unique advantages and limitations of the two sensor types. The sensor's behaviour will be discussed in detail in the following sections.

5.2.4 Temperature Sensitivity of Fibre Bragg Gratings

The sensitivity of FBGs inscribed in a length of silica based optical fibres to ambient temperature fluctuations (ΔT) [133] is well studied and is given by:

$$\frac{\Delta\lambda_{Bragg}}{\lambda_{Bragg}} = (\alpha_\Lambda + \alpha_n)\Delta T, \quad (46)$$

where λ_{Bragg}, the Bragg wavelength is the centre wavelength of the FBG, α_Λ the thermal expansion coefficient of the optical fibre and α_n is the thermo-optic coefficient. As the FBG is subjected to a change in ambient temperature, the Bragg wavelength shifts towards red or blue wavelengths with the increase or decrease in the ambient temperature respectively. This property of the FBG has been widely exploited as thermometers.

CFBGs and SSFBGs behave in a similar way as the normal FBGs when subjected to temperature changes. The whole spectrum of the grating experiences a change, at times in differing magnitudes and directions. This sensitivity to temperature can be a source of problem for Bragg grating based optical refractometers that also relies on the wavelength shift as an indication of RI changes. However, if suitably decoupled, the sensor can be used to simultaneously measure both RI and temperature. This capability is desirable in order to gain sufficient information from a sample under test as it had been long established that RI of a substance is function of temperature [134].

5.3 Sensor Fabrication

Sensor fabrication for both the SSFBG and CFBG sensors are two-step processes beginning with Bragg grating inscription with respective inscription techniques, followed by precise cleaving at the desired cavity length.

5.3.1 Fabrication of Chirped Fibre Bragg Grating Sensor

The CFBG was inscribed with a chirped phase mask using the scanning phase mask technique (Figure 41) for FBG inscription with a 266 nm frequency quadrupled solid state laser into a length of PS1250 photosensitive optical fibre. The mask used was a 20 mm long chirped mask (Chirp rate:9nm/cm) with central pitch of 1067.5 nm. The laser beam was translated across the 20 mm phase mask over the host fibre at a speed which is experimentally determined to deposit fluence that leads to a broadband reflection bandwidth of around 10% reflectivity. At the 3mm mark of the phase mask, irradiation was blocked for the duration equal to a translation distance of 0.5mm to form a let band in the sensor's spectrum (see Figure 48). This is so that the resulting pit can be used as a clear indicator of a spectral shift.

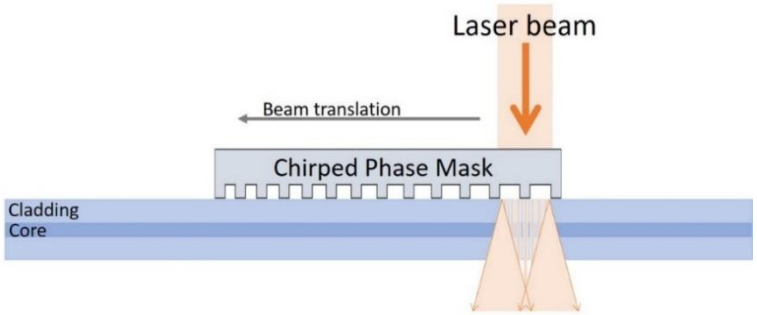

Figure 41: chirped fibre Bragg grating fabrication method.

The optical fibre was cleaved at 12 mm from the centre of the CFBG towards the low pitch side resulting in an effective Fabry–Perot cavity across the CFBG of 2mm from the lowest wavelength end to 22mm at highest wavelength end of the CFBG. It is obvious from the resulting FPI spectra that multiple cavity was formed with continuously increasing length as inferred by the evolution of FSR formed at different wavelengths. The resulting sensor with a single 20 mm long CFBG is depicted in Figure 42.

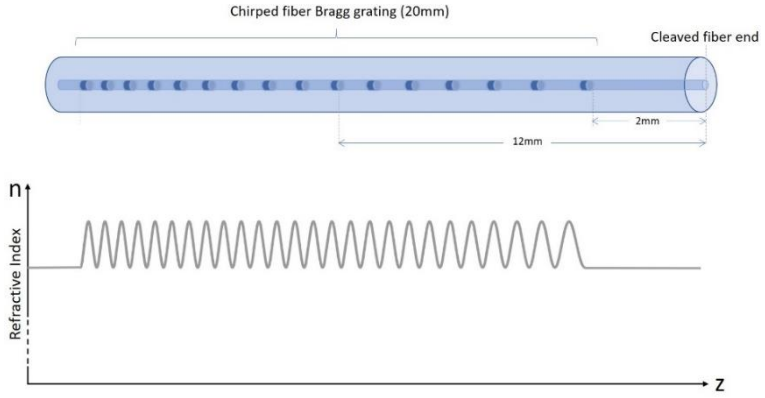

Figure 42: Sensor schematics diagram of sensor configuration and refractive index modulation resulting in chirped fibre Bragg grating sensor.

Behaviour of the CFBG sensor to variations in RI and temperature is characterized and results discussed in section 5.4.

5.3.2 Fabrication of Superstructure Fibre Bragg Grating Sensor

A 1 mm SSFBG was inscribed onto a short length of photosensitive single mode fibre PS1250. The grating inscription was carried out using a 266 nm pulsed UV laser with a spot size of 1 mm with a system of masks (Figure 43) consisting of an amplitude mask of pitch 545 µm positioned 4 mm in front of a phase mask grating plane with pitch of 1075.2 nm.

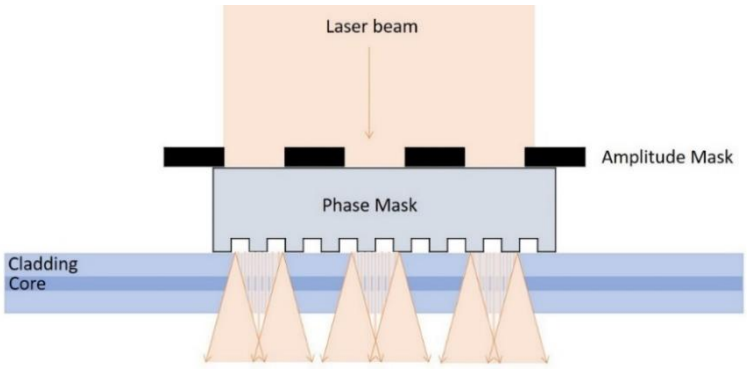

Figure 43: superstructure fibre Bragg grating fabrication method.

The laser beam was translated across the mask system multiple times for 1 mm (grating length) while the transmission spectrum was monitored, and inscription ceased when a reflectivity of around 4% was observed for the centre peak.

The fibre was cleaved 5 mm away from the centre of the SSFBG to form a Fabry–Perot cavity. Cavity length of the sensor was experimentally determined to optimize various factors. A shorter cavity is desired for the sensor to be as compact as possible. A compact sensor makes it easier for the entire sensor to be submerged in test solutions so that simultaneous measurements of RI (from visibility of FPI) and temperature (from Bragg wavelength shift) can be carried out. Shorter cavity resulting in larger FSR improves resolvability of the interference fringes. However, if the cavity length is too short, the resulting large FSR can exceed the linewidth of the SSFBG reflection peaks rendering the FPI unresolvable. The resulting sensor is made up of 4 short 222.5 µm long FBGs in series at regular interval as depicted in Figure 44.

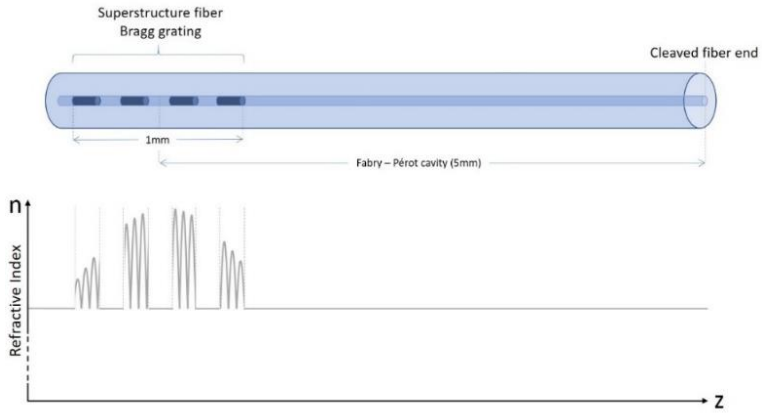

Figure 44: Sensor schematics diagram of sensor configuration and refractive index modulation resulting in superstructure fibre Bragg grating sensor.

The behaviour of the SSFBG sensor to variations in RI and temperature is characterized and results discussed in section 5.4.

5.4 Experiment and Results

5.4.1 Experimental Set-Up

Both the CFBG and the SSFBG sensors were subjected to the same experimental procedures for the investigation and characterisation of the sensor's response to change in ambient environmental RI and temperature. Fourteen RI liquids of different RIs within the range of 1.333 to 1.470 were prepared by diluting Glycerine in deionised water (DI water) in 0.010 RI

unit increments. The sample RI liquids were measured with a commercial refractometer (Model: KRUSS GmbH DR201-95, (Hamburg, Germany)) with 10^{-4} accuracy.

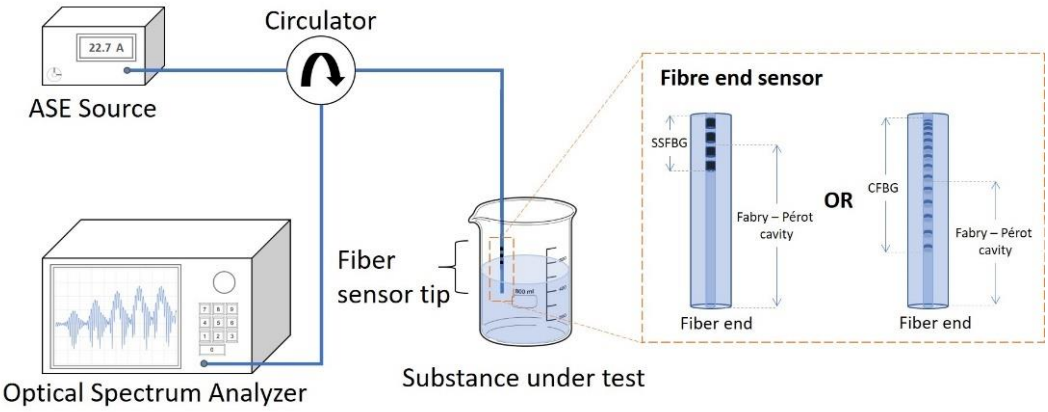

Figure 45: Experimental set up for refractive index measurement.

The sensors were illuminated by a broadband ASE light source with significant optical power in the wavelength range of 1420nm to 1690nm and an optical spectrum analyser (Model: ANDO AQ6317B; Wavelength resolution: 0.01 nm; Power resolution: 0.01 dB) through an optical fibre circulator connected to observe the reflection spectrum, as shown in Figure 45. The fibre sensor tip was immersed in the RI liquids with RI ranging from 1.333 to 1.471. It is to be noted that in the case where only the tip of the sensor fibre is immersed and not the FBGs, the temperature information cannot be measured. For temperature information to be encoded in the sensor response, the FBGs on the sensors must also be submerged in the liquid.

A similar set up as RI characterisation but with a hotplate heated DI water bath instead of RI liquids was used for temperature characterisation of both the CFBG and SSFBG sensors (Figure 46). The sensors were both tested with cold water of 10°C and gradually heated by the hot plate to 60°C and measured in 10°C increment. The sensors were illuminated and interrogated by the same equipment as for the RI measurement. Care was taken to ensure that the FBGs in the sensor fibres are fully submerged in the DI water.

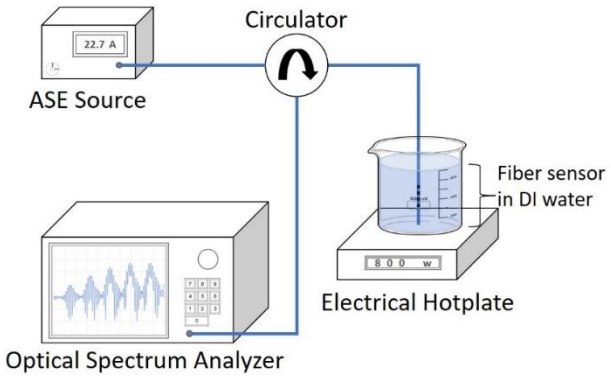

Figure 46: Experimental setup for temperature characterisation of fibre sensors

5.4.2 Refractive Index Response Characterisation

For characterisation of the sensors' capability for RI measurement, the sensor tips were immersed in all fourteen RI liquids in random order and the reflection spectrum of the sensors captured by the optical spectrum analyser. Between each measurement, the sensor was submerged fully in a 1 litre volume beaker of DI water for 1 minute and flushed with more DI water before the next measurement, ensuring that the fibre sensor ends are free from residual glycerine of significant concentration.

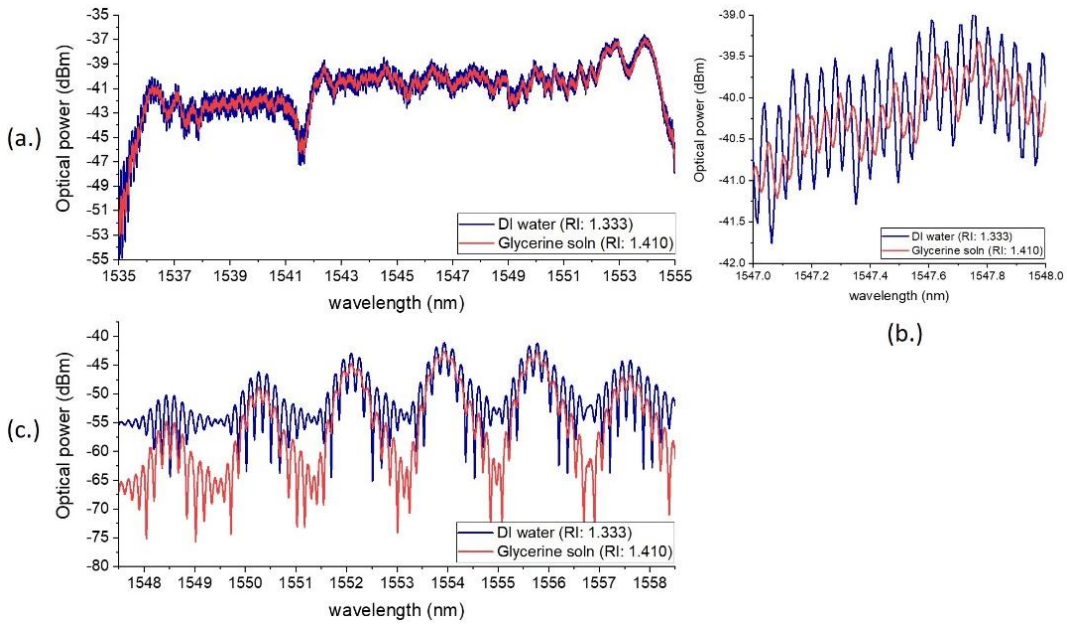

Figure 47: Reflection spectrum when interfaced with DI water (refractive index:1.333) and Glycerine solution(refractive index: 1.410 for chirped fibre Bragg grating and 1.433 for superstructure fibre Bragg grating) for (a.) Chirped fibre Bragg grating fibre end sensor, (b.) Chirped fibre Bragg grating fibre end sensor zoomed to 1 nm spectral width and (c.) Superstructure fibre Bragg grating fibre end sensor.

Figure 47 shows the evolution of both the CFBG and SSFBG sensors when exposed to DI water of RI 1.333 and Glycerine solution of RI 1.410 for CFBG and RI 1.433 for SSFBG

measured from the reflection port of the circulator. For the ease of referral, we number the peaks of the SSFBG sensor with respect to the zeroth order reflection (centre peak at 1554.10nm). It is visually obvious from the spectra that as the sensors are interfaced with environment of different RI, the visibility of the interference fringes changes accordingly. However, due to the different reflection spectral and characteristics of the CFBG and SSFBG, RI measurement sensitivity and method of readout from the spectrum varies and are discussed separately in the following two sections.

5.4.2.1 Chirped Fibre Bragg Grating Sensor Refractive Index Response

As the CFBG is a broad spectrum reflection, it is possible to measure RI by tracking the visibility change of any single period of the interference patterns formed. However, this requires high resolution equipment such as the optical spectrum analyser used in our experiments due to the sub nanometre FSRs. The use of such equipment is not always feasible in actual applications of fibre sensing technologies. The CFBG variant of the sensor allows one to use a duo envelope function on the spectrum, subtracting the top and bottom envelopes, to trace the change in visibility of the FPI (Figure 48).

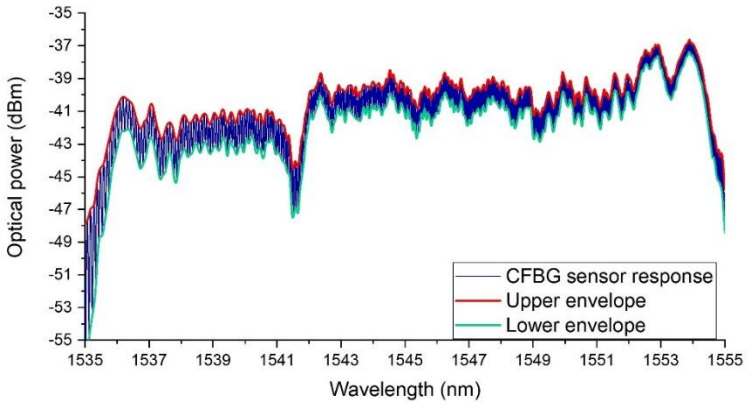

Figure 48: Spectral response of chirped fibre Bragg grating sensor interfaced with de-ionised water, with top and bottom envelop functions.

The area between the top and bottom envelope functions can then be used to represent the visibility of the FPI across the entire spectrum range of interest.

Due to the strong reflection of the CFBG at ~10%, the sensor is found to only be resolvable from 1.333 to 1.410. The relationship of the area between envelop and ambient RI is plotted in Figure 49.

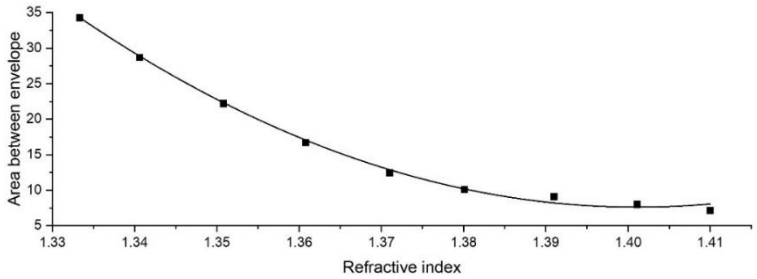

Figure 49: Refractive index response for chirped fibre Bragg grating sensor.

Resolvability of the sensor is best within the range of 1.333 to 1.380. Highest sensitivity of 679.66/RIU is achieved in the range of 1.333 to 1.351. The sensor becomes relatively insensitive to RI changes from 1.380 onwards and losses sensitivity entirely from 1.410. This is so as the cleaved fibre end Fresnel reflection becomes much smaller as compared to the ~10% Bragg reflection. Hence, the resulting FPI becomes irresolvable. The CFBG in this work is designed to be 10% due to limitation of the fabrication method. Lower reflection CFBGs below 10% becomes extremely noisy due to phase mask imperfection. This in turn, translates to the CFBG sensor's limitation as compared to the SSFBG variant.

5.4.2.2 Superstructure Fibre Bragg Grating Sensor Refractive Index Response

The SSFBG spectral response is shown in Figure 50. Multiple peaks of different reflectivity were observed with the central peak ($Peak^0$) being the most reflective. The FPI formed in this sensor is between the broadband fibre end Fresnel reflection and each individual SSFBG reflection peak. Therefore, each peak of the sensor is sensitive only in a range where the reflectivity of the peak and the cleaved fibre end results in FPI measurable visibility.

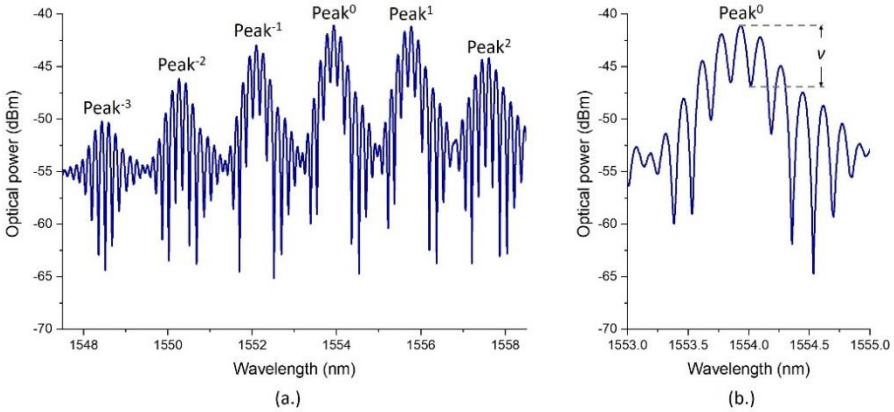

Figure 50: (a.) Spectral response of superstructure fibre Bragg grating sensor interfaced with de-ionised water, (b.) expended view of peak 0 of the spectrum.

Visibility of FPI at each SSFBG reflection peak ($Peak^{-2}$ to $Peak^{2}$) can be found by measuring the difference between the central fringe peak and the adjacent valley as shown in Figure 50(b).

The multipeak spectral characteristic of the SSFBG enabled sensing range to be extended to close to the effective index of the host optical fibre at around 1.445, beyond which the fibre end Fresnel condition will not be satisfied. This is possible, as the weaker reflection in the higher order SSFBG Bragg reflection can still present a high visibility FPI even when the fibre end reflection approaches zero percent.

For example, the FPI visibility at peak 0 becomes unresolvable beyond the RI of 1.420 due to the large reflectivity mismatch between the SSFBG reflection of peak 0 and the fibre end Fresnel reflection. At ambient RI of 1.420, the fibre end Fresnel reflectivity is close to 0.4%, while the SSFBG peak 0 reflectivity remains at 3.7%. Though there should theoretically still be FPI observed at the peak, our existing lab equipment is not able to record this spectrum.

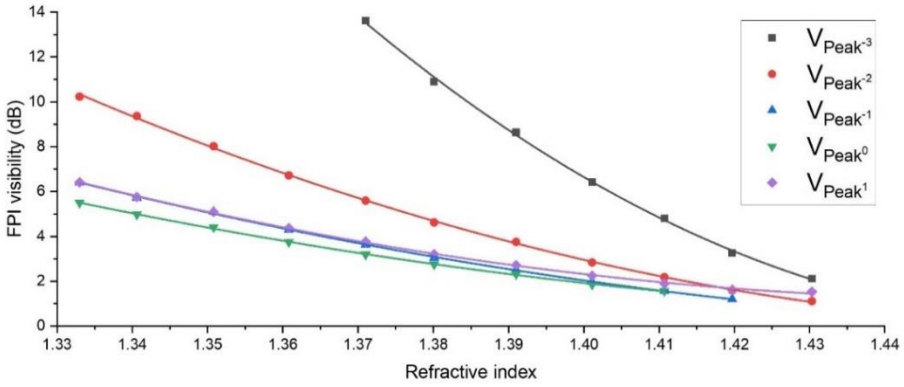

Figure 51: Refractive index response for superstructure fibre Bragg grating sensor

The sensor is found to have a working range of 1.333 to 1.433, where at least one of the SSFBG peaks within peak -3 to peak 1 forms a resolvable FPI with the fibre end Fresnel reflection. The maximum sensitivity of the sensor is 230dB/RIU in the RI range of 1.370 to 1.390 with reference to reflection peak -3 which only becomes resolvable from RI of 1.370 onwards due to its weak reflection being much lower than fibre end Fresnel reflection at lower ambient RI.

5.4.3 Temperature Response Characterisation

For characterisation of the sensors' response to change in ambient temperature, the sensor was immersed in a beaker of DI water chilled to 10°C, gradually heated up to 60°C over a hotplate. The sensor, including the FBGs were fully immersed in the DI water bath at each temperature step for 1 minute, and reflection spectrum of the sensor was captured by the optical spectrum analyser.

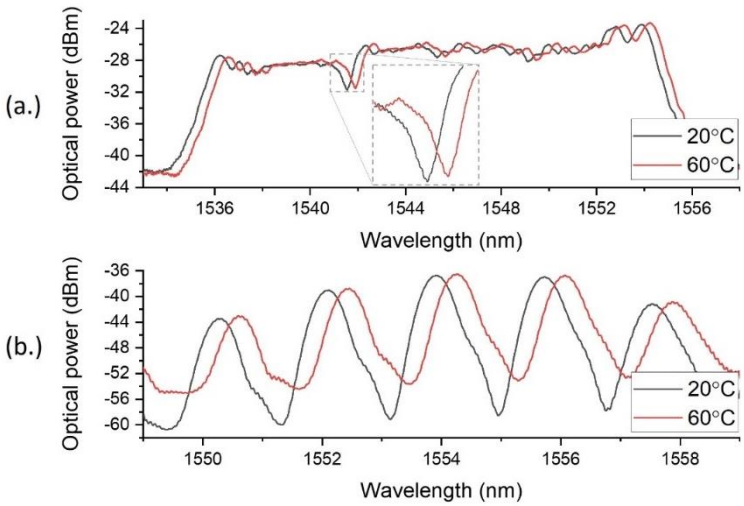

Figure 52: Reflection spectrum when submerged in 20°C and 60°C DI water for (a.) Chirped fibre Bragg grating fibre end sensor, (b.) Superstructure Bragg grating fibre end sensor measured at lower resolution to remove interference fringes.

Figure 52 shows clear spectral red shift for both the CFBG and SSFBG sensors when immersed in DI water bath at 20ºC and at 60ºC. As it is difficult to track wavelength shift for CFBGs with no obvious peaks or pits in the spectrum, a let band at around 1541.8nm was created in the spectrum by stopping irradiation of UV light for a set period during the inscription process. This pit is then used to track wavelength shifts for the CFBG sensor while any of the SSFBG reflection peaks can used for the same purpose.

As both the sensors are of similar material, the effect of temperature change on spectral shift is similar. The temperature response plot in Figure 53 shows almost identical slope for both the sensors. The temperature sensitivity found for CFBG is 8.24pm/ºC while SSFBG is 8.43pm/ºC.

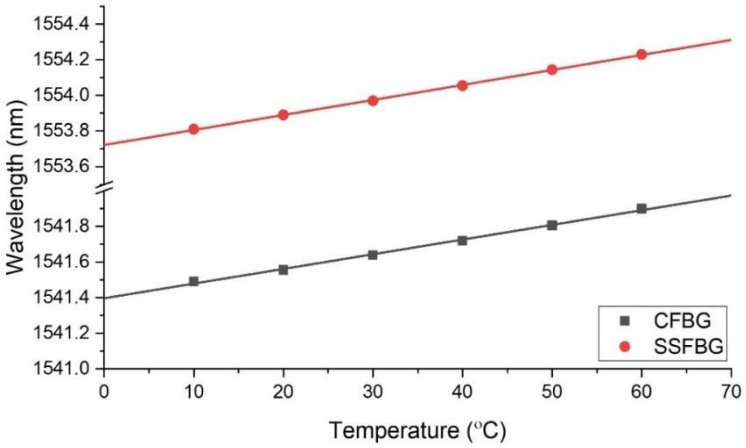

Figure 53: Temperature response for chirped fibre Bragg grating and superstructure fibre Bragg grating sensor.

5.4.4 Further Discussions on Results

Both the SSFBG and CFBG demonstrated good sensitivity to ambient RI and temperature changes. Each scheme presented their unique advantages and limitations. The SSFBG sensor has a much larger sensing range as compared to the CFBG sensor due to the multi-peak reflection characteristics of the SSFBG. Lower reflectivity reflection peak of the SSFBG becomes sensitive to RI changes while higher reflectivity reflection peaks losses sensitivity to RI changes as the fibre end reflected power becomes lower. This larger sensing range enables the sensor to be adaptable for a wider range of applications. However, to interrogate the sensor, a high-resolution optical spectrum analyser must be employed to observe a single FPI period.

On the other hand, the CFBG can be interrogated more cost effectively since it has a broadband spectrum which can be easily resolved by equipment with lower resolutions such as the micron optics fibre interrogators instead of a laboratory grade optical spectrum analyser. It's small range of RI sensitivity as compared to the SSFBG sensor makes it relatively undesirable as an environmental RI sensor where RI of the ambient environment can vary widely.

In the interest of extending the RI sensing range of the SSFBG sensor which is currently limited by the effective index of the host fibre because the sensor loses sensitivity when ambient RI matches the host fibre's effective RI. Such sensing schemes can adopt a higher effective RI host fibre such as the high Ge-doped fibres. As a result, RI sensing range can be raised up to the index of 1.5871 if a pure Germania core fibre is being used. For initial investigation, we implemented the same SSFBG sensor in a length of commercially available high Ge-doped optical fibre (UHNA 7) with effective RI of ~1.480 at an operating wavelength of 1550nm.

5.5 Fibre Host Comparative Studies for Superstructure Fibre Bragg Grating Sensors

This section investigates the suitability of high Ge-doped optical fibres for the application of this FBG to fibre end FPI RI sensor schemes and its capability to increase RI sensing range in comparison to the common PS1250 photosensitive fibres. The high Ge-doped optical fibre is naturally photosensitive to UV irradiation due to it high Ge-doping level resulting in defect centres with the glass structure of the fibre core. The high index step increases light confinement within the sensor, making it less susceptible to bending losses.

The high RI of Germanium raises the effective RI of the fibre. This high effective RI of the fibre is beneficial to this fibre-end sensor where the sensing range is limited by the host fibre's effective RI. In this work, as a mean for easy reference, we name the SSFBG sensors to be sensor A for SSFBG hosted in PS1250 and sensor B for SSFBG hosted in UHNA 7.

5.5.1 Sensor Fabrication

A SSFBG was written in a length of high Ge-doped fibre (UHNA 7) using the same inscription system described in section 5.3.2, forming sensor B. The SSFBG is found to require a length of 6mm with maximum irradiation for the grating to achieve peak reflectivity of ~4%. In comparison, the high Ge-doped UHNA 7 fibre is less photosensitivity than the Ge/B co-doped PS1250.

Due to the narrow linewidth resulting from the long grating length, sensor B is formed by cleaving 30mm away from the centre of the SSFBG (5mm for sensor A) so that FSR of the

resulting FPI is well within the linewidth of the SSFBG reflection peaks. The SSFBG in sensor B is made up of 15 short FBGs of 222.5µm in length as depicted in Figure 54.

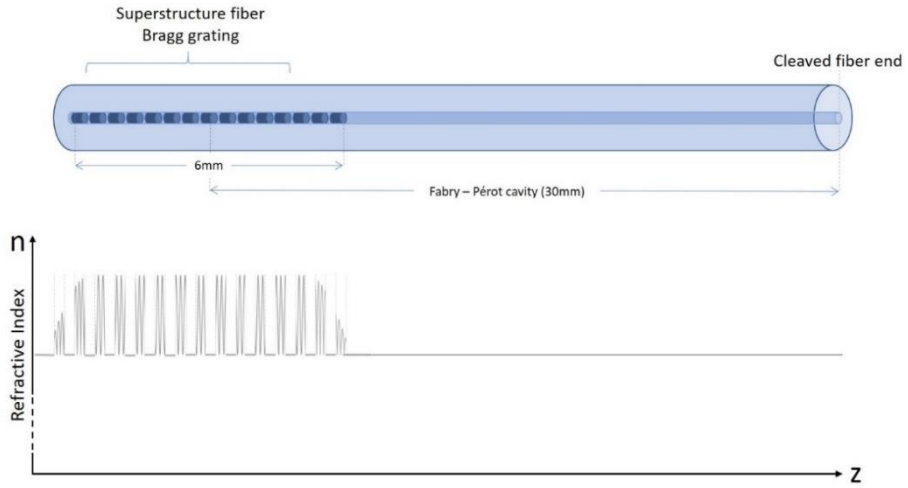

Figure 54:Schematics diagram of sensor configuration and refractive index modulation resulting in superstructure fibre Bragg grating sensor hosted in UHNA 7 high Ge-doped Optical fibre.

When interfaced with DI water after cleaving the fibre at 30mm from the centre of the grating, sensor B exhibits FPI at each of the SSFBG peaks. Sensor A and B were observed to have distinctly different spectral response under the same environmental conditions. The main differences are Bragg wavelengths due to the higher effective RI of sensor B fibre, linewidth due to longer grating length in sensor B and shorter FSR of the FPIs in sensor B due to longer cavity length.

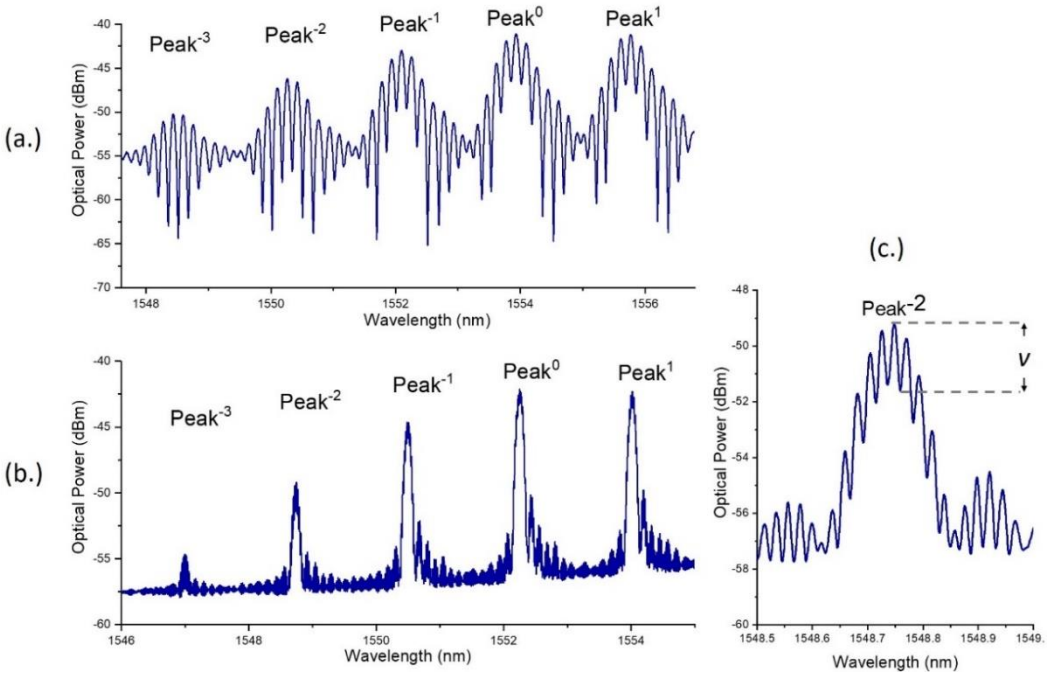

Figure 55:Spectral response of superstructure fibre Bragg grating sensor interfaced with deionised water of (a.) Sensor A and (b.) Sensor B. (c.) expended view of peak -2 of the spectrum for Sensor B.

Visibility of FPI at each SSFBG reflection peak for Sensor B can be found by measuring the difference between the central fringe peak and the adjacent valley. The extremely short linewidth makes interrogation of Sensor B more difficult, requiring a higher resolution equipment, as compared to Sensor A.

5.5.2 Refractive Index Response

Sensor B was found to remain resolvable up till RI of 1.471, a marginal improvement from the RI resolvability limit of 1.433 for Sensor A. The spectral response of Sensor B when interfaced with DI water and with glycerine solution of RI 1.4710 is plotted in Figure 56. When interfaced with different RI environment, the fringes of FPI at each reflection peak of the sensors varies accordingly.

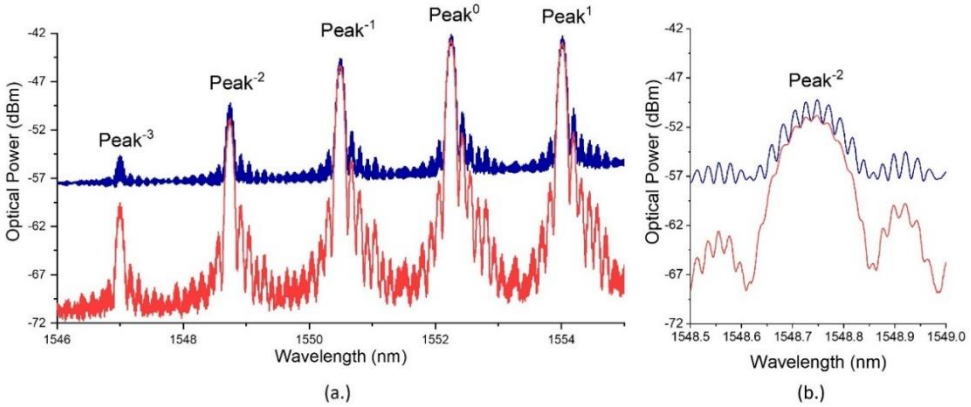

Figure 56: (a.) Reflection spectrum of Sensor B when interfaced with DI water (refractive index:1.333) and Glycerine solution (refractive index: 1.4710) and (b.) expanded view of peak -2.

Sensor B was characterised with the same set of RI liquid prepared with diluted Glycerine solution, in the RI range from 1.3333 to 1.4910. Between each measurement, the sensor was submerged in 1 litre of DI water in a large beaker for 1 minute and flushed with more DI water before the next measurement. This is to ensure that the fibre sensor end is free from residual glycerine of significant concentration.

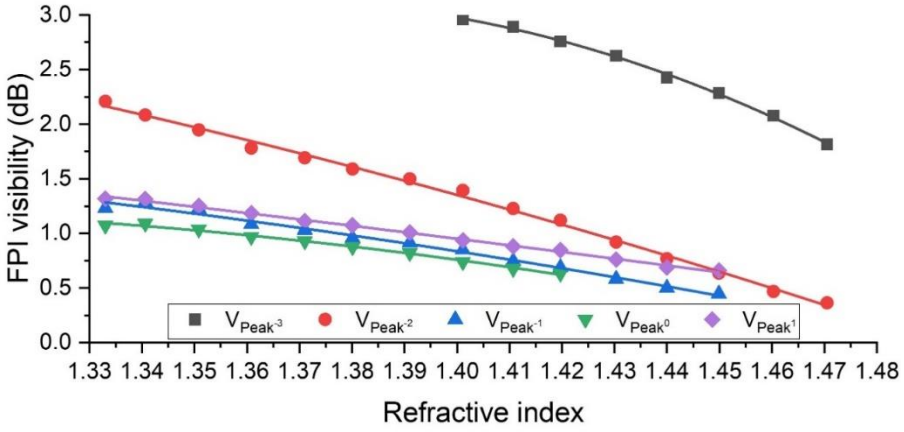

Figure 57: Refractive index response for superstructure fibre Bragg grating sensor B

From the results of the experiment, the sensor showed a working range of 1.333 to 1.471, where at least one of the SSFBG peaks within peak -3 to peak 1 forms a resolvable FPI with the fibre end Fresnel reflection. The maximum sensitivity of the sensor is 24dB/RIU in the RI range of 1.433 to 1.460 with reference to reflection peak -3, which only becomes resolvable from RI of 1.405 onwards due to its weak reflection being much lower than fibre end Fresnel reflection at lower ambient RI.

Comparing Sensor A and Sensor B, there are clear differences in spectral response to RI change caused by differences in physical characteristics of the fibre gratings and the host optical fibres.

Table 2: Refractive index response comparison table for superstructure fibre Bragg grating sensors hosted in PS1250 and UHNA 4 optical fibres.

Attributes	**Sensor A**	**Sensor B**
Grating length	1 mm	6mm
Cavity length	5 mm	30mm
Peak reflectivity	~4%	~4%
3dB Bragg linewidth	481 pm	112 pm
Sensitive range	1.333 - 1.410	1.333 - 1.471
Max sensitivity	230dB/RIU	24dB/RIU

From this work, it was found that implementing the SSFBG sensor in a high Ge-doped single mode fibre at telecommunication wavelength adds little value to the sensor scheme, apart from marginal increase of RI sensing range.

Although the use of high Ge-doped fibres increases sensing range, a longer grating length required in these fibres resulted in shorter Bragg linewidth, and a shorter FSR. Shorter FSR can only be achieved by using a longer cavity which increases the physical length of the sensor. The short FSR is also difficult to interrogate with common field application equipment with lower resolution than the optical spectrum analyser used in this work.

The sensitivity of Sensor B is also found to be an order of magnitude lower than Sensor A. This could be because Sensor B is hosted in UHNA 7, a fibre with high NA and small core, which naturally has a much smaller Mode Field Diameter (MFD) as compared to Sensor A hosted in PS1250, a photosensitive optical fibre that was designed for MFD matching with standard single mode fibre (i.e., SMF28e). As sensitivity of a fibre-end sensor is limited by light ambient interaction area, determined by MFD of the fundamental guided mode at the fibre end, Sensor B suffered lower sensitivity.

5.5.3 Temperature Response Characterisation

Sensor B alike Sensor A was also immersed in a beaker of DI water chilled to 10°C, gradually heated up to 60°C on an electrical hotplate. The sensor, including the FBGs were fully immersed in the DI water at each temperature step for 1 minute and reflection spectrum of the sensor captured by the optical spectrum analyser. At each temperature interval, the spectral shift is consistent for all reflection peaks of the first 4 orders as seen below.

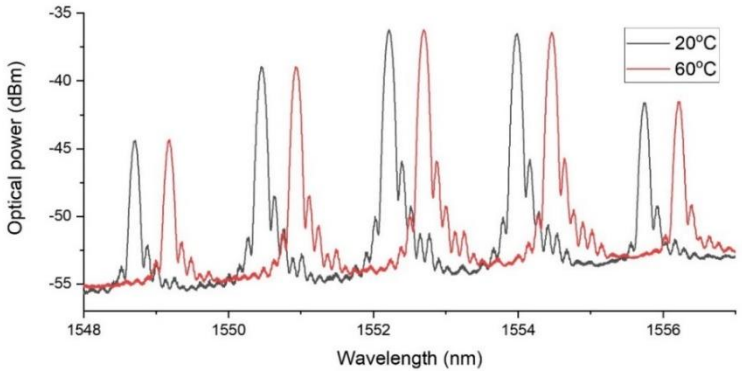

Figure 58:Reflection spectrum when submerged in 20°C and 60°C DI water for Sensor B.

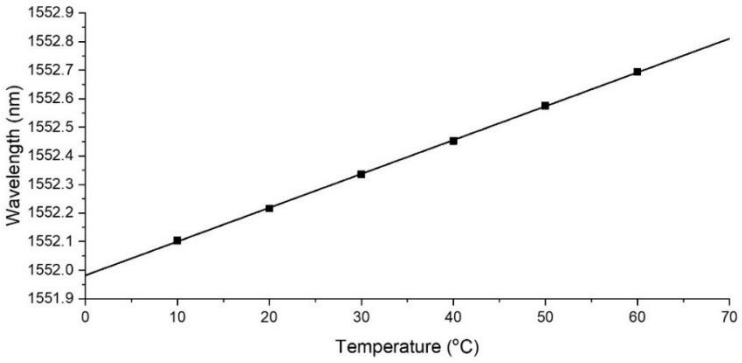

Figure 59: Temperature response for superstructure fibre Bragg grating Sensor B.

The temperature sensitivity of Sensor A is found to be 11.84pm/ºC. This sensitivity is higher than that of sensor A (8.43pm/ºC). This difference can be attributed to the fibre core material difference resulting in a higher thermal expansion coefficient (α_Λ) and thermo-optic coefficient (α_n) of the optical fibre.

5.5.4 Further Discussions

Despite being able to extend the RI sensing range due to the inherent physical properties of the host fibre, Sensor B fabricated with high Ge-doped optical fibres suffers from low RI sensitivity due to its small MFD. The design restrictions also resulted in Sensor B being ~6 time longer than Sensor A. The RI sensing fibre end and temperature sensing FBG is hence further apart, introducing impracticality for simultaneous sensing of RI and temperature for small volume of the sample. Despite the additional benefit of slight improvements in RI sensing range and temperature sensitivity, Sensor B did not prove to be an overall superior sensor using the SSFBG scheme.

5.6 Concluding Remarks

An FBG fibre end RI sensor based on FPI formed between a FBG and the cleaved end of the fibre was demonstrated. The sensor decoupled temperature sensitivity from RI sensitivity. Two different FBG types, CFBG, and SSFBG were investigated as suitable gratings for the sensing scheme. Each sensor type was implemented on a length of PS1250 photosensitive optical fibre and found to present unique advantages and limitations.

The RI sensing range is generally limited by the effective RI of the host fibre. CFBG variant of the sensor is sensitive to RI range of 1.333 to 1.391 while the SSFBG sensor is sensitive in the range of 1.333 to 1.410. A maximum sensitivity of 679.66/RIU and 230dB/RIU was achieved for the CFBG and SSFBG sensors respectively.

Due to the wider sensing range of the SSFBG sensor type, a comparative study of the SSFBG sensor type hosted on different fibres were carried out. The SSFBG were written on a length of PS 1250 (common B/Ge co-doped photosensitive fibre) and a length of UHNA 7 which has high Ge concentration in its core. As a result, the UHNA 7 hosted sensor with larger effective RI has a higher RI detection limit. It was found that the UHNA 7 hosted sensor exhibited RI sensitivity in the range of 1.333 to 1.471 but only with a maximum sensitivity of 24dB/RIU due to the optical fibre's small MFD.

All three implemented sensors have largely linear temperature response and with no observable hysteresis. Hence, the sensors can be implemented to carry out simultaneous temperature and RI measurement.

6 BIREFRINGENT FIBRE BRAGG GRATING REFRACTOMETERS

6.1 Introduction

Side exposed fibre Bragg grating (FBG) refractive index (RI) sensors had proven to be a good solution to a temperature insensitive optical fibre refractometer. As discussed in section 2.3.2, works in this type of sensing schemes had inherent robustness in discriminating temperature from RI measurement but can be complex to fabricate and difficult to replicate due to the need for precisely controlled post processes such as etching and tapering. Although there had been various reported methods of controlling etching for good repeatability [135], etching of silica fibres with micrometre precision inevitably adds complexity to the sensor fabrication process. Furthermore, sensitization techniques such as etching, and tapering weakens the fibre structurally causing them to be prone to breakages and hence unsuitable for deployment in harsher environments. Therefore, this section aims to address the temperature cross-sensitivity issue that plagues many optical fibre refractometer designs with a simple to fabricate side exposed optical FBG sensor that do not require sensitization by etching or tapering.

A side exposed FBG sensor based on a C-shaped, single point core exposed optical fibre (C-fibre), is proposed. An FBG was written directly into the drawn-into-shape C-fibre in which the fundamental guided modes are naturally sensitive to the environment due to the geometry of the fibre, thus encouraging the core guided modes to be extended into the ambient environment. This design allows consistent fabrication of the sensor with good repeatability as post processing is not required since the fibre is inherently sensitive to its environment right off the draw tower. Much like drawn-to-shape microfibres but with higher structural robustness, the C-fibre can be easily reproduced as preform machining and fibre drawing on draw towers are matured technologies.

Since the fibre core and its guided modes are only exposed to the environment at a single point and approximately three quarters of the cladding is unmodified. The sensor can then be

easily attached to rigid surfaces on its unmodified side using common adhesives. This not only further improves the sensor's physical rigidity, but also enables modular distributed deployment of a network of such sensors. It is noteworthy that with the progress of fibre draw tower grating inscription, fabrication of proposed sensor can potentially be integrated into a fibre drawing tower, further simplifying fabrication and lowering the cost.

6.2 Theory

6.2.1 Fibre Bragg Grating Inscribed Birefringent Waveguides

Birefringent waveguides such as a common panda fibre, when inscribed with a FBG results in two distinctive back reflected wavelengths (Bragg Wavelength, λ_{Bragg}) corresponding to orthogonal polarizations. For the sake of discussion, we label the orthogonal axis x and y axis and their respective polarization modes *x* and *y* polarization.

The λ_{Bragg} of a uniform FBG inscribed in a length of non-birefringent fibre follows the following relationship.

$$\lambda_{Bragg} = 2n_{eff}\Lambda \tag{47}$$

λ_{Bragg} of a uniform FBG is dependent on the effective RI (n_{eff}) of the optical waveguide at the FBG site. For unpolarized light, λ_{Bragg} is a function of the FBG fringe pitch (Λ) and effective RI of the waveguide. When the uniform FBG is inscribed on a birefringent fibre, equation (47) now breaks up according to fibre axis as follows.

$$\lambda_{Bragg_x} = 2n_{eff_x}\Lambda \tag{48}$$

$$\lambda_{Bragg_y} = 2n_{eff_y}\Lambda \tag{49}$$

where λ_{Bragg_x} and λ_{Bragg_y} are Bragg wavelengths and n_{eff_x} and n_{eff_y} are the effective RIs of the optical fibre along *x* and *y* axes respectively. FBG reflected light now results in two Bragg wavelengths for two orthogonal axes due to fibre birefringence. The wavelength separation between the Bragg wavelength can be changed by altering the fibre's birefringence.

6.2.2 Side Exposed Single Mode Fibre

For fundamental modes propagating in a single mode fibre, the appropriate design of index profile and choice of operating wavelength determines characteristics of light modes propagating through the fibre. Light can be made loosely guided in the optical fibre with significant portion of the power at the tail end of the gaussian intensity profile of light propagating in the cladding with appropriate design. Removing part of the cladding breaks the circular geometry of a regular fibre and may expose the guided fundamental modes to the ambient environment differently in different polarization axis, introducing sensitivity of guided modes to the environment, thus causing birefringence.

A D-shaped optical fibre (Figure 60a) usually fabricated by either etching or side polishing the cladding of a standard optical fibre to partially expose the fibre core, is one of the common examples of this class of side exposed birefringent fibres. The D-shape fibre is also a candidate of research as interferometric sensor host [136] due to its part mode expose characteristics. Sensitivity of the optical fibre to ambient environment has direct dependency on the extent of cladding removal towards the fibre core. A C-shaped optical fibre as depicted in Figure 60b is like a D-shaped optical fibre in operational principles. The C-fibre however, is not post-processed to obtain the desired shape. The fibre is drawn into its final geometrical shape from the fibre drawing tower using a modified preform. The C-fibre's shape also allows one polarization mode to be exposed to the environment to a much larger extent than the orthogonal polarization, as compared to a D-shaped optical fibre.

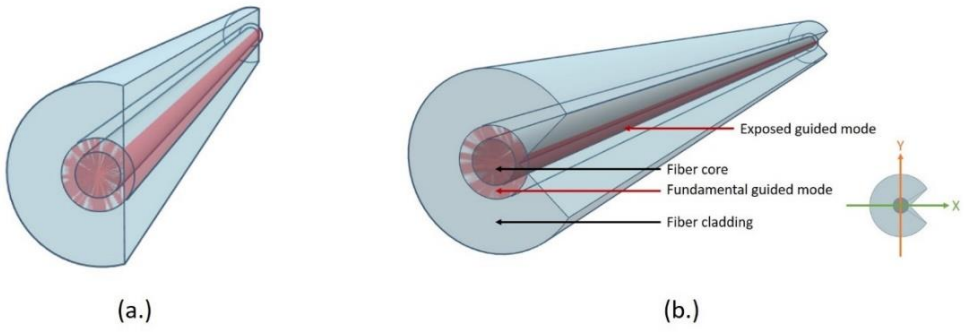

Figure 60: Schematic of (a.) D-shape and (b.) C-shape single mode fibres.

For a gaussian distributed intensity beam of light propagating through the C-fibre, polarization mode along the *x* axis will be exposed to the environment with the tail end of the gaussian beam propagating out of the fibre. This exposed tail end of the polarisation mode contributes significantly to the effective RI of its propagation in the C-fibre, resulting in ambient RI coupled modal effective RI along *x* axis. Therefore, the C-fibre becomes a birefringent waveguide where it's birefringence is coupled to the ambient RI.

6.2.3 Fibre Bragg Grating In C-Shape Optical Fibre

The C-fibre's birefringence is a result of the guided mode being exposed to the ambient environment differently in orthogonal polarisation axis. Therefore, an FBG written in the fibre will then result in similar spectral response to that of an FBG written in a length of polarisation maintaining fibres [137]. In addition, the FBG in C-fibre is sensitive to changes in ambient RI due to the C-fibre's sensitivity to the ambient environment. FBGs in birefringent waveguides exhibits two reflection peaks in its reflection spectrum corresponding to the orthogonally polarised *x* and *y* axes.

By splicing a FBG inscribed in a length of C-fibre to standard single mode fibres (Figure 61), and connecting it to a light source and an interrogator such as an optical spectrum analyser (Figure 67), a sensor can be formed for ambient RI sensing.

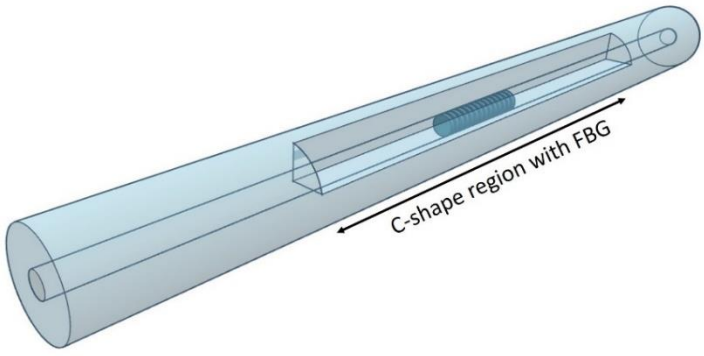

Figure 61: Schematics of C-fibre with FBG spliced to standard single mode fibres as inline refractive index sensor.

6.2.4 Temperature-Refractive Index Decoupling of C-Fibre Bragg Grating Refractometer

A FBG is normally sensitive to temperature fluctuations that the host optical fibre experiences. The change usually results in a shift in Bragg wavelength due to a series of physical changes that heat induced on the grating and the optical fibre. This phenomena is well investigated and widely adopted into optical systems as optical fibre temperature sensing schemes [138]. The governing relationship of a FBG's spectral shift as a result of temperature change is given as:

$$\frac{\Delta\lambda_{Bragg}}{\lambda_{Bragg}} = (\alpha_\Lambda + \alpha_n)\Delta T \tag{50}$$

where α_Λ is thermal expansion coefficient and α_n is thermo-optic coefficient of the host optical fibre.

Many FBG based RI sensors such as the etched or tapered FBG sensors [139, 140] relies on the shift of Bragg wavelength as an indicator of ambient RI change. For these sensors, temperature induced Bragg wavelength shifts then becomes a source of cross-sensitivity as the effect of both RI change and temperature change are coupled into the Bragg wavelength shift. This cross sensitivity can result in significant measurement error.

Our proposed sensing scheme using C-fibre hosted FBG infers RI change by the change in spectral separation of Bragg wavelengths attributed to orthogonal polarization modes. Temperature changes will cause Bragg wavelength of both polarisations to experience equal wavelength shift in the same direction, while not affecting the polarisation mode spectral separations.

6.3 Sensor Fabrication

6.3.1 Fabrication of C-Shape Optical Fibre

Fabrication of the C-fibre was done in house in Nanyang Technological University's Centre for Optical Fibre Technologies. It is a two-step process starting with preform processing with mechanical milling equipment, followed by fibre drawing on a fibre drawing tower. Due

to consideration of cost, resource availability and photosensitivity for grating inscription, a Germanium doped single mode fibre preform (G.652D) was chosen for C-fibre fabrication. The pristine preform has an outer diameter of 19.95 mm and a Germanium doping level of ~5 mol %.

The preform was affixed to a customized jig designed to hold the preform securely in place to be processed by a high precision knee mill. It was determined that to expose the preform core at only one point, an isosceles triangle of 90° apex and sides of 9.35mm is to be cut out from the preform (see Figure 63a). The apex of the isosceles triangle will then be exactly touching the edge of the preform core. Milling equipment used in this work is a Sonic-Mill Rotary Series 10 Ultrasonic Machine with a 25 mm diameter milling bit. The mill was set to operate at a spin speed of 2000rpm moving in repeated horizontal passes along the preform axis systematically removing materials at a speed of 30mm/min. As each pass of the milling bit only cuts 1mm into the preform, multiple passes had to be made in order to precisely make the desired cut. The milling process has an accuracy tolerance of ±100μm. During the entire process of milling, a jet spray nozzle constantly applied coolant to the work piece from between the milling bit and the preform.

Figure 62: Milling of preform on customized milling stage with Standard Series 10 Rotary Knee mill from SONIC-MILL.

This milling process removed a quadrant of the preform whereby the apex of the triangle cut off is designed to be exactly touching the edge of the core (Figure 63a).

The processed preform was loaded into a fibre drawing tower to be drawn into optical fibre. The fibre drawing tower furnace was set at 2000°C and the preform was drawn into optical

fibre at a draw speed of 10m/min. The resulting fibre has an outer diameter of 122μm along the *y* axis (Figure 63b).

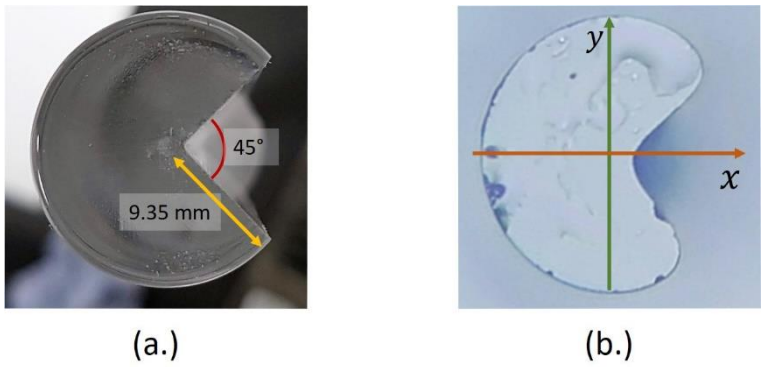

Figure 63: (a.) Preform of standard single mode fibre with quadrant cut out. (b.) fibre end image of C-shaped fibre.

As the quadrant cut out introduced asymmetry to the fibre preform, fluid dynamics during the process of fibre drawing caused the exposed point of the fibre to be coated by a thin layer of mixed cladding/core material. This is as if there is a thin layer of high RI cladding applied at the exposed point (Figure 64), allowing the fibre to retain light guiding properties while facilitating guided modes' interaction with the ambient environment.

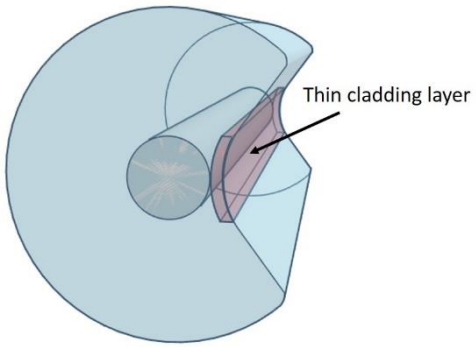

Figure 64: Thin cladding layer formed through fibre drawing process.

The linear RI profiles of both polarisation axes shown in Figure 65 were measured with an IFA-100 fibre profiler.

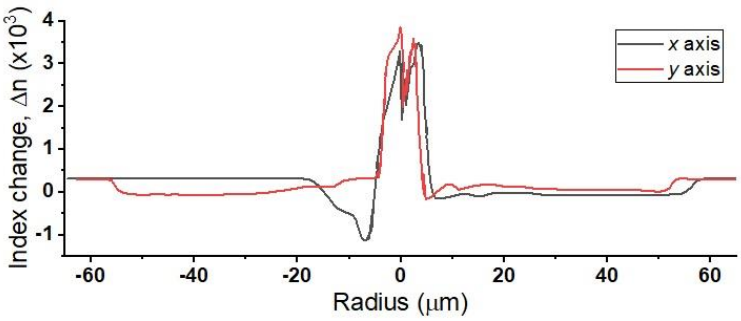

Figure 65: Index profile of C-Shape optical fibre along x and y axes.

It is obvious from the RI profile that the cladding is thinned to an effective thickness of less than 5 μm along the *x* axis (distance from middle of index dip at ~ -10 μm to core surface at ~ -6 μm), resulting in guided modes of corresponding polarisation extending out of the fibre into the ambient environment. Hence, the polarisation modes are exposed to the environment more along *x* axis as compared to *y* axis.

It is apparent that the performance and repeatability of the sensor is dependent on the physical structure of the optical fibre. Once the process of milling and fibre drawing is optimized, the undesired variation of the fibre structure can be minimised. The milling machine used in this work has an accuracy tolerance of ±100μm which translate to a less than ±1μm variation at the fibre level, given that the preform is >100x larger than the fibre. The fibre drawing process is a matured technology where the fibre tower furnace temperature can be controlled at a resolution of 1°C. Therefore, variation of the fibre's physical structure is minimized. However, as the fibre sensor performance can still be affected by the small differences like other fibre RI schemes, each fabricated sensor must be individually characterised.

6.3.2 Fibre Bragg Grating Inscription

A scanning phase mask system (phase mask pitch: 1072.90nm) was used to inscribe a 10 mm long uniform FBG of fringe pitch 536.45nm into the middle of an 80mm long segment of C-fibre. The inscription UV irradiation source used was a 244nm frequency doubled Argon ion laser. As the C-fibre is of unconventional shape, extra care was taken to orientate the fibre on the fibre stage so that the UV laser beam incidents squarely on the unmodified (round) side

of the fibre. This is to ensure that the irradiation is not being diffracted by the abrupt corners on the C-fibre. Taking deionised (DI) water (Measured RI: 1.333, Measurement equipment: KRUSS GmbH DR201-95, (Hamburg, Germany)) as a reference ambient environment, the c-fibre Bragg grating was found to present dual polarized Bragg wavelengths at 1550.435nm in the *x* direction and 1553.212nm in the *y* direction.

6.4 Experiment

Upon fabrication of the C- fibre Bragg grating, the grating was spliced between lengths of standard single mode optical fibre. The 8mm segment of C-fibre was aligned to the middle of a 3D printed nylon sensor holder with a V groove (Figure 66). The sensor was then oriented and adhered to the holder within the V groove so that the thin cladding side of the sensor is unaffected and exposed outwards to the ambient environment, forming a sensing module. The module can be affixed to any structure by the means of adhesive on the back of the nylon holder.

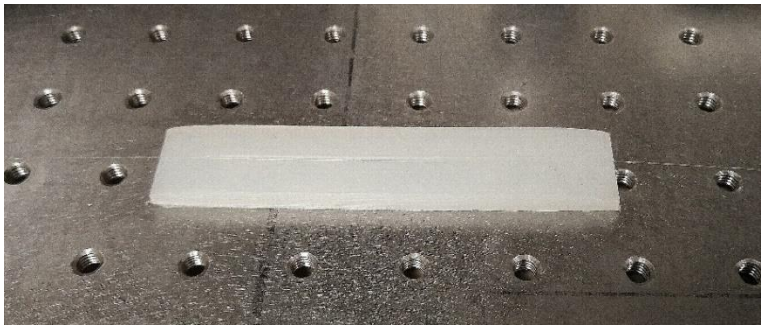

Figure 66: C-Shape optical fibre with fibre Bragg grating inscribed affixed to a nylon block with V-groove.

The sensor module was connected to an amplified spontaneous emission source with significant optical power in the wavelength range of 1480nm to 1620nm and an optical spectrum analyser through a circulator (Figure 67). Measurements of the reflection spectrum of the sensor was made with 5 substances of different RIs. These 5 substances are deionised water (DI water) and four Glycerine solutions diluted to RI of 1.410 1.380, 1.360 and 1.340 with DI water. The RI range was chosen to be significantly lower than the RI of the optical fibre core, to limit the optical power loss due to out coupling of light from the light guiding core.

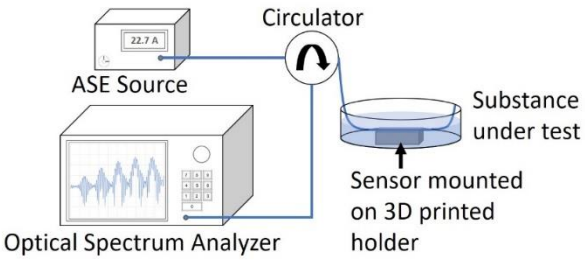

Figure 67: Experimental setup.

An ambient environment of 25°C was maintained and monitored in the laboratory when the experiment was conducted. The sensor was flushed under running DI water between measurements and the experiment was repeated 3 times under the same condition. To prevent temperature fluctuation due to handling of the sample substance, each measurement was taken only after allowing the sensor module to sit in the test substance for exactly 1 hour. It was found that all three sets of measurements showed highly similar results that is indistinguishable within the resolution of the measurement equipment. (Optical spectrum analyser: ANDO AQ6317B; Wavelength resolution: 0.01 nm; Power resolution: 0.01 dB).

To study the response of the sensor under the influence of temperature changes, the sensor module was immersed in a DI water bath in the temperature range of 25°C to 34°C. The water bath was heated up with an electrical hot plate. The temperature range was chosen so that the results of this experiment will not be significantly affected by the change of RI of the DI water bath due to heating. As the sensitivity of the sensor is in the order of 10^{-3}, the change of DI water's RI as a result of heating during the experiment is to be kept below 10^{-3}. The maximum temperature range that results in RI change of less than 10^{-3} was approximated [141] using Equation (51).

$$n_1(\lambda, t_1) - n_2(\lambda, t_2) < 10^{-3} \tag{51}$$

$$\mathrm{n_i}(\lambda, \mathrm{t_i}) = \mathrm{A(t_i)} + \frac{\mathrm{B(t_i)}}{\lambda^2} + \frac{\mathrm{C(t_i)}}{\lambda^4} + \frac{\mathrm{D(t_i)}}{\lambda^6} \tag{52}$$

where λ is the operating wavelength, t_i is temperature in °C and A, B, C, D are temperature dependent Cauchy coefficients determined experimentally in [141]. RI changes of $9.9\text{x}10^{-4}$ RIU is found to be resulted from a 9°C increase in temperature from 25°C to 34°C. Therefore, this

experiment limits our temperature response investigation within the 9°C range with measurements taken at 3°C step starting at 25°C to 34°C.

6.5 Results and Discussions

6.5.1 Sensor Response to Refractive Index Change

Figure 68 shows the reflection spectral responses of the sensor when submerged in DI water and Glycerine solution with RI of 1.410. It was observed that as the sensor changes from an RI 1.333 (DI water) environment to one of RI 1.410 (Glycerine solution), the increase in ambient RI caused the Bragg wavelength of both orthogonal polarizations to red shift. However, due to the different extent of mode exposure for *x* and *y* polarizations axes, the Bragg wavelength of the orthogonal polarizations red shifts with different magnitude. This phenomenon forms the operating basis of the C-fibre Bragg grating sensor.

The reflection spectra also show that there exist a Mach-Zehnder interference that could be attributed by the interference of light of different light path as they couple from the C-fibre into the standard single mode fibre. Mach-Zehnder interference of this nature is the basis of some optical fibre RI sensor [142]. This effect is a source of noise in the C-fibre Bragg grating sensor but can be ignored in this case as the magnitude of visibility of the resulting Mach-Zehnder interference is insignificantly small and does not cause a change to Bragg reflection wavelength.

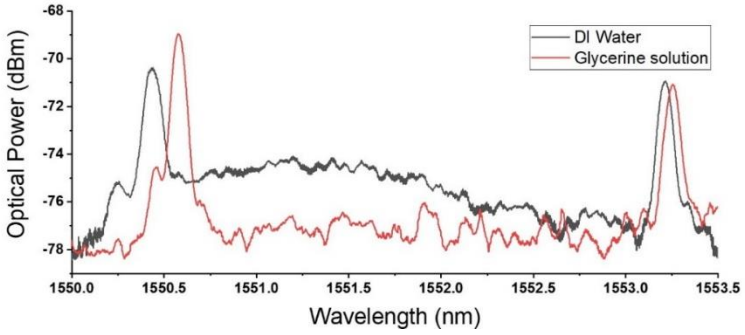

Figure 68: Spectral response in deionized water and Glycerine solution of refractive index 1.410.

In DI water ambient environment, the Bragg wavelength separation of the orthogonal polarisations is 2.777nm with Bragg wavelengths of *x* and *y* polarizations at 1550.435nm and 1553.212nm respectively. As Bragg wavelength is a function of modal effective RI of the host optical fibre described by equation (47), modal effective RI of light propagating in the C-fibre was then calculated to be 1.445 along the *x* axis and 1.448 along the *y* axis in ambient RI of 1.333. The birefringence of the C-fibre is higher than expected but can be attributed to stress within the fibre structure induced during fibre drawing process of the irregularly shaped preform.

Replacing the DI water with Glycerine solution of RI 1.410 caused a shift in Bragg wavelengths of the sensor to 1550.578nm and 1553.255nm for the *x* and *y* polarisations respectively. The spectral separation between the Bragg wavelengths of orthogonal polarizations is reduced to 2.677nm. This 100pm change in Bragg wavelength spectral separation is indicative of the 5.8% change in ambient RI with a sensitivity of 1300pm/RIU within the range of RI from 1.333 to 1.410. The same measurements were conducted for 5 ambient RIs from 1.333 to 1.410 using the prepared RI liquids.

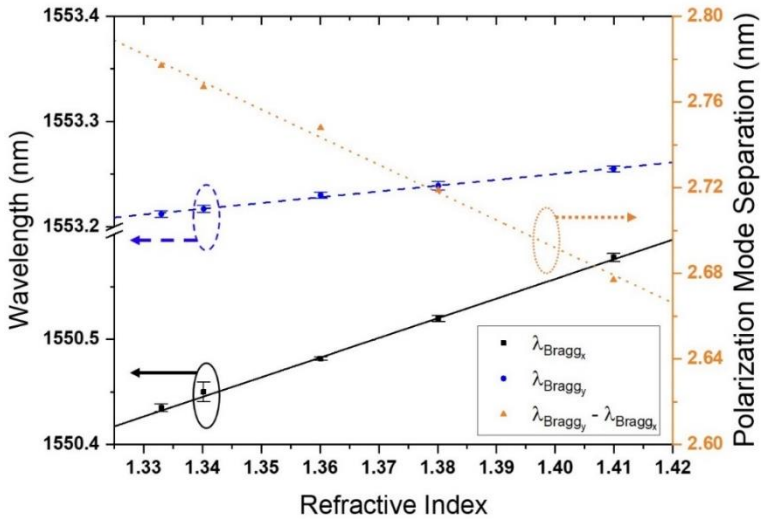

Figure 69: Sensor response to change in ambient refractive index.

Figure 69 shows that Bragg wavelengths for both polarisations experience linear red shifts but *x* polarisation experiences a larger wavelength shift, indicated by steeper slope for x polarisation as compared to y polarisation. Hence, the linearly decreasing spectral distance

between the Bragg wavelengths of both polarisations can be used as a measurement of ambient RI change.

6.5.2 Sensor Response to Temperature Change

The same sensor module was submerged in a DI water bath heated by a hotplate. The temperature was varied from 25 to 34°C in step increment of 3°C. As the C- fibre Bragg grating was affixed to the nylon material sensor holder, response to temperature change of the entire module is a contribution of the fibre, nylon holder and epoxy thermal properties. Both the Bragg wavelengths of orthogonal polarizations experience linear spectral shifts with temperature change. Considering the evolution of spectral separation (Figure 70) between the two polarisation's Bragg wavelengths, it was observed that the small 9°C fluctuation in ambient temperature did not complicate the sensor's ability to measure RI.

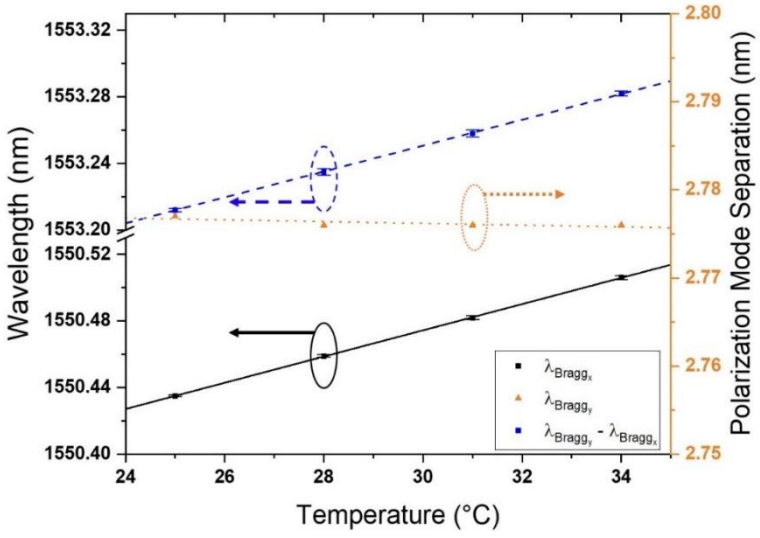

Figure 70: Sensor response to change in ambient temperature.

Although a slight change in Bragg wavelength separation was also observed, it is likely to be due to the small change in the RI of the DI water bath resulting from heating. A 9ºC increase in temperature is approximated to induce an 9.90×10^{-4} RIU RI change for DI water due to heating. As a 1pm polarization mode separation change was observed and with sensor sensitivity of 1300pm/RIU, a 7.69×10^{-4} RIU increase in ambient RI is implied, close to the approximated increase of 9.90×10^{-4} RIU. It is reasonable to suggest that the minor decrease in

mode separation is indeed due to the change of DI water bath's RI due to heat. If a more significant temperature range was considered, the RI of the DI water bath will be significantly changed, producing a more prominent change in Bragg wavelength spectral separation of the sensor.

6.6 Concluding Remarks

A new polarisation assisted RI sensor employing a birefringent FBG was presented in this work. The Bragg grating was inscribed in a special C-shaped fibre which is naturally sensitive to ambient environment due to its physical geometry. Post fibre drawing processes such as arc-tapering or chemical etching is not required to sensitise the fibre.

The C-fibre Bragg grating sensor is simple to fabricate, and it retains the original fibre's physical robustness. Without enhancement, the sensor's sensitivity to ambient RI is 1300pm/RIU. Although the sensitivity of the sensor is not as high as other reported fibre RI sensing schemes, the C-fibre sensor has advantages which makes it a good candidate for many applications. Some of these advantages are the simplicity of fabrication, potential for draw tower fabrication of long distributed array for multi-point sensing in large water bodies, physically robust and temperature insensitivity. As the C-fibre is only modified at one quadrant exposing the guided modes only at one point, the sensor can be easily attached to physical structure such as dam and water reservoir walls.

7 SURFACE FUNCTIONALIZED GRATING BASED REFRACTOMETERS FOR CHEMICAL SENSING APPLICATIONS

7.1 Introduction

Functionalisation of refractive index (RI) optical fibre sensors at the sensing surface with chemical compounds designed to react with or trap specific chemical molecules transforms a refractometer into a targeted chemical sensor. These functionalisation coating usually changes in RI after being bonded either chemically or physically with the target chemical. The change in RI from this interaction can then be measured by the optical fibre refractometer.

In this thesis, two analytes, heavy metal ions in water and ethylene gas in air are of interest. An RI sensor (Superstructure Bragg grating to fibre end Fabry–Perot interferometric refractive index sensor) presented in the chapter 5 was chosen for the implementation of heavy metal ion and ethylene gas sensing by functionalisation of the fibre sensor with two different coatings.

Water pollution is a global concern and environmental agencies worldwide have expressed tremendous interest in robust refractometers suitable for implementation in large water bodies. Although a change in RI can be indicative of the severity of pollution, normal refractometers are unable to identify the pollutants. One of the most dangerous group of pollutants in water, especially in water for consumption, are heavy metal ions. Optical micro fibre RI sensors designed to sense heavy metal ions have previously been reported [143] but these sensors are unsuitable for unsupervised long term monitoring as they are cross-sensitive to strain and temperature fluctuation which are unavoidable in practical implementation.

The level of ethylene, a hydrocarbon gas in farms, fruit storage and fruit transports indicates ripeness and conditions of the produce [144]. Production of ethylene gas, a type of plant hormone is a natural process in plants and can encourage the ripening of fruits [145, 146].

Therefore, monitoring of ethylene in farms and other fruit processing and handling facilities is of interest in the agricultural and fruit processing industries.

Two chemical sensors implemented in this thesis were based on the superstructure fibre Bragg grating (SSFBG) to fibre end Fabry–Perot interferometric refractometer. The sensors were functionalised at the surface of the cleaved fibre end with Ethylenediaminetetraacetic acid (EDTA) for heavy metal ion detection and Molybdenum disulphide (MoS_2) for ethylene gas sensing.

7.2 Heavy Metal Detection

7.2.1 Ethylenediaminetetraacetic Acid as Chelating Agent for Metal Chelates

Chelating agents also known as chelators for metal ions are multidentate legends of which the molecular structure contains binding sites or donor atoms for metal ions. Upon interactions with metal ions, the chelating agent forms a chelate, an extremely stable complex ring-like structures [147]. Examples of donor atoms include chemical groups such as *-SH, -S-S, -NH2, =NH, -OH, -OPO3H* and *>C=O* [148]. A universal metal chelator, Ethylenediaminetetraacetic Acid (EDTA), was chosen as a coating to be deposited on the cleaved fibre end surface of the SSFBG refractometer.

EDTA is a hexadentate ligand comprising six potential binding sites made up of four carboxylate and two amine groups for metal ions such as cadmium (Cd^{2+}) and lead (Pb^{2+}) [149]. Despite the fact that EDTA is a universal metal chelator capable of binding most metal ions to its binding sites, the chelation properties of the compound in contact with different metal ions is different depending on the stability constant (k) of the resulting chelate [148]. Heavier metal ions tend to form a much more stable chelate with EDTA as compared to lighter metal ions and hence have a higher stability constant. In cases where the environment is made up of a mixture of metal ions and heavy metal ions are of interest, the heavy metal with higher k constant will compete and displace those of lower k constant from the binding sites of the EDTA. Therefore, functionalization of the SSFBG sensor cleaved fibre end surface allows heavy metal ions to be

captured at the fibre tip surface. The resulting change in RI of the EDTA coating can be measured by the host fibre refractometer.

7.2.2 Ethylenediaminetetraacetic Acid Coating Process on Fibre End for Heavy Metal Sensitivity

The coating of the SSFBG sensor tip with EDTA is a three-step process, namely fibre sensor surface preparation, coating preparation and optical deposition process.

First, the sensor fibre cleaved ends were cleaned by immersion in acetone to dislodge and remove any foreign particles. The fibre is rinsed with running deionised (DI) water and then dipped into a small test tube of Piranha solution with the chemical compositional makeup of three part of sulfuric acid to one part of hydrogen peroxide for 30 mins inside a fume hood. The fibre end was once again rinsed thoroughly under running DI water and dried with inert nitrogen gas from a low flow rate air gun. Silanisation of the fibre sensor was then carried out using a 2% *v*/*v* of 3-aminotrimethoxysilane in toluene solution. The solution was heated to 70°C and the fibre was immersed in it for 90 minutes. The salinized sensor fibre was then removed from the solution and rinsed with ethanol and dried in a furnace at 80°C for 90 minutes to remove any weakly binding amine groups from the sensor fibre surfaces. The sensor fibre is then ready for coating of EDTA.

The EDTA coating solution was prepared using 20mg of EDTA with 15 mL of phosphate buffer saline solution. A trace amount of cross-linker, 1-ethyl-3-(3-dimethylaminopropyl) carbodiimide hydrochloride (EDC) was then added to the solution for activation of the EDTA solution's carboxyl groups. 10mg of stabilizer in the form of *N*-hydroxy succinimide (NHS) was added to the solution and left to rest in room temperature for 15 minutes.

Finally, the silanized sensor fibre tip was lowered into a test tube of the activated chelating agent and left to sit for 2 hours. This allows covalent bonds between the silanized silica sensor fibre tip and ETDA. At the end of the 2 hours, the reaction was stopped by the addition

of 10mg of hydroxylamine to the solution. The coated sensor fibre (Figure 71) was then rinsed under running DI water for one last time before it is ready for sensing of heavy metal ions.

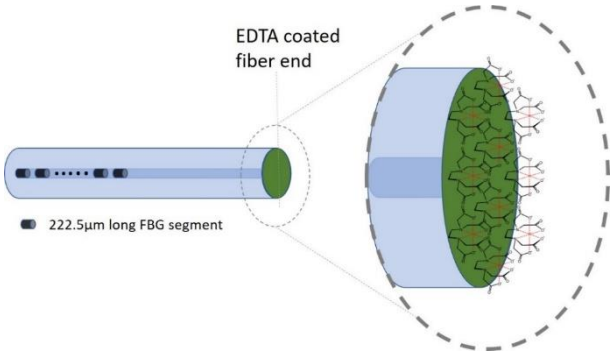

Figure 71: Superstructure fibre Bragg grating refractometer fibre end coated with Ethylenediaminetetraacetic acid.

7.2.3 Experiment and Results

The EDTA coated SSFBG sensor was connected to a light source and interrogation circuit (Figure 72). The sensor was immersed in DI for 15 hours to ensure that EDTA is properly coated on the sensor fibre end surface.

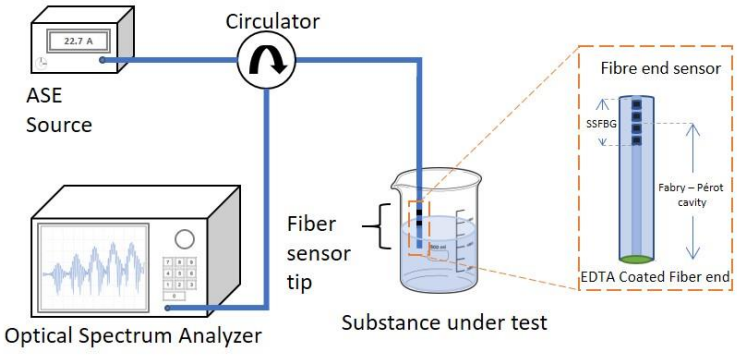

Figure 72: Experimental set up for metal ion detection with EDTA coated sensor.

The fibre was found to be insensitive to ambient refractive index change, indicated by the absence of spectral change when the sensor was immersed in air and water (Figure 73).

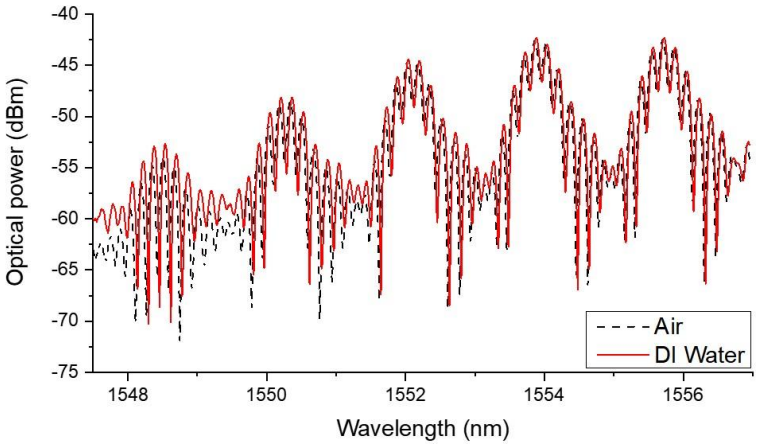

Figure 73: Ethylenediaminetetraacetic acid coated sensor response when exposed to air and in deionized water

This observation is likely to be because the sensor fibre end is covered with a thin layer of EDTA which insulated light guided in the fibre to the fibre end from interfacing directly with the ambient environment. The RI of the EDTA coating without any metal chelate is found to be 1.356 from the RI characterisation in section 5.4.2.

Five samples of Cd^{2+} mixed in DI water with concentration of 1ppm, 10ppm, 100ppm and 200ppm were prepared along with pure DI water for experimentation of the sensor's capability to detect traces of heavy metal ions. Figure 74 shows the spectral response of the sensor when immersed in DI water and DI water mixed with Cd^{2+} ions of concentrations of 100ppm and 200ppm.

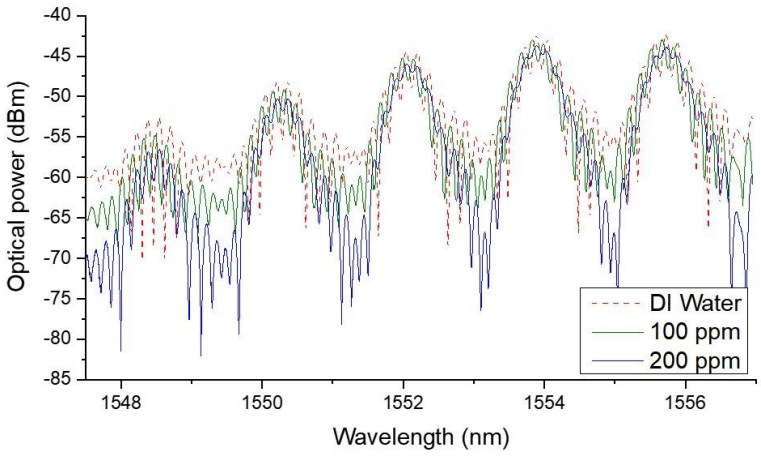

Figure 74: Ethylenediaminetetraacetic acid coated Sensor response when exposed to deionized water and in 100 ppm and 200 ppm solution of Cd2+

The fibre was immersed into each of the five samples for 10 seconds and reflection spectrum capture by the optical spectrum analyser. Between each measurement, the sensor was immersed into large quantity of DI water until the reflection spectrum returns to that of measurement in pure DI water. A clear spectrally observable change in the fringe visibility could be observed between some doping levels, demonstrating the sensor's ability to detect ppm levels of Cd^{2+} ions.

The minimum detectable concentration of Cd^{2+} ions causing a significant change in the RI of the EDTA coating is 10ppm. However, at that level, the measurement is not sufficiently stable to be conclusive as the magnitude of fringe visibility change falls within the error range of the optical spectrum analyser. Therefore, a significantly conclusive reading was achieved only from samples with lowest concentration of 100 ppm. This is evident from Figure 74 showing that the Fabry–Perot interference fringes significantly decreases when the sensor was placed into the solution of 100 ppm Cd^{2+} ions, and further decreased in the solution of 200 ppm Cd^{2+} ions for the same duration of 10 seconds.

The sensor's sensitivity to low concentration of Cd^{2+} ions in water under 100 ppm was found to be 0.150 dB/10ppm and 0.143 dB/10ppm in the range of 100ppm to 200ppm.

7.3 Ethylene Gas Sensing

7.3.1 Molybdenum Disulphide for Ethylene Gas Sensing

The interaction between MoS_2 and ethylene gas is not yet known. However, it is observed that upon encounter with ethylene gas, both the resistivity and RI of the MoS_2 experience a change. One suggestion to this observation is that the MoS_2 complex layers traps the gas like graphene's ability to retain ammonia gas within its structure. The mechanism of change in RI of the compound remains a subject for further studies. Nevertheless, relying on this observation, MoS_2 could be a feasible coating on fibre refractometers for ethylene gas sensing.

7.3.2 Molybdenum Disulphide Coating Process on Fibre End for Ethylene Gas Sensitivity

The coating of the SSFBG sensor tip with MoS_2 is also a three-step process like the coating of EDTA. The steps are fibre sensor surface preparation, coating preparation and drop casting process.

Acetone was used to clean the surface of the sensor fibre, dislodging and removing any foreign particles, and then rinsing with running DI. The clean sensor fibre was dipped into a small test tube of Piranha solution with the chemical compositional make up of three parts of sulfuric acid to one part of hydrogen peroxide for 15 mins inside a fume hood. The fibre end was once again rinsed thoroughly under running DI water and dried with inert nitrogen gas from a low flow rate air gun. The sensor fibre is then ready for coating of MoS_2.

MoS_2 nanosheets were prepared by dissolving 10mg/ml of MoS_2 powder in dimethylformamide (DMF) and sonicated for 60 minutes in room temperature. The mixture was then centrifuged for 90 minutes at 3500 rpm to separate the MoS_2 nanosheets from the unexfoliated flakes of MoS_2. Supernatant of the process containing the MoS_2 nanoparticles were then extracted from the mixture.

MoS_2 nanosheets were drop casted onto the sensor fibre tip and left in the oven at 50°C to evaporate the DMF, and for the MoS_2 to properly adhere to the fibre tip. To generate a multilayer MoS2 coating and to fully coat the entire fibre end surface, the process was repeated 5 times. The coated sensor fibre (Figure 75) was then flushed with nitrogen gas before it is ready for sensing of ethylene gas.

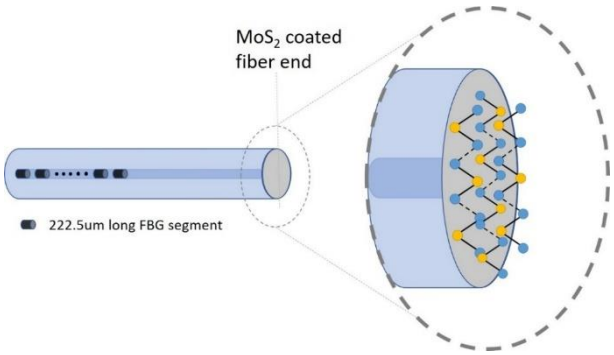

Figure 75: Superstructure fibre Bragg grating refractometer fibre end coated with Molybdenum Disulphide

7.3.3 Experiment and Results

The MoS_2 coated SSFBG sensor was connected to a light source and interrogation circuit (Figure 76). To produce natural occurring ethylene gas for the experiment, a pair of fresh apples were placed in a container. A commercial ethylene gas sensor (resolution of 0.5ppm), commonly used by fruit handlers to monitor ethylene gas, and water, to raise the humidity of the container to 100% (for controlling of humidity at a fixed level), were also placed in the container. The MoS_2 coated fibre end sensor was inserted through a small hole drilled through one of the container walls.

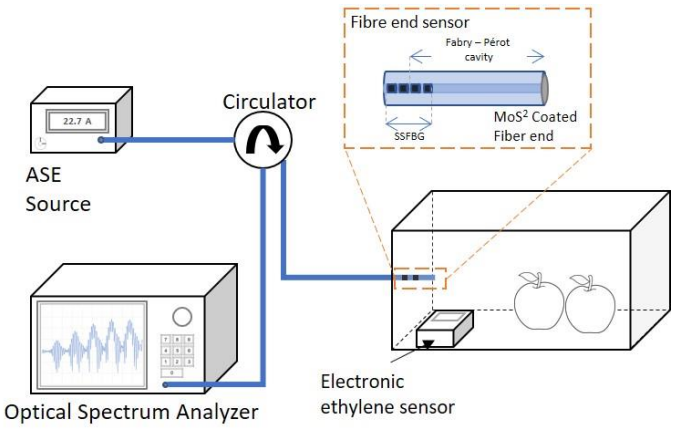

Figure 76:Experimental set up for metal ion detection with MoS^2 coated sensor.

A separate experiment with the coated fibre sensor was carried out to study the sensor's response over time in a constant 100% relative humidity environment by placing the sensor into the same container with a dish of water after relative humidity of the container had reached 100%

indicated by a hygrometer. It was found that in a 24 hours period no significant changes to the reflection spectrum of the sensor was observed.

Measurements of the refection spectrum of the sensor when in contact with ethylene gas were made at the beginning of the experiment when the commercial gas sensor presents a measurement of 0 ppm and then at 2 levels where the commercial sensor showed 0.5 and 1 ppm. Humidity level in the container remained at close to 100%. The amount of time between the measurements is around 12 hours.

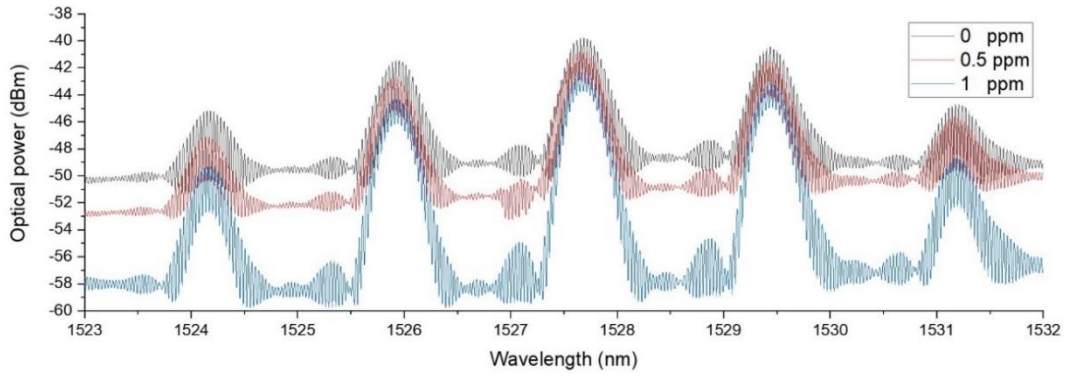

Figure 77: Molybdenum Disulphide coated Sensor response when exposed to air and ethylene gas of 0.5ppm and 1ppm of ethylene gas.

Figure 77 shows the reflection spectrum of the sensor when interrogated at different ethylene concentration levels. There is an obvious decrease in the fringe visibility of the FPI at the reflection peaks with increased concentration of ethylene gas.

It is well known that MoS_2 is also sensitive to humidity and in fact used in many humidity sensing works [150-152]. Complication could arise from the fact that the fruits in the container also contributes to humidity within the container. Therefore, to minimise the influence of humidity changes, water was added to the container and the experiment only began when humidity has reached close to 100%. Therefore, it is reasonable to conclude that while slight fluctuation in humidity indeed affects the sensor response, the major contributor is ethylene gas. This work serves only as an initial prove of concept of the sensor. In-depth study of the cross sensitivity of the sensor for humidity and ethylene gas is not in the focus of this thesis and has been furthered by other works since the penning of this chapter.

Figure 78 takes a closer look at the central peak of the sensor spectrum. Clear evolution of FPI fringe visibility can be observed. Fringe visibility is 3.374dBm at 0 ppm taken at the 0th hour, 2.114dBm at 0.5 ppm taken at the 12th hour and 1.432dBm at 1ppm taken at the 24th hour of the experiment.

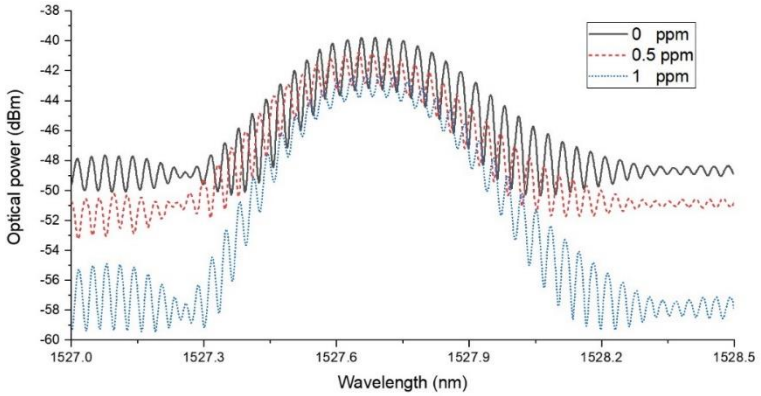

Figure 78: Central peak of Molybdenum Disulphide coated Sensor response when exposed to air and ethylene gas of 0.5ppm and 1ppm of ethylene gas.

Further works on this sensor should include humidity compensation studies and it is not always feasible to keep humidity at constant level where such sensors are designed to be deployed. Apart from this shortcoming of the design, MoS_2 functionalised refractometers are viable schemes for high sensitivity monitoring of ethylene gas.

7.4 Concluding Remarks

This chapter explored the potential of optical fibre RI sensor for targeted chemical sensing by functionalising the sensing surfaces of the sensors. Two applications were presented using the same refractometer design that relies on a low finesse FP cavity formed between a SSFBG and the cleaved fibre end. This sensor was discussed in chapter 5. With this scheme, the detection of metal ions in water was shown to be sensitive at the ppm level by coating the SSFBG sensor end with EDTA, a metal chelating agent. When in contact with metal ions in water, a chelate is formed and the overall RI of the coating is changed. This change in RI was then measured by the refractometer.

A gas sensor was also proposed by coating the SSFBG sensor with thin layers of MoS_2. The mechanism of ethylene gas capturing on the MoS_2 complex is not known now but is thought to be like graphene's capabilities in trapping ammonia gases in its structure. The interaction between the MoS_2 and ethylene gas resulting in a measurable change in RI is captured by the host SSFBG sensor.

8 FINAL DISCUSSIONS, CONCLUSION AND RECOMMENDATIONS FOR FUTURE WORK

8.1 Final Discussions

Communal effort by the scientific community in designing an ideal optical fibre refractive index (RI) sensor suitable for all applications had yield little results. Different sensing schemes presents unique advantages but also some unavoidable limitations. This thesis focuses on applying fibre Bragg grating (FBG) technology in addressing some of the limitations with existing optical fibre refractometers. Despite resolving fibre refractometers' issues of cross-sensitivity between RI and physical distortion of the sensor from heat and strain, these novel sensing schemes do face challenges in some other areas.

8.1.1 Advantages and Limitation of Fibre Bragg Grating Refractometers

FBGs had become subject of interest since its discovery and had been applied widely in optics. The operating principles of such devices have been well understood and fabrication process of these devices are mature. Therefore, researchers can creatively apply this technology in a wide range of applications. Naturally, some works adopted FBGs into fibre sensing schemes of physical parameters, exploiting the obvious interactions of FBG with the environment. More recently, the technology had found applications in chemical and biological sensors in which the fibre devices' role might not be obvious.

Some advantages of using fibre grating based refractometers is then the ease of fabrication, excellent repeatability and versatility. Incorporating a Bragg grating in refractometers as exemplified by the two FBG RI sensing schemes discussed in chapter 5 and 6 of this thesis, not only resolve the issues of cross sensitivity by making it possible to simultaneously measure RI along with temperature or strain. These advantages of the FBG schemes do come with limitations.

FBG is not inherently sensitive to RI of the ambient environment unlike its capability of responding to surrounding temperature and strain changes. Therefore, sensitization techniques such as cladding thinning or special grating designs are commonly adopted. However, these simple designs also present cross sensitivity issues. Moreover, cladding thinning causes the sensor to be structurally weak and special gratings such as the tilted FBG are not only difficult to fabricate but also difficult to interrogate. Therefore, more complex designs need to be adopted.

This thesis sets the effort of addressing these issues with advanced FBG refractometer designs in motion. In the last section of this chapter, possible future directions of research in this area were spelt out.

8.1.2 Advantages and Limitation of Surface Functionalisation of Fibre Refractometers

Leveraging on the fact that certain chemical reactions or physical interactions between compounds results in RI changes. Coating these materials onto a fibre refractometer's sensing surfaces enabled the refractometers to detect RI changes because of these interactions, detecting specific chemicals responsible for these changes. As a result, surface coating can be applied to most optical RI sensor designs. In some applications where reaction between the coating compound and reagent is highly unique, high specificity can be achieved.

Specificity is also the greatest limitation of these sensors. Coating of the sensors can be concurrently sensitive to more than one reagent and at times difficult to discriminate by the sensor. These sensors will then encounter high error rate when more than one of its coating's reagent exist in the same environment concurrently. There are discrimination techniques developed to resolve such problem including exploiting the fact that each reagent type has different rates of reaction with the coating. However, to extract enough information from the sensor to post process the results in order to discriminate the contribution of RI change of the coating by different reagent can be difficult and impractical. Nevertheless, as compared to

alternative more complex solutions to chemical sensing such as spectrometry, surface functionalisation of fibre refractometers remained a good candidate for further research.

8.2 Conclusion

This thesis focused on FBG technology's application in chemical sensing. It started by conducting an initial investigation on high germanium doped (>20% Ge-dopant) optical fibres as Bragg grating fibre host for sensing applications. It was found that although the fibres are generally more photosensitive to UV irradiation than standard optical fibres, at very low fluence dose irradiation, the photosensitivity mechanism is complex and hence difficult to control. It was also found that at extremely high Ge concentration of above 70%, the fibres start to lose its photosensitivity. This result is consistent with the theory that photosensitivity of the optical fibres arises from GeO defect states. At high Ge concentration, the optical fibre core essentially becomes Ge core doped with small amount of Si, resulting in less defect states in the glass structure. Being a very new class of optical fibres with tremendous potential due to its high nonlinearity, high Ge-doped optical fibres rightfully deserves more attention from the scientific community.

Addressing the issue of RI sensing, it was found that FBGs can play roles on top of being a sensing device in the sensor system as the interrogator. A two FBG cascaded interrogator design was proposed and implemented to interrogate a common tapered fibre RI sensor. This interrogator has removed the need for bulky electronic equipment in an optical sensor system, this lowering the complexity of design and cost of implementation. The interrogator circuit can be implemented in any interferometric RI sensors.

The major contribution of this thesis are the two fibre RI sensing schemes. The schemes decoupled RI sensitivity from the effect of temperature, they can also be used to measure temperature given RI is constant. The first of these demonstrated schemes is a fibre end RI sensor which sensing mechanism relies on an FBG to a cleaved fibre end low finesse Fabry-Perot cavity. The FBG reflection forms a Fabry-Perot interference (FPI) with the broadband

Fresnel reflection at the cleaved fibre end. As the Fresnel reflection is modulated by the changing RI of the environment, the characteristic of the FPI (visibility) is also modulated. Therefore, the FPI visibility change can be used to indicate RI change of the ambient environment. Temperature and strain applied to the sensor induces an all spectrum wavelength shifts and will not affect the visibility of the FPI which is strictly a function of the Fresnel fibre end reflection. Therefore, in the absence of strain, the sensor is capable of measuring RI and temperature simultaneously. Two different FBG types, superstructure FBG (SSFBG) and chirped FBG (CFBG) where implemented with different advantages. The SSFBG sensor has a maximum sensing range of 1.333 to 1.471 and sensitivity of 230 dB/RIU while the CFBG achieved a maximum sensitivity range of 1.333 to 1.410 and sensitivity of 679.66 RIU^{-1}.

The second RI sensing scheme relies on a specialty fibre (C-fibre) designed and fabricated in house. The special fibre has a cross dimensional geometry of a C shape with quadrant of the fibre removed at the preform stage. This causes one polarisation of the fundamental guided mode to be purposefully exposed to the environment. Essentially, the C-fibre is a birefringent waveguide as the orthogonal polarisation fundamental guided modes experiences different modal effective RI. One polarisation's modal effective RI is more significantly affected by the RI of the ambient environment than the other. By inscribing an FBG in the C-fibre, the Bragg reflection splits into two Bragg reflections according to the orthogonal modes. The separation between these two Bragg reflections changes with changes in ambient RI. Therefore, the polarisation mode separation can indicate ambient RI changes. As temperature and strain do not influence the birefringence of the fibre, the RI measurement from this sensor is not cross sensitive to temperature and strain. Temperature and strain changes however, results in equal shifts of both the Bragg wavelengths. In the absence of either strain or temperature, the sensor can then be used to simultaneously measure RI and either temperature or strain. The sensor reported has achieved a maximum RI sensitivity of 1300pm/RIU and range of 1.333 to 1.410.

Lastly, the SSFBG sensor reported in chapter 5 was chosen to be implemented as chemical sensor for heavy meatal ion in water and ethylene gas. This is achieved by functionalising the sensors with Ethylenediaminetetraacetic acid (EDTA) and Molybdenum disulphide (MoS_2) respectively. EDTA was coated onto the fibre end by chemical silanlisation followed by dip coating in EDTA solution. MoS_2 on the other hand was drop casted onto the fibre end surface. The EDTA coated sensor was found to be capable of detecting 10s of ppm level of heavy metal ions in water while the MoS_2 coated sensor can pick up traces of ethylene gas in the ppm level.

All in all, the series of work have showed that FBG based refractometers presents various merits in RI sensing not only as the sensing element but also as an interrogator for fibre sensors. Surface functionalisation of these sensors transforms the refractometers into targeted chemical sensor depending on the coating chosen.

8.3 Recommendations for Future Work

8.3.1 Detail Study of High Germanium Doped Fibres

UV photosensitivity of high Ge-doped fibres remains a relatively unchartered area of study with only one reported article on strong grating inscription into the fibre. For sensing applications, weak gratings can be useful. However, to inscribe weak gratings of specific characteristics, photosensitivity characteristics of the host fibre needs to be well known. This thesis found interesting competing mechanism of photosensitivity in this class of fibres, as compared to traditional photosensitive optical fibres. Therefore, in order to design and inscribe gratings into such fibres with high level of control, in depth analysis and investigation should be furthered.

8.3.2 On Tower Inscription of C-Fibre Bragg Gratings

As chapter 6 of this thesis suggests, on-tower inscription of FBG into C-fibre during the fibre drawing process can be interesting for cost effective fast fabrication and creation of long

sensor array. The existing challenges of on-tower grating inscription naturally applies, and new challenges will also arise. Due to the asymmetry of the fibre, freshly drawn C-fibre on the tower before coating is less steady than regular fibre. It then can be difficult to focus grating inscription irradiation onto the fibre core. The sharp corners of the fibre also diffract light and hence, more advance control system may be needed to tightly control the inscription pulses.

8.3.3 Further Investigation of Molybdenum Disulphide Interaction with Ethylene Gas Molecules

The mechanism behind the interaction of MoS_2 and ethylene gas that results in RI change of the coating is not confirmed. More experimentation and closer study of the phenomena is required to better understand the mechanisms to better optimise the application of the coating. MoS_2 is also cross sensitive to changes in humidity which is difficult to avoid in any natural environment. Robust humidity decoupling or compensation techniques needs to be explored for MoS_2 coated fibre sensors to be a feasible design for environmental sensing.

REFERENCES

[1] A. C. van Heel, "A new method of transporting optical images without aberrations," *Nature,* vol. 173, no. 4392, p. 39, 1954.

[2] P. C. Schultz, "Making the first low-loss optical fibers," *Optics and Photonics News,* vol. 21, no. 10, pp. 30-35, 2010.

[3] T. G. Giallorenzi *et al.*, "Optical fiber sensor technology," *IEEE transactions on microwave theory and techniques,* vol. 30, no. 4, pp. 472-511, 1982.

[4] J. Turán and E. Ovsenik, "Modern monitoring system for water pollution by petrochemical products based on optical fibre refractometer," in *Information and Communication Technology, Electronics and Microelectronics (MIPRO), 2014 37th International Convention on*, 2014, pp. 100-103: IEEE.

[5] J. Ascorbe, J. M. Corres, F. J. Arregui, and I. R. Matias, "Recent developments in fiber optics humidity sensors," *Sensors,* vol. 17, no. 4, p. 893, 2017.

[6] B. Xu, J. Li, Y. Li, J. Xie, and X. Dong, "Liquid seal for temperature sensing with fiber-optic refractometers," *Sensors,* vol. 14, no. 8, pp. 14873-14884, 2014.

[7] I. O. B. Luan, "Singapore water management policies and practices," *International Journal of Water Resources Development,* vol. 26, no. 1, pp. 65-80, 2010.

[8] J. Bürck, J.-P. Conzen, and H.-J. Ache, "A fiber optic evanescent field absorption sensor for monitoring organic contaminants in water," *Fresenius' journal of analytical chemistry,* vol. 342, no. 4-5, pp. 394-400, 1992.

[9] A. Dybko, W. Wroblewski, J. Maciejewski, R. S. Romaniuk, and Z. Brzozka, "Fiber optic probe for monitoring of drinking water," in *Chemical, Biochemical and Environmental Fiber Sensors IX*, 1997, vol. 3105, pp. 361-367: International Society for Optics and Photonics.

[10] M. Guarnieri and J. R. Balmes, "Outdoor air pollution and asthma," *The Lancet,* vol. 383, no. 9928, pp. 1581-1592, 2014.

[11] J. Lelieveld, J. S. Evans, M. Fnais, D. Giannadaki, and A. Pozzer, "The contribution of outdoor air pollution sources to premature mortality on a global scale," *Nature,* vol. 525, no. 7569, p. 367, 2015.

[12] P. E. Zerbini *et al.*, "Optical properties, ethylene production and softening in mango fruit," *Postharvest biology and technology,* vol. 101, pp. 58-65, 2015.

[13] R. Pitarma, G. Marques, and B. R. Ferreira, "Monitoring indoor air quality for enhanced occupational health," *Journal of medical systems,* vol. 41, no. 2, p. 23, 2017.

[14] Y. Shono and T. Inuzuka, "New image transmission method using planar plates and rectangular fibers," *Applied optics,* vol. 24, no. 3, pp. 361-364, 1985.

[15] A. Boucouvalas, M. Greaves, and N. Rayit, "D Shaped Optical Fibre For Sensing Applications," in *Fiber Optic Sensors II*, 1987, vol. 798, pp. 370-376: International Society for Optics and Photonics.

[16] G. Keiser, *Optical fiber communications*. McGraw-Hill, 2008.

[17] G. P. Agrawal, "Nonlinear fiber optics," in *Nonlinear Science at the Dawn of the 21st Century*: Springer, 2000, pp. 195-211.

[18] W. B. Allan, *Fibre optics: theory and practice*. Springer Science & Business Media, 2012.

[19] S. B. Poole, D. N. Payne, R. J. Mears, M. E. Fermann, and R. I. Laming, "Fabrication and characterization of low-loss optical fibers containing rare-earth ions," *J. Lightwave Technol,* vol. 4, no. 7, pp. 870-876, 1986.

[20] A. B. Seddon, Z. Tang, D. Furniss, S. Sujecki, and T. M. Benson, "Progress in rare-earth-doped mid-infrared fiber lasers," *Optics express,* vol. 18, no. 25, pp. 26704-26719, 2010.

[21] A. Sincore, J. D. Bradford, J. Cook, L. Shah, and M. C. Richardson, "High average power thulium-doped silica fiber lasers: Review of systems and concepts," *IEEE Journal of Selected Topics in Quantum Electronics,* vol. 24, no. 3, pp. 1-8, 2018.

[22] C. Wang, M. Wang, and J. Wu, "Heavily germanium-doped silica fiber with a flat normal dispersion profile," *IEEE Photonics Journal,* vol. 7, no. 2, pp. 1-10, 2015.

[23] O. I. Medvedkov, S. A. Vasiliev, P. I. Gnusin, and E. M. Dianov, "Photosensitivity of optical fibers with extremely high germanium concentration," *Optical Materials Express,* vol. 2, no. 11, pp. 1478-1489, 2012.

[24] D. Williams, B. Ainslie, J. Armitage, R. Kashyap, and R. Campbell, "Enhanced UV photosensitivity in boron codoped germanosilicate fibres," *Electronics Letters,* vol. 29, no. 1, pp. 45-47, 1993.

[25] D. Marcuse, "Field deformation and loss caused by curvature of optical fibers," *JOSA,* vol. 66, no. 4, pp. 311-320, 1976.

[26] L. Faustini and G. Martini, "Bend loss in single-mode fibers," *Journal of lightwave technology,* vol. 15, no. 4, pp. 671-679, 1997.

[27] A. Argyros, R. Lwin, and M. C. Large, "Bend loss in highly multimode fibres," *Optics Express,* vol. 16, no. 23, pp. 18590-18598, 2008.

[28] M. Lines, "Scattering losses in optic fiber materials. II. Numerical estimates," *Journal of applied physics,* vol. 55, no. 11, pp. 4058-4063, 1984.

[29] K. Hill, Y. Fujii, D. C. Johnson, and B. Kawasaki, "Photosensitivity in optical fiber waveguides: Application to reflection filter fabrication," *Applied physics letters,* vol. 32, no. 10, pp. 647-649, 1978.

[30] R. Kashyap, *Fiber bragg gratings*. Academic press, 2009.

[31] P. S. J. Russell, L. Poyntz-Wright, and D. P. Hand, "Frequency doubling, absorption, and grating formation in glass fibers: effective defects or defective effects?," in *Fiber laser sources and amplifiers II*, 1991, vol. 1373, pp. 126-140: International Society for Optics and Photonics.

[32] G. Meltz and W. W. Morey, "Bragg grating formation and germanosilicate fiber photosensitivity," in *International workshop on photoinduced self-organization effects in optical fiber*, 1991, vol. 1516, pp. 185-200: International Society for Optics and Photonics.

[33] T. Tsai, C. Askins, and E. Friebele, "Photoinduced grating and intensity dependence of defect generation in Ge‐doped silica optical fiber," *Applied physics letters,* vol. 61, no. 4, pp. 390-392, 1992.

[34] M. Gallagher and U. Osterberg, "Spectroscopy of defects in germanium‐doped silica glass," *Journal of applied physics,* vol. 74, no. 4, pp. 2771-2778, 1993.

[35] D. L. Williams, S. T. Davey, R. Kashyap, J. Armitage, and B. J. Ainslie, "Photosensitive germanosilicate preforms and fibers," in *Glasses for Optoelectronics II*, 1991, vol. 1513, pp. 158-168: International Society for Optics and Photonics.

[36] L. Dong, J. Pinkstone, P. S. J. Russell, and D. Payne, "Study of UV absorption in germanosilicate fiber preforms," in *Conference on Lasers and Electro-Optics*, 1994, p. CWK4: Optical Society of America.

[37] D. Marcuse, "Loss analysis of single-mode fiber splices," *Bell System Technical Journal*, vol. 56, no. 5, pp. 703-718, 1977.

[38] R. Sidharthan *et al.*, "Stress-loss correlation and dispersion control in highly GeO2-doped Fibers," *IEEE Photonics Technol. Lett.*, vol. 28, no. 14, pp. 1521-1524, 2016.

[39] P. J. Lemaire, R. Atkins, V. Mizrahi, and W. Reed, "High pressure H/sub 2/loading as a technique for achieving ultrahigh UV photosensitivity and thermal sensitivity in GeO/sub 2/doped optical fibres," *Electronics Letters*, vol. 29, no. 13, pp. 1191-1193, 1993.

[40] R. Atkins, P. Lemaire, T. Erdogan, and V. Mizrahi, "Mechanisms of enhanced UV photosensitivity via hydrogen loading in germanosilicate glasses," *Electronics Letters*, vol. 29, no. 14, pp. 1234-1235, 1993.

[41] P. Lemaire, A. Vengsarkar, W. Reed, V. Mizrahi, and K. Kranz, "Refractive-index changes in optical fibers sensitized with molecular hydrogen," in *Optical Fiber Communication Conference*, 1994, p. TuL1: Optical Society of America.

[42] P. J. Lemaire, "Reliability of optical fibers exposed to hydrogen: prediction of long-term loss increases," *Optical engineering*, vol. 30, no. 6, pp. 780-790, 1991.

[43] K. Noguchi, N. Shibata, N. Uesugi, and Y. Negishi, "Loss increase for optical fibers exposed to hydrogen atmosphere," *Journal of lightwave technology*, vol. 3, no. 2, pp. 236-243, 1985.

[44] K. Awazu, H. Kawazoe, and M. Yamane, "Simultaneous generation of optical absorption bands at 5.14 and 0.452 eV in 9 SiO2: GeO2 glasses heated under an H2 atmosphere," *Journal of Applied Physics*, vol. 68, no. 6, pp. 2713-2718, 1990.

[45] G. Meltz, W. W. Morey, and W. Glenn, "Formation of Bragg gratings in optical fibers by a transverse holographic method," *Optics letters*, vol. 14, no. 15, pp. 823-825, 1989.

[46] T. Guo, F. Liu, B.-O. Guan, and J. Albert, "Tilted fiber grating mechanical and biochemical sensors," *Optics & Laser Technology*, vol. 78, pp. 19-33, 2016.

[47] G. Laffont and P. Ferdinand, "Tilted short-period fibre-Bragg-grating-induced coupling to cladding modes for accurate refractometry," *Measurement Science and Technology*, vol. 12, no. 7, p. 765, 2001.

[48] C. Caucheteur and P. Mégret, "Demodulation technique for weakly tilted fiber Bragg grating refractometer," *IEEE Photonics Technology Letters*, vol. 17, no. 12, pp. 2703-2705, 2005.

[49] C.-F. Chan, C. Chen, A. Jafari, A. Laronche, D. J. Thomson, and J. Albert, "Optical fiber refractometer using narrowband cladding-mode resonance shifts," *Applied optics*, vol. 46, no. 7, pp. 1142-1149, 2007.

[50] K. Byron, K. Sugden, T. Bricheno, and I. Bennion, "Fabrication of chirped Bragg gratings in photosensitive fibre," *Electronics letters*, vol. 29, no. 18, pp. 1659-1660, 1993.

[51] J. Cruz, L. Dong, S. Barcelos, and L. Reekie, "Fiber Bragg gratings with various chirp profiles made in etched tapers," *Applied optics*, vol. 35, no. 34, pp. 6781-6787, 1996.

[52] F. Ouellette, "Dispersion cancellation using linearly chirped Bragg grating filters in optical waveguides," *Optics letters*, vol. 12, no. 10, pp. 847-849, 1987.

[53] B. Eggleton, P. Krug, L. Poladian, and F. Ouellette, "Long periodic superstructure Bragg gratings in optical fibres," *Electronics letters,* vol. 30, no. 19, pp. 1620-1622, 1994.

[54] A. Martinez, M. Dubov, I. Khrushchev, and I. Bennion, "Direct writing of fibre Bragg gratings by femtosecond laser," *Electronics Letters,* vol. 40, no. 19, pp. 1170-1172, 2004.

[55] K. Itoh, W. Watanabe, S. Nolte, and C. B. Schaffer, "Ultrafast processes for bulk modification of transparent materials," *MRS bulletin,* vol. 31, no. 8, pp. 620-625, 2006.

[56] C. Askins, M. Putnam, G. Williams, and E. Friebele, "Stepped-wavelength optical-fiber Bragg grating arrays fabricated in line on a draw tower," *Optics letters,* vol. 19, no. 2, pp. 147-149, 1994.

[57] R. F. Idrisov *et al.*, "Spectral characteristics of draw-tower step-chirped fiber Bragg gratings," *Optics & Laser Technology,* vol. 80, pp. 112-115, 2016.

[58] M. W. Rothhardt, M. Becker, E. Lindner, C. Chojetzki, and H. Bartelt, "Strain sensor chains beyond 1000 individual fiber Bragg gratings made during fiber drawing," in *Bragg Gratings, Photosensitivity, and Poling in Glass Waveguides*, 2010, p. JThA53: Optical Society of America.

[59] A. M. Vengsarkar, P. J. Lemaire, J. B. Judkins, V. Bhatia, T. Erdogan, and J. E. Sipe, "Long-period fiber gratings as band-rejection filters," *Journal of lightwave technology,* vol. 14, no. 1, pp. 58-65, 1996.

[60] T. Erdogan, "Cladding-mode resonances in short-and long-period fiber grating filters," *JOSA A,* vol. 14, no. 8, pp. 1760-1773, 1997.

[61] S. A. Vasil'ev *et al.*, "Properties of the cladding modes of an optical fibre excited by refractive-index gratings," *Quantum Electronics,* vol. 29, no. 1, pp. 65-68, 1999.

[62] M. Artiglia, G. Coppa, P. Di Vita, M. Potenza, and A. Sharma, "Mode field diameter measurements in single-mode optical fibers," *Journal of Lightwave Technology,* vol. 7, no. 8, pp. 1139-1152, 1989.

[63] W. Liang, Y. Huang, Y. Xu, R. K. Lee, and A. Yariv, "Highly sensitive fiber Bragg grating refractive index sensors," *Applied physics letters,* vol. 86, no. 15, p. 151122, 2005.

[64] A. Iadicicco, A. Cusano, A. Cutolo, R. Bernini, and M. Giordano, "Thinned fiber Bragg gratings as high sensitivity refractive index sensor," *IEEE Photonics Technology Letters,* vol. 16, no. 4, pp. 1149-1151, 2004.

[65] A. Iadicicco, A. Cusano, S. Campopiano, A. Cutolo, and M. Giordano, "Thinned fiber Bragg gratings as refractive index sensors," *IEEE Sensors Journal,* vol. 5, no. 6, pp. 1288-1295, 2005.

[66] S.-M. Lee, S. S. Saini, and M.-Y. Jeong, "Simultaneous measurement of refractive index, temperature, and strain using etched-core fiber Bragg grating sensors," *IEEE Photonics Technology Letters,* vol. 22, no. 19, pp. 1431-1433, 2010.

[67] N. Chen, B. Yun, Y. Wang, and Y. Cui, "Theoretical and experimental study on etched fiber Bragg grating cladding mode resonances for ambient refractive index sensing," *JOSA B,* vol. 24, no. 3, pp. 439-445, 2007.

[68] J. Kumar *et al.*, "Wavelength independent chemical sensing using etched thermally regenerated FBG," *Sensors and Actuators B: Chemical,* vol. 244, pp. 54-60, 2017.

[69] X. Liu, T. Wang, Y. Wu, Y. Gong, and Y.-J. Rao, "Dual-parameter sensor based on tapered FBG combined with microfiber cavity," *IEEE Photonics Technology Letters,* vol. 26, no. 8, pp. 817-820, 2014.

[70] Y. Ran *et al.*, "193nm excimer laser inscribed Bragg gratings in microfibers for refractive index sensing," *Optics express,* vol. 19, no. 19, pp. 18577-18583, 2011.

[71] X. Fang, C. Liao, and D. Wang, "Femtosecond laser fabricated fiber Bragg grating in microfiber for refractive index sensing," *Optics letters,* vol. 35, no. 7, pp. 1007-1009, 2010.

[72] K. Zhou, X. Chen, L. Zhang, and I. Bennion, "Implementation of optical chemsensors based on HF-etched fibre Bragg grating structures," *Measurement Science and Technology,* vol. 17, no. 5, p. 1140, 2006.

[73] J. Li, H. Wang, L.-P. Sun, Y. Huang, L. Jin, and B.-O. Guan, "Etching Bragg gratings in Panda fibers for the temperature-independent refractive index sensing," *Optics Express,* vol. 22, no. 26, pp. 31917-31923, 2014.

[74] O. Frazão, T. Martynkien, J. Baptista, J. Santos, W. Urbanczyk, and J. Wojcik, "Optical refractometer based on a birefringent Bragg grating written in an H-shaped fiber," *Optics letters,* vol. 34, no. 1, pp. 76-78, 2009.

[75] Y. Ran, L. Jin, L.-P. Sun, J. Li, and B.-O. Guan, "Bragg gratings in rectangular microfiber for temperature independent refractive index sensing," *Optics letters,* vol. 37, no. 13, pp. 2649-2651, 2012.

[76] Q. Zhang, L. Hu, Y. Qi, G. Liu, N. Ianno, and M. Han, "Fiber-optic refractometer based on a phase-shifted fiber Bragg grating on a side-hole fiber," *Optics express,* vol. 23, no. 13, pp. 16750-16759, 2015.

[77] H. Meng, W. Shen, G. Zhang, C. Tan, and X. Huang, "Fiber Bragg grating-based fiber sensor for simultaneous measurement of refractive index and temperature," *Sensors and Actuators B: Chemical,* vol. 150, no. 1, pp. 226-229, 2010.

[78] J. Yang, X. Dong, Y. Zheng, K. Ni, C. C. Chan, and P. P. Shum, "Magnetic field sensing with reflectivity ratio measurement of fiber Bragg grating," *IEEE Sensors Journal,* vol. 15, no. 3, pp. 1372-1376, 2015.

[79] C.-B. Kim and C. B. Su, "Measurement of the refractive index of liquids at 1.3 and 1.5 micron using a fibre optic Fresnel ratio meter," *Measurement Science and Technology,* vol. 15, no. 9, p. 1683, 2004.

[80] V. Bhatia and A. M. Vengsarkar, "Optical fiber long-period grating sensors," *Opt Lett,* vol. 21, no. 9, pp. 692-4, May 1 1996.

[81] B. H. Lee, Y. Liu, S. B. Lee, S. S. Choi, and J. N. Jang, "Displacements of the resonant peaks of a long-period fiber grating induced by a change of ambient refractive index," *Opt Lett,* vol. 22, no. 23, pp. 1769-71, Dec 1 1997.

[82] O. Duhem, J. F. Henninot, M. Warenghem, and M. Douay, "Demonstration of Long-Period-Grating Efficient Couplings with an External Medium of a Refractive Index Higher than that of Silica," *Appl Opt,* vol. 37, no. 31, pp. 7223-8, Nov 1 1998.

[83] X. Shu, L. Zhang, and I. Bennion, "Sensitivity characteristics near the dispersion turning points of long-period fiber gratings in B/Ge codoped fiber," *Opt Lett,* vol. 26, no. 22, pp. 1755-7, Nov 15 2001.

[84] J. L. Tang and J. N. Wang, "Chemical Sensing Sensitivity of Long-Period Grating Sensor Enhanced by Colloidal Gold Nanoparticles," *Sensors (Basel),* vol. 8, no. 1, pp. 171-184, Jan 21 2008.

[85] I. Del Villar, I. R. Matias, and F. J. Arregui, "Enhancement of sensitivity in long-period fiber gratings with deposition of low-refractive-index materials," *Opt Lett,* vol. 30, no. 18, pp. 2363-5, Sep 15 2005.

[86] X. Chen, K. Zhou, L. Zhang, and I. Bennion, "Dual-peak long-period fiber gratings with enhanced refractive index sensitivity by finely tailored mode dispersion that uses the light cladding etching technique," *Applied optics,* vol. 46, no. 4, pp. 451-455, 2007.

[87] Q. Ling, Z. Gu, and K. Gao, "Smart design of a long-period fiber grating refractive index sensor based on dual-peak resonance near the phase-matching turning point," *Applied optics,* vol. 57, no. 10, pp. 2693-2697, 2018.

[88] S. Khaliq, S. W. James, and R. P. Tatam, "Enhanced sensitivity fibre optic long period grating temperature sensor," *Measurement Science and Technology,* vol. 13, no. 5, p. 792, 2002.

[89] Y.-P. Wang, L. Xiao, D. Wang, and W. Jin, "Highly sensitive long-period fiber-grating strain sensor with low temperature sensitivity," *Optics letters,* vol. 31, no. 23, pp. 3414-3416, 2006.

[90] H. Patrick, C. Chang, and S. Vohra, "Long period fibre gratings for structural bend sensing," *Electronics Letters,* vol. 34, no. 18, pp. 1773-1775, 1998.

[91] M. N. Ng, Z. Chen, and K. S. Chiang, "Temperature compensation of long-period fiber grating for refractive-index sensing with bending effect," *IEEE Photonics Technology Letters,* vol. 14, no. 3, pp. 361-362, 2002.

[92] X. Bevenot, A. Trouillet, C. Veillas, H. Gagnaire, and M. Clement, "Surface plasmon resonance hydrogen sensor using an optical fibre," *Measurement Science and Technology,* vol. 13, no. 1, p. 118, 2001.

[93] J. Villatoro and D. Monzón-Hernández, "Fast detection of hydrogen with nano fiber tapers coated with ultra thin palladium layers," *Optics express,* vol. 13, no. 13, pp. 5087-5092, 2005.

[94] A. Trouillet, E. Marin, and C. Veillas, "Fibre gratings for hydrogen sensing," *Measurement Science and Technology,* vol. 17, no. 5, p. 1124, 2006.

[95] B. D. MacCraith *et al.*, "Fibre optic oxygen sensor based on fluorescence quenching of evanescent-wave excited ruthenium complexes in sol–gel derived porous coatings," *Analyst,* vol. 118, no. 4, pp. 385-388, 1993.

[96] M. Krihak and M. Shahriari, "Highly sensitive, all solid state fibre optic oxygen sensor based on the sol-gel coating technique," *Electronics Letters,* vol. 32, no. 3, pp. 240-242, 1996.

[97] M. Penza *et al.*, "Carbon nanotube acoustic and optical sensors for volatile organic compound detection," *Nanotechnology,* vol. 16, no. 11, p. 2536, 2005.

[98] A. Abdelghani *et al.*, "Optical fibre sensor coated with porous silica layers for gas and chemical vapour detection," *Sensors and Actuators B: Chemical,* vol. 44, no. 1-3, pp. 495-498, 1997.

[99] J. F. Alder, D. C. Ashworth, R. Narayanaswamy, R. E. Moss, and I. O. Sutherland, "Communication. An optical potassium ion sensor," *Analyst,* vol. 112, no. 8, pp. 1191-1192, 1987.

[100] R. Verma and B. D. Gupta, "Detection of heavy metal ions in contaminated water by surface plasmon resonance based optical fibre sensor using conducting polymer and chitosan," *Food chemistry,* vol. 166, pp. 568-575, 2015.

[101] O. B. Miled, D. Grosso, C. Sanchez, and J. Livage, "An optical fibre pH sensor based on dye doped mesostructured silica," *Journal of Physics and Chemistry of solids,* vol. 65, no. 10, pp. 1751-1755, 2004.

[102] S. Dong, M. Luo, G. Peng, and W. Cheng, "Broad range pH sensor based on sol–gel entrapped indicators on fibre optic," *Sensors and Actuators B: Chemical,* vol. 129, no. 1, pp. 94-98, 2008.

[103] S. E. Khalil, L. Bansal, and M. A. El-Sherif, "Intrinsic fiber optic chemical sensor for the detection of dimethyl methylphosphonate," *Optical Engineering,* vol. 43, no. 11, pp. 2683-2689, 2004.
[104] J. Yuan and M. A. El-Sherif, "Fiber-optic chemical sensor using polyaniline as modified cladding material," *IEEE sensors journal,* vol. 3, no. 1, pp. 5-12, 2003.
[105] B. MacCraith, C. McDonagh, G. O'keeffe, A. McEvoy, T. Butler, and F. Sheridan, "Sol-gel coatings for optical chemical sensors and biosensors," *Sensors and Actuators B: Chemical,* vol. 29, no. 1-3, pp. 51-57, 1995.
[106] W. C. Michie *et al.,* "Fibre optic/hydrogel probe for distributed chemical measurements," in *Tenth International Conference on Optical Fibre Sensors,* 1994, vol. 2360, pp. 130-134: International Society for Optics and Photonics.
[107] R. Bogdanowicz *et al.,* "Improved surface coverage of an optical fibre with nanocrystalline diamond by the application of dip-coating seeding," *Diamond and Related Materials,* vol. 55, pp. 52-63, 2015.
[108] K. Kashiwagi, S. Yamashita, and S. Y. Set, "In-situ monitoring of optical deposition of carbon nanotubes onto fiber end," *Optics express,* vol. 17, no. 7, pp. 5711-5715, 2009.
[109] R. M. Atkins, "Measurement of the ultraviolet absorption spectrum of optical fibers," *Optics letters,* vol. 17, no. 7, pp. 469-471, 1992.
[110] J. P. Bernardin and N. Lawandy, "Dynamics of the formation of Bragg gratings in germanosilicate optical fibers," *Optics communications,* vol. 79, no. 3-4, pp. 194-199, 1990.
[111] H.-J. Deyerl, H. Sorensen, J. B. Jensen, N. Plougmann, and M. Kristensen, "Fabrication and stability of fiber Bragg gratings for WDM applications using a 266 nm CW-laser," in *Lasers and Electro-Optics, 2003. CLEO'03. Conference on,* 2003, p. 3 pp.: IEEE.
[112] S. A. Slattery, D. N. Nikogosyan, and G. Brambilla, "Fiber Bragg grating inscription by high-intensity femtosecond UV laser light: comparison with other existing methods of fabrication," *JOSA B,* vol. 22, no. 2, pp. 354-361, 2005.
[113] P. Swart, M. Shlyagin, A. Chtcherbakov, and V. Spirin, "Photosensitivity measurement in optical fibre with Bragg grating interferometers," *Electronics Letters,* vol. 38, no. 24, pp. 1508-1510, 2002.
[114] J. Canning and A. Carter, "Modal interferometer for in situ measurements of induced core index change in optical fibers," *Optics letters,* vol. 22, no. 8, pp. 561-563, 1997.
[115] E. Brinkmeyer, D. Johlen, F. Knappe, and H. Renner, "Methods for experimental characterization of uv-written gratings and waveguides," in *Bragg Gratings, Photosensitivity, and Poling in Glass Waveguides,* 1999, p. BC1: Optical Society of America.
[116] D. S. Gunawardena *et al.,* "Photosensitivity of gallium-doped silica core fiber to 193 nm ArF excimer laser," *Applied optics,* vol. 54, no. 17, pp. 5508-5512, 2015.
[117] W. B. Ji, H. H. Liu, S. C. Tjin, K. K. Chow, and A. Lim, "Ultrahigh sensitivity refractive index sensor based on optical microfiber," *IEEE Photonics Technology Letters,* vol. 24, no. 20, pp. 1872-1874, 2012.
[118] Q. Rong, X. Qiao, R. Wang, H. Sun, M. Hu, and Z. Feng, "High-sensitive fiber-optic refractometer based on a core-diameter-mismatch Mach–Zehnder interferometer," *IEEE Sensors Journal,* vol. 12, no. 7, pp. 2501-2505, 2012.
[119] Y. Ma *et al.,* "Mach-Zehnder interferometer based on a sandwich fiber structure for refractive index measurement," *IEEE Sensors Journal,* vol. 12, no. 6, pp. 2081-2085, 2012.

[120] J. Zheng *et al.*, "Temperature and index insensitive strain sensor based on a photonic crystal fiber in line Mach–Zehnder interferometer," *Optics Communications,* vol. 297, pp. 7-11, 2013.
[121] Y. Li, Z. Liu, and S. Jian, "Multimode interference refractive index sensor based on coreless fiber," *Photonic Sensors,* vol. 4, no. 1, pp. 21-27, 2014.
[122] D. Wu, T. Zhu, K. S. Chiang, and M. Deng, "All single-mode fiber Mach–Zehnder interferometer based on two peanut-shape structures," *Journal of Lightwave Technology,* vol. 30, no. 5, pp. 805-810, 2012.
[123] W. B. Ji, Y. C. Tan, B. Lin, S. C. Tjin, and K. K. Chow, "Nonadiabatically tapered microfiber sensor with ultrashort waist," *IEEE Photonics Technology Letters,* vol. 26, no. 22, pp. 2303-2306, 2014.
[124] Z. Tian *et al.*, "Refractive index sensing with Mach–Zehnder interferometer based on concatenating two single-mode fiber tapers," *IEEE Photonics Technology Letters,* vol. 20, no. 8, pp. 626-628, 2008.
[125] K. Q. Kieu and M. Mansuripur, "Biconical fiber taper sensors," *IEEE Photonics Technology Letters,* vol. 18, no. 21, pp. 2239-2241, 2006.
[126] D. Wu *et al.*, "Refractive index sensing based on Mach–Zehnder interferometer formed by three cascaded single-mode fiber tapers," *Applied optics,* vol. 50, no. 11, pp. 1548-1553, 2011.
[127] G. Brambilla, "Optical fibre nanowires and microwires: a review," *Journal of Optics,* vol. 12, no. 4, p. 043001, 2010.
[128] G. Y. Chen, M. Ding, T. Newson, and G. Brambilla, "A review of microfiber and nanofiber based optical sensors," *The Open Optics Journal,* vol. 7, no. 1, 2013.
[129] L. Tong, F. Zi, X. Guo, and J. Lou, "Optical microfibers and nanofibers: A tutorial," *Optics Communications,* vol. 285, no. 23, pp. 4641-4647, 2012.
[130] S. F. Silva, O. Frazão, P. Caldas, J. L. Santos, F. Araújo, and L. A. Ferreira, "Optical fiber refractometer based on a Fabry-Pérot interferometer," *Optical Engineering,* vol. 47, no. 5, p. 054403, 2008.
[131] C. Gouveia, P. Jorge, J. Baptista, and O. Frazão, "Fabry–Pérot cavity based on a high-birefringent fiber Bragg grating for refractive index and temperature measurement," *IEEE Sensors Journal,* vol. 12, no. 1, pp. 17-21, 2012.
[132] J. Santos, A. Leite, and D. A. Jackson, "Optical fiber sensing with a low-finesse Fabry–Perot cavity," *Applied Optics,* vol. 31, no. 34, pp. 7361-7366, 1992.
[133] K. O. Hill and G. Meltz, "Fiber Bragg grating technology fundamentals and overview," *Journal of lightwave technology,* vol. 15, no. 8, pp. 1263-1276, 1997.
[134] J. Gladstone, "On the Influence of Temperature on the Refraction of Light," *Proceedings of the Royal Society of London,* vol. 9, pp. 328-331, 1857.
[135] M. F. Namiq and M. Ibsen, "Hydrofluoric Acid Refractive Index Determination using In-situ Monitoring of Etched Fibre Bragg Gratings," in *Optical Sensors*, 2015, p. SeS3C. 4: Optical Society of America.
[136] H. H. Qazi, A. B. Mohammad, H. Ahmad, and M. Z. Zulkifli, "D-shaped polarization maintaining fiber sensor for strain and temperature monitoring," *Sensors,* vol. 16, no. 9, p. 1505, 2016.
[137] M. Wuilpart, C. Caucheteur, S. Bette, P. Mégret, and M. Blondel, "Polarization properties of uniform fiber Bragg gratings written in highly birefringent fibers," *Optics communications,* vol. 247, no. 4-6, pp. 239-245, 2005.
[138] B.-O. Guan, H.-Y. Tam, X.-M. Tao, and X.-Y. Dong, "Simultaneous strain and temperature measurement using a superstructure fiber Bragg grating," *IEEE Photonics Technology Letters,* vol. 12, no. 6, pp. 675-677, 2000.

[139] Q. Zhang, N. J. Ianno, and M. Han, "Fiber-optic refractometer based on an etched high-Q π-phase-shifted fiber-Bragg-grating," *Sensors*, vol. 13, no. 7, pp. 8827-8834, 2013.

[140] P. Ray, K. Srijith, and B. Srinivasan, "Enhanced sensitivity etched fiber Bragg gratings for precise measurement of refractive index," in *International Conference on Optics and Photonics 2015*, 2015, vol. 9654, p. 965415: International Society for Optics and Photonics.

[141] A. N. Bashkatov and E. A. Genina, "Water refractive index in dependence on temperature and wavelength: a simple approximation," in *Saratov Fall Meeting 2002: Optical Technologies in Biophysics and Medicine IV*, 2003, vol. 5068, pp. 393-396: International Society for Optics and Photonics.

[142] C. Liao, Y. Wang, D. Wang, and M. Yang, "Fiber in-line Mach–Zehnder interferometer embedded in FBG for simultaneous refractive index and temperature measurement," *IEEE Photonics Technology Letters*, vol. 22, no. 22, pp. 1686-1688, 2010.

[143] W. B. Ji *et al.*, "Detection of low-concentration heavy metal ions using optical microfiber sensor," *Sensors and Actuators B: Chemical*, vol. 237, pp. 142-149, 2016.

[144] S. Janssen, K. Schmitt, M. Blanke, M. Bauersfeld, J. Wöllenstein, and W. Lang, "Ethylene detection in fruit supply chains," *Phil. Trans. R. Soc. A*, vol. 372, no. 2017, p. 20130311, 2014.

[145] K. L.-C. Wang, H. Li, and J. R. Ecker, "Ethylene biosynthesis and signaling networks," *The plant cell*, vol. 14, no. suppl 1, pp. S131-S151, 2002.

[146] B. Esser, J. M. Schnorr, and T. M. Swager, "Selective detection of ethylene gas using carbon nanotube-based devices: utility in determination of fruit ripeness," *Angewandte Chemie International Edition*, vol. 51, no. 23, pp. 5752-5756, 2012.

[147] G. T. Morgan and H. D. K. Drew, "CLXII.—Researches on residual affinity and co-ordination. Part II. Acetylacetones of selenium and tellurium," *Journal of the Chemical Society, Transactions*, vol. 117, pp. 1456-1465, 1920.

[148] S. J. Flora and V. Pachauri, "Chelation in metal intoxication," *International journal of environmental research and public health*, vol. 7, no. 7, pp. 2745-2788, 2010.

[149] Z. Mohammadi, S. Shalavi, and H. Jafarzadeh, "Ethylenediaminetetraacetic acid in endodontics," *European journal of dentistry*, vol. 7, no. Suppl 1, p. S135, 2013.

[150] S.-L. Zhang, H. Jung, J.-S. Huh, J.-B. Yu, and W.-C. Yang, "Efficient exfoliation of MoS2 with volatile solvents and their application for humidity sensor," *Journal of nanoscience and nanotechnology*, vol. 14, no. 11, pp. 8518-8522, 2014.

[151] J. Zhao *et al.*, "Highly sensitive MoS2 humidity sensors array for noncontact sensation," *Advanced Materials*, vol. 29, no. 34, p. 1702076, 2017.

[152] B. Du *et al.*, "MoS2-based all-fiber humidity sensor for monitoring human breath with fast response and recovery," *Sensors and Actuators B: Chemical*, vol. 251, pp. 180-184, 2017.

LIST OF PUBLICATIONS

Journals

- **Rex Xiao Tan**, Stephanie Hui Kit Yap, Yung Chuen Tan, Swee Chuan Tjin, Morten Ibsen, Ken-Tye Yong, and Wenn Jing Lai, "Functionalized Fiber End Superstructure Fiber Bragg Grating Refractive Index Sensor for Heavy Metal Ion Detection," MDPI Sensors, vol. 18, no. 6, p. 1821, Jun. 2018. (DOI:10.3390/s18061821)

- **Rex Xiao Tan**, Yung Chuen Tan, Daryl Ho, Chun Ho Tse, Swee Chuan. Tjin, Morten Ibsen, "Birefringent Bragg Grating in C-Shaped Optical Fiber as a Temperature-Insensitive Refractometer," MDPI Sensors, vol. 18, no. 10, p. 3285, Sept. 2018. (DOI:10.3390/s18103285.)

- Stephanie Hui Kit Yap, Yi-Hsin Chien, **Rex Xiao Tan**, Abdul Rahman Ahiak Alauddin, Wen Bin Ji, Swee Chuan Tjin, Ken-Tye Yong, "An advanced handheld microfiber-based sensor for ultra-sensitive lead ion detection," ACS Sensors, Nov. 2018. (DOI: 10.1021/acssensors.8b01031)

- Wenjie Lai, Lin Cao, **Rex Xiao Tan**, Yung Chuen Tan, Xiaoguo Li, Phuoc Thien Phan, Anthony Meng Huat Tiong, Swee Chuan Tjin, Soo Jay Phee, "An Integrated Sensor-Model Approach for Haptic Feedback of Flexible Endoscopic Robots," Ann Biomed Eng, Aug. 2019. (DOI: 10.1007/s10439-019-02352-8)

- Wenjie Lai, Lin Cao, **Rex Xiao Tan**, Phuoc Thien Phan, Jianzhong Hao, Swee Chuan Tjin, Soo Jay Phee, "Force Sensing with 1mm Fiber Bragg Gratings for Tendon-Sheath Driven Mechanisms and Tendon Driven Mechanisms in Flexible Surgical Robots," IEEE/ASME Trans. on Mechatronics, Nov. 2019. (DOI: 10.1109/TMECH.2019.2951540).

- **Rex Tan Xiao**, Morten Ibsen, Swee Chuan Tjin, "Optical Fiber Refractometer Based Metal Ion Sensors", MDPI Chemosensors, Dec. 2019.

Conferences

- **Rex Xiao Tan**, Stephanie Hui Kit Yap, Swee Chuan Tjin. "Strain and temperature insensitive optical fibre grating refractive index sensor.," Fibre-optic and Photonic Sensors for Industrial and Safety Applications (OFSIS), 2nd International Conference for. IEEE, 2017.

- **Rex Xiao Tan**, Stephanie Hui Kit Yap, Swee Chuan Tjin. "Fiber gratings enabled interrogation of Mach-Zehnder interferometer tapered fiber sensor.," Lasers and Electro-Optics Pacific Rim (CLEO-PR), 2017 Conference on. IEEE, 2017.

- **Rex Xiao Tan**, Daryl Ho, Chun Ho Tse, Seong Woo Yoo, Swee Chuan Tjin, Morten Ibsen, "Bragg Grating Inscribed C-Shape Optical Fiber for Temperature and Strain Insensitive Refractive Index Sensing." 6th International Symposium on Sensor Science (I3S 2018), 2018.

- **Rex Xiao Tan**, Swee Chuan Tjin. "Light-Environment Interface Functionalized Fiber Grating Sensors for Environmental Monitoring.," 7th Annual Conference of AnalytiX (AnalytiX), 2019